GRUPO DE SISTEMAS RADIANTES
Departamento de Física Aplicada
Facultad de Física.
Santiago de Copostela, SPAIN

FINAL REPORT OF THE CONTRACT

ANTENNA ARRAY PATTERN SYNTHESIS IN THE PRESENCE OF NEAR-ZONE SCATTERERS

GRUPO DE SISTEMAS RADIANTES
Departamento de Física Aplicada
Facultad de Física.
Santiago de Copostela, SPAIN

FINAL REPORT OF THE CONTRACT

ANTENNA ARRAY PATTERN SYNTHESIS IN THE PRESENCE OF NEAR-ZONE SCATTERERS

Contract Number: F61708-98-W0018

Prepared by: Grupo de Sistemas Radiantes.

Revised by: Manuel Vicente Lozano.

Approved by: Francisco J. Ares Pena.

UNIVERSIDADE DE SANTIAGO DE COMPOSTELA GRUPO DE SISTEMAS RADIANTES * Facultade de Física *

Date: 8th March 1999

REPORT DOCUMENTATION PAGE

Form Approved OMB No. 0704-0188

1. AGENCY USE ONLY (Leave blank)	2. REPORT DATE	3. REPORT TYPE AND DATES COVERED
	8 March 1999	Final Report

4. TITLE AND SUBTITLE

Antenna Array Pattern Synthesis In The Presence Of Near-Zone Scatterers

5. FUNDING NUMBERS

F6170898W0018

6. AUTHOR(S)

Prof. Francisco Jose Ares Pena

7. PERFORMING ORGANIZATION NAME(S) AND ADDRESS(ES)

Universidae De Santiago De Compostela
Facultade de Fisica, Campus Universitario Sur., 15706 Santiago de Compostela (Espana)
Espana
Spain

8. PERFORMING ORGANIZATION REPORT NUMBER

N/A

9. SPONSORING/MONITORING AGENCY NAME(S) AND ADDRESS(ES)

EOARD
PSC 802 BOX 14
FPO 09499-0200

10. SPONSORING/MONITORING AGENCY REPORT NUMBER

SPC 98-4011

11. SUPPLEMENTARY NOTES

12a. DISTRIBUTION/AVAILABILITY STATEMENT

Approved for public release; distribution is unlimited.

12b. DISTRIBUTION CODE

A

13. ABSTRACT (Maximum 200 words)

This report results from a contract tasking Universidae De Santiago De Compostela as follows: The contractor will investigate techniques of simulated annealing and/or genetic algorithms of an N-element array to synthesize a desirable far-field electro-magnetic radiation pattern. The approach will take into account polarization, sidelobe topography, dynamic range ratio in the aperture distribution, and the bandwidth for both linear and planar array pattern synthesis. The contractor will consider infinite and finite scatterers, and conduct a comparative study on the results obtained using near-field nulling and those obtained using direct synthesis in the presence of the scatterers.

14. SUBJECT TERMS

EOARD, Antennas, Electromagnetics, C3I

15. NUMBER OF PAGES

144

16. PRICE CODE

N/A

17. SECURITY CLASSIFICATION OF REPORT	18. SECURITY CLASSIFICATION OF THIS PAGE	19. SECURITY CLASSIFICATION OF ABSTRACT	20. LIMITATION OF ABSTRACT
UNCLASSIFIED	UNCLASSIFIED	UNCLASSIFIED	UL

FINAL REPORT OF THE CONTRACT: ANTENNA ARRAY PATTERN SYNTHESIS IN THE PRESENCE OF NEAR-ZONE SCATTERERS.

(Contract number F61708-98-W0018)

We have been studied and developed the following points that constitute the articles referenced below. In all of them it has been included the support of the European Office of the U.S. Aerospace Research and Development Board (EOARD) and the U.S. Air Force Office of Scientific research (AFOSR) in the acknowledgements:

a) Extension of the Olen-Compton method using the simulated annealing technique [1].
b) Optimization of the performance of antenna arrays in presence of defective elements [2,5].
c) Antenna array design taking into account the mutual coupling effects [3,4].
d) Far field null fixing in linear, planar and conformal arrays [5-7].
e) Synthesis of antenna arrays in presence of infinite scatters: Two-dimensional problem.
   e.1) Synthesis fixing nulls in near field [8].
   e.2) Direct synthesis [9].
f) Study of the extension of the previous methods [8,9] considering the presence of finite scatterers (3D problem) taking into account the polarization [10].
g) Phase-only synthesis of continuous linear apertures [11].
h) Pattern synthesis using orthogonal beams [12].
i) Matching of beam forming feeds [13].

[1] PATTERN SYNTHESIS OF ARRAY ANTENNAS WITH ARBITRARY ELEMENTS BY SIMULATED ANNEALING AND ADAPTIVE ARRAY THEORY.

ABSTRACT: A method to carry out the pattern synthesis of arbitrary array antennas is presented. This method uses the simulated annealing technique to calculate the power interferences described in the Olen-Compton method. Its application to a linear array of 16 unequally spaced non-identical elements and to a circular arc array of 25 axial dipoles is shown in order to illustrate its efficiency and accuracy.

Published in Microwave and Optical Technology Letters, Vol. 20, No. 1, pp. 48-50, Jan 1999.

Presented in the Spanish U.R.S.I. Symposium, Pamplona, pp. 521-522 Sept. 1998 (Spain).

[2] OPTIMIZATION OF THE PERFORMANCE OF ARRAYS WITH FAILED ELEMENTS USING THE SIMULATED ANNEALING TECHNIQUE

ABSTRACT: A method is described which optimizes the performance of antenna arrays with defective elements, by numerically finding a new excitation for the remaining ones. Two approaches for recovering the patterns have been investigated. In the first, new excitations are obtained by changing their amplitude distribution, whereas in the second, only the phase distribution is modified while keeping the original amplitudes. These optimum values for new excitations are calculated by the application of the simulated annealing technique. Examples for both sum and shaped beam patterns are presented to illustrate the optimal results obtained.

Published in Journal of Electromagnetic Waves and Applications, Vol. 12, pp. 1625-1637, 1998.

[3] REAL LINEAR ARRAY EXCITATIONS WITH NO EDGE BRIGHTENING FOR EFFICIENT SUM PATTERNS.

ABSTRACT: The paper reports the application of the simulated annealing optimization technique to the synthesis of linear array sum patterns by highly efficient real aperture distributions with no edge brightening.

Accepted for publication in the Microwave and Optical Technology Letters and will appear in the March 20, 1999 issue.

Presented in the Spanish U.R.S.I. Symposium, Pamplona (Spain), pp. 447-448 Sept. 1998.

[4] DESIGN OF EFFICIENT, EASILY FEED-MATCHED ARRAY ANTENNAS BY JOINT OPTIMIZATION OF EXCITATIONS AND ELEMENT GEOMETRY: PENCIL BEAM EXAMPLE

ABSTRACT: By using simulated annealing for simultaneous optimization of the geometries and excitations of the array elements, it is often possible to design array antennas that generate specified radiation power patterns, have elements with real active impedances, and are easily feed-matched. The example of a twelve-element pencil beam antenna fed by coaxial cables of practical dimensions with no additional circuitry is described.

Published in Electronics Letters, Vol. 34, No. 13, pp. 1280-1282, Jun. 1998.

Presented in JINA-98 Symposium, Nice (France), pp. 374-377 Nov. 1998.

[5] RECALCULATING LINEAR ARRAY ANTENNAS TO COMPENSATE FOR FAILED ELEMENTS WHILE MAINTAINING FIXED NULLS

ABSTRACT: A new technique for the synthesis of linear array antenna patterns is presented. This technique allows to fix nulls in prescribed directions, to simulate the presence of failed elements and to obtain power patterns when both situations occur at the same time. These patterns are synthesized by finding the optimal configuration of the array factor roots using the simulated annealing technique. Examples of fixing nulls and/or failed elements in both sum and flat-topped beam patterns are presented.

Published in Journal of Electromagnetic Waves and Applications, Vol. 13, pp. 397-412, 1999.

Submitted to the 1999 IEEE, AP-S International Symposium & URSI Radio Science Meeting.

[6] OPTIMAL COMPROMISE BETWEEN SUM AND DIFFERENCE PATTERNS WHILE FIXING QUASI-NULLS IN BOTH.

ABSTRACT: Methods previously developed for designing linear array monopulse antennas with relatively simple feed network requirements are extended to allow the suppression of jamming signals in both sum and difference modes.

Accepted for publication in the Journal of Electromagnetic Waves and Applications, and will appear in Vol. 13, pp. 655-664, 1999.

[7] PLACING QUASI-NULLS IN PLANAR AND CONFORMAL ARRAYS

ABSTRACT: We describe the use of the simulated annealing optimization method to introduce minimal modifications in the excitations and/or geometries of planar and circular arc antenna arrays so as to depress the radiation pattern in arbitrary directions while maintaining side lobe levels and beamwidth.

Accepted for publication in the Electromagnetics Journal.

Presented in the Spanish U.R.S.I Symposium, Pamplona (Spain), pp. 445-446, Sep. 1998.

[8] PATTERN SYNTHESIS OF ARRAY ANTENNAS WITH ADDITIONAL ISOLATION OF NEAR-FIELD ARBITRARY OBJECTS.

ABSTRACT: In this Letter we present a new technique to synthesize array antennas in presence of arbitrary obstacles in its near-field region. This technique allows to synthesize a prescribed far-field pattern trying to avoid the coupling with near-field obstacles through the constraint of minimizing the radiated power over the obstacle surface. Some results have been obtained showing that the obstacles are finally isolated from the array antenna radiation.

Published in Electronics Letters, Vol. 34, N° 16, pp. 1540-1542, August 1998.

[9] ANTENNA ARRAY PATTERN SYNTHESIS IN THE PRESENCE OF NEAR-ZONE SCATTERERS: TWO-DIMENSIONAL SCALAR CASE.

ABSTRACT: A new method for the array pattern synthesis in the presence of near-zone scatterers in the two-dimensional scalar case is presented. The synthesis is based on the minimization of an objective function using the simulated annealing technique. To take into account the effects of the scatterers the physical optics approximation is used. Examples for a 41-element linear array in presence of perfectly electric conducting cylinders are performed.

Accepted for publication in Microwave and Optical Technology Letters, and it will appear in the May 1999 issue.

[10] ANTENNA ARRAY PATTERN SYNTHESIS IN THE PRESENCE OF NEAR-ZONE SCATTERERS: THREE-DIMENSIONAL VECTOR CASE

ABSTRACT: A method for the array pattern synthesis in the presence of near-zone scatterers in the three-dimensional vector case is presented. The synthesis is based on the minimization of an objective function using the simulated annealing technique. In order to take into account the effects of the scatterers, the physical optics approximation is used. The polarization in both the incident and the scattered fields is also taken into account. Examples for a 10x10-element planar array of dipoles in the presence of a perfectly electric conducting cylinder are presented.

Submitted to Journal of Electromagnetic Waves and Applications.

Submitted to the 29th European Microwave Conference.

[11] PHASE-ONLY SYNTHESIS OF CONTINUOUS LINEAR APERTURE DISTRIBUTION PATTERNS WITH ASYMMETRIC SIDE LOBES

ABSTRACT: A method for synthesizing linear aperture distribution patterns with different side lobe levels (SLLs) on both sides of the main beam is proposed. This phase-only control method was applied to a Taylor distribution as well as to a uniform amplitude distribution and achieved differences in the SLL on both sides of the main beam as great as 23 dB, improving on a previous procedure that had achieved a gap of little more than 10 dB.

Published in Electronics Letters, Vol. 34 No. 20, pp., 1916-1917, October 1998.

[12] SHAPED POWER PATTERNS PRODUCED BY EQUISPACED LINEAR ARRAYS: OPTIMIZED SYNTHESIS USING ORTHOGONAL sin(Nx)/sin(x) BEAMS.

ABSTRACT: The major defects of the Woodward-Lawson method of shaped patterns synthesis (lack of control over side lobes and ripple, and high dynamic range ratios) can be overcome by perturbing the field samples weighting the component $\sin(Nx)/\sin(x)$ beams. If a real field is not necessary, further improvement (especially as regards dynamic range ratio) can be achieved by optimizing the phases of the coefficients of the component beams. These procedures are illustrated by linear arrays producing a symmetric flat-topped beam and a cosecant squared pattern.

Accepted for publication in the Journal of Electromagnetic Waves and Applications, and will appear in Vol. 13, pp. 985-992, 1999.

Submitted to the International Conference on Electromagnetics in advanced applications (ICEAA 99).

[13] MINIMISING THE VARIABILITY OF CHARACTERISTIC IMPEDANCES IN MULTISECTION QUARTER-WAVELENGTH TRANSFORMERS

ABSTRACT: The widely used first-order polynomial representation of the voltage reflection coefficient in multisection quarterwavelength transformers is assumed. The roots of this polynomial are displaced iteratively to obtain, through the simulated annealing technique, low variability between the characteristic impedances of adjacent transformers. Besides, for each problem configuration, the bandwidth is maintained close to its maximum possible value. An example is presented obtaining an important decrease in the characteristic impedances variability of the transformers.

Submitted to Electronics Letters

Submitted to the 7th International Symposium on Recent Advances in Microwave Technology.

MICROWAVE AND OPTICAL TECHNOLOGY LETTERS

VOLUME 20 / NUMBER 1 JANUARY 5 1999

A WILEY INTERSCIENCE PUBLICATION
John Wiley & Sons, Inc.

4. S. González García, I. Villó Pérez, R. Gómez Martín, B. García Olmedo, Extension of Berenger's PML to adapt bi-isotropic media, IEEE Microwave Guided Wave Lett (1998).
5. J. P. Berenger, A perfectly matched layer for the absorption of electromagnetic waves, J Comput Phys (1994), 185–200.
6. S. González García, T. Materdey Hung-Bao, R. Gómez Martín, and B. García Olmedo, On the application of finite methods in time domain to anisotropic dielectric waveguides, IEEE Trans Microwave Theory Tech 44 (1996), 2195–2206.

CCC 0895-2477/99

PATTERN SYNTHESIS OF ARRAY ANTENNAS WITH ARBITRARY ELEMENTS BY SIMULATED ANNEALING AND ADAPTIVE ARRAY THEORY

J. A. Rodríguez,[1] L. Landesa,[2] J. L. Rodríguez,[2] F. Obelleiro,[2] F. Ares,[1] and A. García-Pino[2]
[1] Departamento de Física Aplicada
Grupo de Sistemas Radiantes Facultade de Física
Universidade de Santiago de Compostela
15706 Santiago de Compostela, Spain
[2] Departamento de Tecnoloxías das Comunicacións
E.T.S.E. Telecomunicacións
Universidade de Vigo
36200 Vigo, Spain

Received 15 June 1998

ABSTRACT: *A method to carry out the pattern synthesis of arbitrary array antennas is presented. This method uses the simulated annealing technique to calculate the power interferences described in the Olen–Compton method. Its application to a linear array of 16 unequally spaced nonidentical elements and to a circular arc array of 25 axial dipoles is shown in order to illustrate its efficiency and accuracy.* © 1999 John Wiley & Sons, Inc. Microwave Opt Technol Lett 20: 48–50, 1999.

Key words: *adaptive theory; antenna array pattern synthesis*

1. INTRODUCTION

In recent years, most of the work in the pattern synthesis of array antennas has been focused on uniformly spaced arrays with isotropic elements [1]. In [2], Olen and Compton proposed a synthesis algorithm for arbitrary arrays (with different elements located in arbitrary positions) which is based on the adaptive array theory described in [3]. The method has some convergence problems since the adjustment for the interference power (namely, a parameter that controls the interference spectrum intentionally imposed to adjust the secondary lobe map) is more likely qualitative than quantitative. An improvement in the convergence of this method by means of the stability criterion of Routh–Hurwitz also has been presented in [4]. And a new extension of the method, based on a linear expansion of the gain near the interference levels, has been developed in [5]. The main drawback of the method is the lack of exhaustive control over every lateral lobe because those whose sidelobe level is lower than the desired one are not considered. As a consequence of that, a beam widening and gain reduction is caused. Furthermore, there is no control over other array parameters such as the excitation dynamic range and adjacent element on excitation ratio. In this paper, we present a method based on [5], but using a simulated annealing technique for the computation of interference levels. The main advantage is that this method allows an exhaustive and simultaneous control of lateral lobes and other significant array design parameters.

2. DESCRIPTION OF THE METHOD

Let us consider an array of N elements, where $\bar{r}_n$ is the position of the nth element ($n = 1, 2, \ldots, N$), $\hat{r}$ is the unit vector in the far-field observation direction. $f_n(\hat{r})$ is the radiation pattern of the nth element, and $W = [w_1, w_2, \ldots, w_N]^T$ are the excitations of the array elements. The radiation pattern can be expressed (in decibels) as

$$p(\hat{r}) = 20 \log|W^T \cdot U(\hat{r})| \tag{1}$$

where $U(\hat{r})$ is given by

$$U(\hat{r}) = \left[f_1(\hat{r}) e^{jk\bar{r}_1 \cdot \hat{r}}, f_2(\hat{r}) e^{jk\bar{r}_2 \cdot \hat{r}}, \ldots, f_N(\hat{r}) e^{jk\bar{r}_N \cdot \hat{r}} \right]^T. \tag{2}$$

The elements of the array are going to be used as those of an adaptive array. So, we assume that all of the elements are receiving a desired signal from the direction $\hat{r}_d$, M interference signals impinging on the antenna from directions $\hat{r}_m$ ($m = 1, 2, \ldots, M$), and uniform thermal noise. The amplitude level of the interference direction $\hat{r}_m$ is a positive magnitude denoted by ξ_m, all of them conforming to the so-called interference spectrum.

The theory of adaptive array establishes that the signal-to-interference-plus-noise power ratio (SINR) can be minimized by choosing optimal excitations w_n. In this synthesis method, an adequate selection of the interference levels will force the adaptive array technique to adjust a certain desired sidelobe level map which allows us to compensate the interference spectrum and to achieve the minimum SINR.

According to the theory of adaptive arrays [3], the optimum excitation coefficients obtained to maximize the ratio between the desired and the interference-plus-noise signals (SINR) are given by

$$W = \Phi^{-1} \cdot U^*(\hat{r}_d) \tag{3}$$

where Φ is a covariance matrix defined as

$$\Phi = I + \sum_{m=1}^{M} \xi_m U^*(\hat{r}_m) \cdot U^T(\hat{r}_m) \tag{4}$$

where I denotes the identity matrix, superscript (*) denotes the conjugate, and (T) the transpose.

The novelty of the proposed method consists in the selection of the interference levels. A cost function, which takes into account the sidelobe level of the patterns as well as other significant parameters of the array such as the dynamic range of excitations, is defined and minimized by a simulated annealing technique [6]. The cost function we have defined can be written as

$$C = c_1 \cdot \sum_{p=1}^{P} [SLL_{p,o} - SLL_{p,d}]^2 + c_2 \cdot \left| \frac{w_{\max}}{w_{\min}} \right| \tag{5}$$

where $SLL_{p,o}$ is the obtained level of the pth lobe, $SLL_{p,d}$ is the desired one. $|w_{\max}/w_{\min}|$ is the excitation dynamic range, and c_i are weights to control the importance given to each term of (5) in the optimization procedure. The potentiality of the method is that any parameter of interest (directivity,

beam width, etc.) can be easily considered by including it in the cost function.

3. EXAMPLE DESIGNS

3.1 Linear Array with Nonuniformly Spaced Elements. In order to illustrate the method, we have synthesized an array of 16 dipoles, placed along the z-axis at distances d_n, with different lengths l_n and different orientations (denoted by the angle τ_n between the dipole and the array axis). The U vector for the nth element is

$$U_n(\theta) = \frac{\cos[\pi l_n \sin(\theta + \tau_n)] - \cos(\pi l_n)}{\cos(\theta + \tau_n)} \cdot \exp\left[j2\pi \left(\sum_{i=0}^{n-1} d_i \right) \sin\theta \right]. \quad (6)$$

The desired pattern has a main beam and two adjacent lobes with a level of -35 dB. A level of -20 dB is required for the rest of the lobes. A discrete spectrum of 58 interference directions is distributed across the sidelobe region. By minimizing the cost function, a set of interference levels is adjusted; then the excitations are computed by (3) and (4). Table 1 shows the geometric parameters of the array elements and their corresponding optimal excitations. Figure 1 shows the far-field pattern computed by using Eqs. (1) and (2), demonstrating the efficiency of the proposed technique.

3.2 Circular Arc Array. Let us consider an array antenna of N dipoles in the z-direction, uniformly distributed on a perfectly conducting cylinder, conforming an arc of radius R between angles $-\phi_0$ and ϕ_0 as shown in Figure 2. In our case, the selected values are $N = 25$, $R = 5.73\lambda$, and $\phi_0 = 60°$ to produce a separation between adjacent elements of 0.5λ. We have introduced 72 interference directions uniformly distributed for $5° \le |\phi| \le 180°$. In this case, we want to synthesize an asymmetric pattern with -40 dB sidelobes on one side of the main lobe and a tapered-sidelobe structure from -25 to -35 dB on the other side. The factor $|w_{max}/w_{min}|$ has to be minimized.

TABLE 1 Parameters of the Linear Array with 16 Arbitrary Dipoles and Element Excitations Obtained After the Optimization

n	l_n	τ_n	d_n	w_n
1	0.25	0.0	0.50	$0.093 \cdot e^{j(+0.054)}$
2	0.25	0.5	0.50	$0.031 \cdot e^{j(-0.569)}$
3	0.24	5.0	0.55	$0.106 \cdot e^{j(+0.020)}$
4	0.20	−32	0.54	$0.086 \cdot e^{j(+0.365)}$
5	0.26	−3.2	0.60	$0.184 \cdot e^{j(-0.083)}$
6	0.27	10	0.45	$0.122 \cdot e^{j(+0.097)}$
7	0.23	1.0	0.46	$0.190 \cdot e^{j(-0060)}$
8	0.24	0.0	0.50	$0.129 \cdot e^{j(-0.332)}$
9	0.25	0.0	0.50	$0.218 \cdot e^{j(+0.222)}$
10	0.21	7.0	0.51	$0.155 \cdot e^{j(-0.286)}$
11	0.28	6.0	0.47	$0.177 \cdot e^{j(+0.181)}$
12	0.30	4.4	0.48	$0.071 \cdot e^{j(-0.573)}$
13	0.29	0.0	0.61	$0.135 \cdot e^{j(+0.199)}$
14	0.19	1.0	0.57	$0.151 \cdot e^{j(-0.186)}$
15	0.22	−2.1	0.65	$0.062 \cdot e^{j(+0.255)}$
16	0.22	3.0	—	$0.153 \cdot e^{j(-0.072)}$

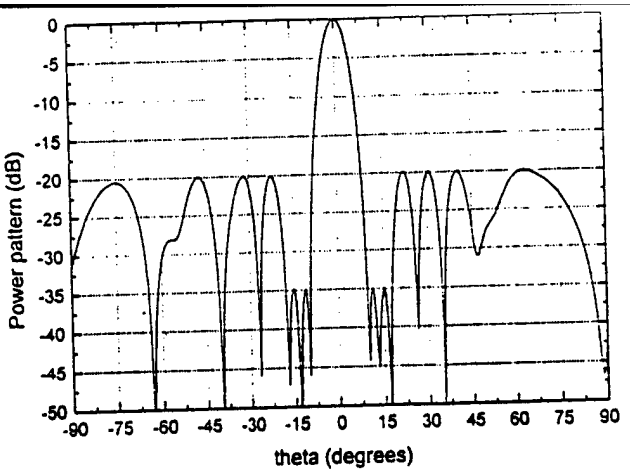

Figure 1 Radiation pattern of the synthesized linear array with 16 arbitrary dipoles

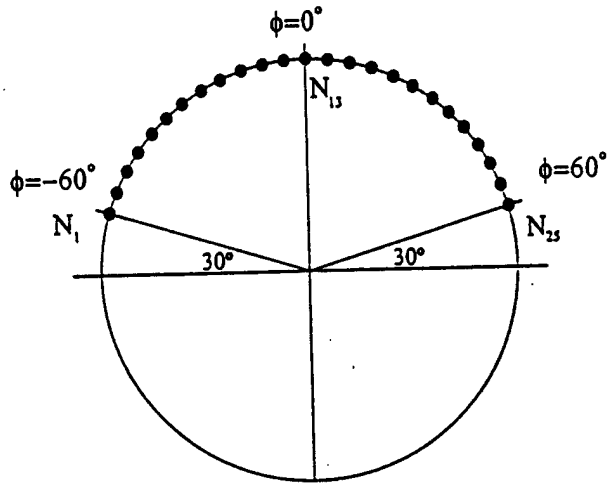

Figure 2 Geometry of the circular arc array

The power pattern of this array can be expressed as

$$F(\phi) = \sum_{n=1}^{N} I_n e^{j\alpha_n} e^{jkR\cos(\phi - \phi_n)} FE(\phi - \phi_n) \quad (7)$$

where I_n and a_n are the amplitude and phase, respectively, of the excitation of the nth element, and $FE(\phi)$ is the pattern of the element in the XY-plane. In conformal arrays, this term is of great importance because each element is independently oriented. The element pattern used in this paper is that proposed by Jiao et al. in [7], based upon results presented by Herper, Hessel, and Tomasic in [8, 9] for a cylindrical array of axial dipoles on a perfectly conducting cylinder. The FE factor for a separation of 0.5λ is given by

$$FE(\theta, \phi) = \tfrac{1}{3}\sin\theta[1 + 2\max(\cos\phi, -1/2)] \quad (8)$$

where the θ-dependence is ignored in our case because we only consider pattern synthesis in the XY-plane.

Figure 3 shows the obtained array pattern, again showing the good performance achieved. Table 2 shows the excitation coefficients of this array, whose $|w_{max}/w_{min}|$ has been minimized to a value of 8.

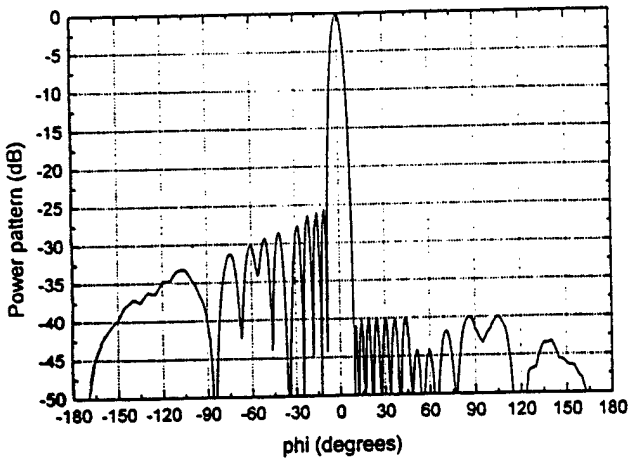

Figure 3 Radiation pattern of the synthesized circular arc array of 25 axial dipoles

TABLE 2 Excitations Obtained for the Synthesis of the Circular Arc Array of 25 Axial Dipoles

n	w_n	n	w_n
1	$0.264 \cdot e^{j(+0.242)}$	14	$0.840 \cdot e^{j(+1.886)}$
2	$0.180 \cdot e^{j(-2.141)}$	15	$0.766 \cdot e^{j(+2.296)}$
3	$0.220 \cdot e^{j(+1.400)}$	16	$0.698 \cdot e^{j(+2.983)}$
4	$0.238 \cdot e^{j(-0.395)}$	17	$0.604 \cdot e^{j(+3.928)}$
5	$0.311 \cdot e^{j(+3.844)}$	18	$0.507 \cdot e^{j(-1.200)}$
6	$0.417 \cdot e^{j(+1.783)}$	19	$0.450 \cdot e^{j(+0.247)}$
7	$0.486 \cdot e^{j(+0.117)}$	20	$0.377 \cdot e^{j(+1.985)}$
8	$0.595 \cdot e^{j(-1.227)}$	21	$0.296 \cdot e^{j(+4.001)}$
9	$0.629 \cdot e^{j(+3.831)}$	22	$0.209 \cdot e^{j(-0.034)}$
10	$0.762 \cdot e^{j(+2.900)}$	23	$0.121 \cdot e^{j(+2.315)}$
11	$0.826 \cdot e^{j(+2.266)}$	24	$0.103 \cdot e^{j(+4.633)}$
12	$0.797 \cdot e^{j(+1.889)}$	25	$0.103 \cdot e^{j(+1.245)}$
13	$0.844 \cdot e^{j(+1.685)}$		

4. CONCLUSIONS

A novel technique for synthesizing arrays by using the adaptive array theory and simulated annealing technique has been presented. The method is based on the optimum selection of a set of interference levels which are combined with an adaptive array scheme to minimize the signal-to-interference-plus-noise power ratio, allowing us to obtain the desired sidelobe map. The potentiality of the method is that it is able to take into account any significant parameter of the array such as the excitation dynamic range, gain, beam width, etc.

ACKNOWLEDGMENT

This work was supported by the U.S. European Office of Aerospace Research and Development (EOARD) and the U.S. Air Force Office of Scientific Research (AFOSR), and by the Spanish Comision Interministerial de Ciencla y Tecnología (CICYT) Project TIC97-0821-C02-01.

REFERENCES

1. R.C. Hansen, Phased array antennas, John Wiley & Sons, New York, 1998.
2. C.A. Olen and R.T. Compton, A numerical pattern synthesis algorithm for arrays, IEEE Trans Antennas Propagat 38 (1990), 1666–1676.
3. R.T. Compton, Adaptive antennas—Concepts and performance, Prentice-Hall, Englewood Cilffs, NJ, 1988.
4. W.A. Swart and J.C. Olivier, Numerical synthesis of arbitrary discrete arrays, IEEE Trans Antennas Propagat 41 (1993), 1171–1174.
5. X. Shi, K. Yoo, J. Park, and H. Lee, Pencil-beam pattern synthesis for arbitrary arrays, Electron Lett 33 (1997), 1007–1008.
6. W.H. Press, S.A. Teukolsky, W.T. Vetterling, and B.P. Flannery, Numericaly recipes, 2nd ed., Cambridge University Press, Cambridge, England, 1992, pp. 444–455.
7. Y.C. Jiao, W.Y. Wei, L.W. Huang, and H.S. Wu, A new low-side-lobe pattern syntheis technique for conformal arrays, IEEE Trans Antennas Propagat 41 (1993), 824–831.
8. J.C. Herper, A. Hessel, and B. Tomasic, Element pattern of an axial dipole in a cylindrical phased array, Part I: Theory, IEEE Trans Antennas Propagat AP-33 (1985), 259–272.
9. J.C. Herper, A. Hessel, and B. Tomasic, Element pattern of an axial dipole in a cylindrical phased array, Part II: Element design and experiments, IEEE Trans Antennas Propagat AP-33 (1985), 273–278.

CCC 0895-2477/99

DESIGN CRITERIA FOR OPTICAL RECEIVERS IN BROADBAND OPTICAL SYSTEMS

Franco Curti,[1] Pasquale Tommasino,[2] and Alessandro Trifiletti[2]
[1] Fondazione Ugo Bordoni
I-00142 Rome, Italy
[2] Dipartimento di Ingegneria Elettronica
Università "La Sapienza"
I-00184 Rome, Italy

Received 20 May 1998

ABSTRACT: *A design criterion for the optimization of bandpass optical receivers based on lossless matching networks has been established. A minimum value for the input-equivalent noise current under the constraint of fixed transimpedance gain and an expression for detuning penalty evaluation with respect to the optimum have been found.* © 1999 John Wiley & Sons, Inc. Microwave Opt Technol Lett 20: 50–53, 1999.

Key words: *optical receivers; noise figure: matching networks*

1. INTRODUCTION

Bandpass optical systems are becoming more and more important owing to the need for bandpass low-loss transmission channels (i.e., CATV AM-SCM systems, microwave links for radar systems). In these applications, the bandwidth requirements are quite moderate with respect to the capability of the optical fiber, but the system designer has to take into account signal degradations produced along the link: the RIN of the transmitting laser, nonlinear distorsions in multioctave and SCM systems, fiber attenuation and dispersion, shot noise, and preamplifier noise figure [1–3]. The noise influence and intermodulation products power are inversely related by the choice of the optical modulation index [3], and the system design is strongly affected by this tradeoff. An improvement of receiver sensitivity allows us to achieve in a simpler way system requirements in terms of one or more of the following parameters: 1) maximum number of users connected to a single node in a star architecture, 2) minimum required transmitted optical power, and 3) maximum length of the single portion of the link.

IBERDROLA
INSTITUTO
TECNOLOGICO

Síntesis de diagramas de radiación en arrays lineales con elementos radiantes arbitrarios

J. A. Rodríguez[†], L. Landesa[††], F. Ares Pena[†], A. García Pino[††]

[†] Departamento de Física Aplicada, Grupo de Sistemas Radiantes
Facultade de Física, Universidade de Santiago de Compostela
15706 Santiago de Compostela
E-mail: faares@usc.es

[††] Departamento de Tecnoloxías das Comunicacións
E.T.S.E. Telecomunicacións, Universidade de Vigo, 36200 Vigo
E-mail: landesa@tsc.uvigo.es

Abstract: A method of pattern synthesis of arbitrary linear arrays is presented. This method uses the simulated annealing technique to calculate the power interferences in the Olen-Compton method. Application to a linear array of 16 unequally spaced non-identical elements is shown.

1. Introducción

El problema de la síntesis de patrones de radiación ha tenido un gran interés en los últimos años, pero la mayoría de los trabajos se centran en arrays lineales con elementos isotrópicos y equiespaciados. De entre éstos, cabe destacar el método de Orchard-Elliott [1]. Olen y Compton [2] propusieron un algoritmo de síntesis que, utilizando la teoría de arrays adaptativos [3], permitía sintetizar arrays con elementos distintos y dispuestos en posiciones arbitrarias. El mayor problema de este método radica en el hecho de que el ajuste del parámetro que mide los niveles de interferencia necesarios para el control de la topografía de lóbulos de los diagramas de radiación se realiza mediante prueba y error, lo que conlleva grandes dificultades a la hora de conseguir que el algoritmo converja. Posteriormente, se introdujo una extensión de dicho algoritmo que, basada en el criterio de estabilidad de Routh-Hurwitz mejoraba la convergencia [4]. En otro trabajo, se consiguió mejorar los resultados obtenidos mediante un desarrollo lineal de la ganancia en torno a los niveles de interferencia. En dicho método, dichos niveles se calculan resolviendo un sistema de ecuaciones lineales, lo que le confiere una gran velocidad de convergencia [5]. Sin embargo, dicho método no permite tener un control exhaustivo sobre cada uno de los lóbulos laterales, ya que, con el fin de asegurar la convergencia, se descartan aquellos lóbulos cuyo nivel es inferior al deseado. Esto provoca un aumento del ancho de haz que conlleva una pérdida en la ganancia. Además, dicho método no tiene control sobre otros parámetros del array, como son el rango dinámico o la variabilidad de las excitaciones entre elementos colindantes. En este trabajo se presenta un método, basado en [5] pero que utiliza la técnica de "simulated annealing" para el cálculo de los niveles de interferencia. El método permite tener un control exhaustivo sobre los lóbulos del diagrama de radiación así como otros parámetros de interés en el diseño.

2. Descripción del método

Considérese un array de N elementos. Sea $\hat{\mathbf{r}}_n$ el vector de posición del elemento n-ésimo (n=1, 2,.., N), $\hat{\mathbf{r}}$ el vector unitario en la dirección de un punto en campo lejano, $f_n(\hat{\mathbf{r}})$ el diagrama del elemento n-ésimo y $\mathbf{W}=[w_1, w_2,..., w_N]^T$ el vector con las excitaciones de cada elemento radiante. Entonces, el vector director del array viene dado por:

$$\mathbf{U}(\hat{\mathbf{r}})=[f_1(\hat{\mathbf{r}})\, e^{jk\mathbf{r}_1\cdot\hat{\mathbf{r}}}, f_2(\hat{\mathbf{r}})\, e^{jk\mathbf{r}_2\cdot\hat{\mathbf{r}}},..., f_N(\hat{\mathbf{r}})\, e^{jk\mathbf{r}_N\cdot\hat{\mathbf{r}}}]^T \quad (1)$$

mientras que el diagrama de radiación, expresado en dB's, viene dado por la siguiente expresión:

$$p(\hat{\mathbf{r}})=20\log|\mathbf{W}^T\mathbf{U}(\hat{\mathbf{r}})| \quad (2)$$

Supóngase que el array es adaptativo y que las señales recibidas por los elementos incluyen una señal deseada procedente de la dirección $-\hat{\mathbf{r}}_d$, M señales de interferencia, en ciertas direcciones denotadas por $-\hat{\mathbf{r}}_m$ (m=1, 2, ..., M), y ruido térmico de igual magnitud para todos los elementos. De acuerdo con la teoría de antenas adaptativas [3], para maximizar la razón de la señal deseada frente a las señales de interferencia y ruido (SINR), las excitaciones óptimas deben verificar la siguiente expresión:

$$\mathbf{W}=\Phi^{-1}\,\mathbf{U}^*(\hat{\mathbf{r}}_d) \quad (3)$$

en donde la matriz de covarianza se calcula mediante la siguiente expresión:

$$\Phi=\mathbf{I}+\sum_{m=1}^{M}\xi_m\,\mathbf{U}^*(\hat{\mathbf{r}}_m)\mathbf{U}^T(\hat{\mathbf{r}}_m) \quad (4)$$

en donde ξ_m es el nivel de la interferencia m-ésima, que debe ser positiva. Se observa que, ajustando dichos niveles, se modifica $\mathbf{W}$ y con ello el diagrama de radiación adaptado. Estos niveles se calculan minimizando una función de costo que tiene en cuenta el nivel de lóbulos laterales de dicho diagrama, así como otros parámetros de interés en la optimización.

Esta función viene dada por la siguiente expresión

$$C=c_1\cdot\sum_{i=1}^{P}[SLL_{i,o}-SLL_{i,d}]^2+c_2\cdot|w_{max}/w_{min}| \qquad (5)$$

en donde $SLL_{i,o}$ y $SLL_{i,d}$ denotan el nivel en potencia del lóbulo i-ésimo obtenido y deseado respectivamente, $|w_{max}/w_{min}|$ es el rango dinámico de las excitaciones, mientras que c_i son los factores de peso que permiten darle más importancia a ciertos parámetros en la optimización. Esta función es minimizada mediante la técnica de "simulated annealing", la cual permite optimizar cualquier parámetro de interés (directividad, ancho de haz, etc.,) sin más que incluirlo en la función de costo.

3. Ejemplo de diseño

Para ilustrar el método se ha utilizado un array lineal de 16 elementos distintos no equiespaciados. El vector director del elemento n-ésimo viene dado por

$$U_n(\theta)=\frac{\cos[\pi l_n \sin(\theta+\tau_n)]-\cos(\pi l_n)}{\cos(\theta+\tau_n)}\times \exp\left(j2\pi\sum_{i=0}^{n-1}d_i\sin(\theta)\right) \qquad (6)$$

en donde θ es el ángulo medido desde el "boresight" del array, l_n es el tamaño del dipolo n-ésimo expresado en longitudes de onda, τ_n es el ángulo que forma éste con el eje del array (en grados) y d_n es su espaciado también en longitudes de onda. Los valores que se han utilizado se muestran en la tabla I (d_0=0).

Se desea sintetizar un diagrama de tipo suma con los dos lóbulos interiores a cada lado del haz principal a un nivel de -35 dB y el resto a -20 dB. Para este propósito, se ha utilizado un total de 58 interferencias distribuidas sobre la región de lóbulos laterales del diagrama de radiación. Tras la minimización de la función de costo se obtienen los niveles ξ_j óptimos de cada una de ellas que más se ajustan a las especificaciones del diseño. Las excitaciones asociadas se calculan utilizando las expresiones (3-4) y se muestran en la tabla I (con el argumento expresado en radianes). Finalmente, el diagrama de radiación se muestra en la fig. 1.

n	l_n	τ_n	d_n	w_n
1	0.25	0.0	0.50	$0.093\cdot e^{j(+0.054)}$
2	0.25	0.5	0.50	$0.031\cdot e^{j(-0.569)}$
3	0.24	5.0	0.55	$0.106\cdot e^{j(+0.020)}$
4	0.20	-32	0.54	$0.086\cdot e^{j(+0.365)}$
5	0.26	-3.2	0.60	$0.184\cdot e^{j(-0.083)}$
6	0.27	10	0.45	$0.122\cdot e^{j(+0.097)}$
7	0.23	1.0	0.46	$0.190\cdot e^{j(+0.060)}$
8	0.24	0.0	0.50	$0.129\cdot e^{j(-0.332)}$
9	0.25	0.0	0.50	$0.218\cdot e^{j(+0.222)}$
10	0.21	7.0	0.51	$0.155\cdot e^{j(-0.286)}$
11	0.28	6.0	0.47	$0.177\cdot e^{j(+0.181)}$
12	0.30	4.4	0.48	$0.071\cdot e^{j(-0.573)}$
13	0.29	0.0	0.61	$0.135\cdot e^{j(+0.199)}$
14	0.19	1.0	0.57	$0.151\cdot e^{j(-0.186)}$
15	0.22	-2.1	0.65	$0.062\cdot e^{j(+0.255)}$
16	0.22	3.0	-	$0.153\cdot e^{j(-0.072)}$

Tabla I. Parámetros del array y excitaciones obtenidas en la síntesis.

4. Agradecimientos

Los autores quieren agradecer la ayuda económica ofrecida por la European Office of Aerospace Research and Development (EOARD) y la Air Force Office of Scientific Research (AFOSR).

Referencias:

[1] H. J. Orchard, R. S. Elliott, and G. J. Stern, "Optimising the synthesis of shaped beam antenna patterns", *Proc. Inst. Elec. Eng.*, vol. 132, part H, pp. 62-68, Feb. 1985.

[2] C. A. Olen, and R. T. Compton, "A numerical pattern synthesis algorithm for arrays", *IEEE Trans.*, AP-38, Nº10, pp. 1666-1676, 1990.

[3] R. T. Compton, "Adaptive antennas - concepts and performance" (Prentice Hall, 1988), Chap. 2.

[4] W. A. Swart, and J. C. Olivier, "Numerical Synthesis of Arbitrary Discrete Arrays", *IEEE Trans.*, Vol. 41, Nº 8, pp. 1171-1174, Aug. 1993.

[5] X. Shi, K. Yoo, J. Park, and H. Lee, "Pencil-beam pattern synthesis for arbitrary arrays", *Electronics Letters*, Vol. 33, Nº 12, pp. 1007-1008, June 1997.

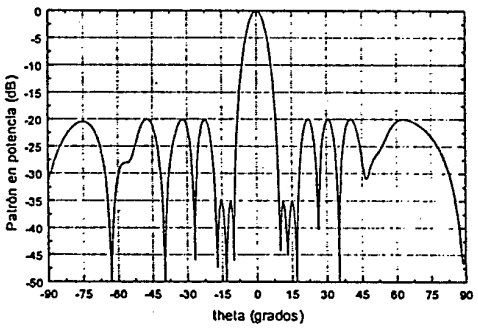

Fig. 1. Diagrama de radiación obtenido.

Journal of Electromagnetic Waves and Applications, Vol. 12, 1625–1637, 1998

OPTIMIZATION OF THE PERFORMANCE OF ARRAYS WITH FAILED ELEMENTS USING THE SIMULATED ANNEALING TECHNIQUE

J. A. Rodriguez and F. Ares

Grupo de Sistemas Radiantes,
Departamento de Fisica Aplicada, Facultad de Fisica
Universidad de Santiago de Compostela,
15706 Santiago de Compostela, Spain.

Abstract–A method is described which optimizes the performance of antenna arrays with defective elements, by numerically finding a new excitation for the remaining ones. Two approaches for recovering the pattems have been investigated. In the first, new excitations are obtained by changing their amplitude distribution, whereas in the second, only the phase distribution is modified while keeping the original amplitudes. These optimum values for new excitations are calculated by the application of the simulated annealing technique. Examples for both sum and shaped beam patterns are presented to illustrate the optimal results obtained.

1. INTRODUCTION

In antenna arrays, element failures destroy symmetry and cause sharp variations in the field intensity across the array aperture, increasing the sidelobe level of the power pattern. Recently there has been an increased interest in developing methods to improve the patterns of arrays in the presence of failed or partially failed elements. A recent work replaces the signals from failed elements in a digitally beamformed receive array [1] . The method is restricted for receive and is only applied to linear arrays. Another approach uses neural networks to produce a new array transfer function and offers advantages in direction finding in a single signal environment [2]. The array failure correction has also been performed by means of a quadratic optimization to achieve a suboptimum beam pattern closely matching the original desired specification [3]. In addition, there are several resynthesis methods based on calculating a new set of excitations for the remaining elements of the array. These excitations are obtained by using a genetic algorithm to

minimize a given cost function [4] or via a conjugate gradient method [5]. Although these resynthesis methods are the only ones appropriate for transmitting, they require to modify both the amplitude and phase distribution of the aperture, which may increase the hardware complexity. The advent of low-power solid-state microwave amplifiers has stimulated interest in phase-only antenna pattern synthesis in recent years, because it is easier and less expensive to modify dynamically the phase of an RF-signal, rather than its power level [6, 7]. Frey and Elliott, have shown that it is possible, for a fixed amplitude distribution, to obtain patterns with asymmetric sidelobes (with respect to the main beam) by phase-only changes [8].

In this paper, we have used the simulated annealing technique [9], to minimize by amplitude-only synthesis or phase-only changes a cost function that is the square of the difference between the obtained and desired sidelobe levels in a set of φ-cuts for the patterns of planar arrays with failed elements. In this way the technique performs an improvement of the degraded pattern in terms of the sidelobe level. Throughout this paper, the elements are assumed to be completely failed, which is the most useful and interesting case since known errors can be quite easily corrected [1]. The main advantage of using the simulated annealing technique, is to eliminate the possibility of getting the cost function stuck in local minima, one of the main problems of the conventional gradient-based methods. Examples using a 10×10 rectangular grid, circular boundary planar array with three elements failures are presented for sum patterns. We also show results relating to shaped-beam patterns using a 16×16 rectangular grid, circular boundary planar array with two defective elements, which are specially difficult to reoptimize since such distributions exhibit more variability than those associated with sum and difference patterns. In fact, in the previous literature, there are no works of failure correction which show results of shaped-beam patterns.

2. DESCRIPTION OF THE METHOD

The pattern in the far field for a planar array of N isotropic elements laying on the XY-plane, with an arbitrary grid and boundary is given by:

$$F(\theta, \phi) = \sum_{n=1}^{N} I_n \exp(jk \sin\theta[x_n \cos\phi + y_n \sin\phi]) \tag{1}$$

where (x_n, y_n) are the positions of the radiating elements and $I_n = A_n \exp(j\alpha_n)$ their complex excitations.

For computing convenience it is useful to express (1) as follows: $F(p)$ represents $F(\theta_{rs}, \phi_s)$ where θ_{rs} is a particular value of θ in the cut ϕ_s. In

a similar way, V_g represents the exponential factor $\exp(jk\sin\theta[x_n\cos\phi + y_n\sin\phi])$. Assigning the index g to a specific value of n and p to the (θ_{rs},ϕ_s) direction we obtain:

$$F(p) = \sum_g I_g V_g(p) \tag{2}$$

$G(p)$, the power in dB, is defined using the relation:

$$G(p) = 10\ \log_{10}[F(p)]^2 \tag{3}$$

The cost function C is defined as the sum of the square of the differences between the actual pattern $G(p)$ and the desired pattern $D(p)$:

$$C = \sum_{p=1}^{p_0}[G(p) - D(p)]^2 = \sum_{p=1}^{p_0}[E(p)]^2 \tag{4}$$

where p_0 is the number of points considered. The cost function is always positive and depends on a finite number of variables (planar array excitations). The minimization process applied to the cost function by changing their variables is equivalent to improve the pattern. For the case of amplitude-only synthesis, the amplitudes of non-defective elements are used as variables, and given by $A_g = A_g^o + \delta A_g$. Phase-only changes are accomplished changing the phase variables of non-defective elements as given by $\alpha_g = \alpha_g^o + \delta\alpha_g$, keeping the amplitudes constant. In other words, the proximity of the actual pattern to the desired one is measured by the numerical value of a cost function. The minimization of this function is performed by means of the simulated annealing method [9]. Using this method, it is possible to include in the cost function some other parameters of interest, such as directivity, dynamic range $|A_{\max}/A_{\min}|$ for amplitude-only synthesis or $|\alpha_{\max} - \alpha_{\min}|$ for phase-only changes, because it is not necessary to know its dependence with the cost function as it happens in gradient based methods.

3. SIMULATED ANNEALING: AN INTRODUCTION

The simulated annealing technique is based on an analogy with thermodynamics, specifically on how the slow cooling of a system allows it to find a minimum energy state. The method is suitable for optimization problems of large scale, especially ones where a desired global extremum is hidden among many, poorer, local extrema. One of the main advantages of the algorithm is its easy implementation and use. Unlike gradient-based methods, this

technique only requires to know the function values and not its derivatives. This means that any design parameter can be optimized by only including it in the cost function. The algorithm always accepts a downhill step, but sometimes accepts an uphill one. In this way, the algorithm can avoid get stuck in local minima, one of the main problems of the gradient-based methods. The probability of an uphill excursion depends on a control parameter T (analog of temperature) and the values of the cost function E (analog of energy).

The flowchart of the simulated annealing technique is shown in Figure 1. The algorithm begins with an encoding of the variables of the problem. Then, the initial temperature is fixed as well as its decrement in each iteration and the initial solution for the variables. After that, this configuration is evaluated, being E_1, the cost function value obtained.

In the next step, a random perturbation in any of the variables is performed, obtaining a new configuration with a cost value equal to E_2. The probability of an energy state E is given by the so-called Boltzmann distribution:

$$\text{Prob}(E) \sim \exp(-E/kT) \tag{5}$$

where k is the Bolzmann's constant. The probability p of choosing the new configuration is then given by:

$$p \sim \exp[-(E_2 - E_1)/kT] \tag{6}$$

This implies that if the cost function decreases, E_2 will be lower that E_1, and therefore p will be greater than 1, which means that the transition is accepted. It is obvious that if the system only accepts those transitions verifying this condition (that is, accepting only downhill steps), the algorithm could easy get stuck in a local minima. The strategy employed to avoid this consist on accepting those transitions whose probability p is greater than a random value x, calculated in the range (0, 1). In this way, the algorithm accepts not only all the downhill steps but some uphill ones too, trying to avoid local minima.

If the new configuration is rejected, a new random perturbation is introduced and the process above described is repeated. If not, the temperature is slightly decreased (in a small amount which guarantees a slow cooling of the system) and the process is iterated, generating a new random configuration. The process ends when the temperature reaches a previously fixed value.

4. APPLICATION

We have synthesized a sum pattern using a 10×10 element planar array

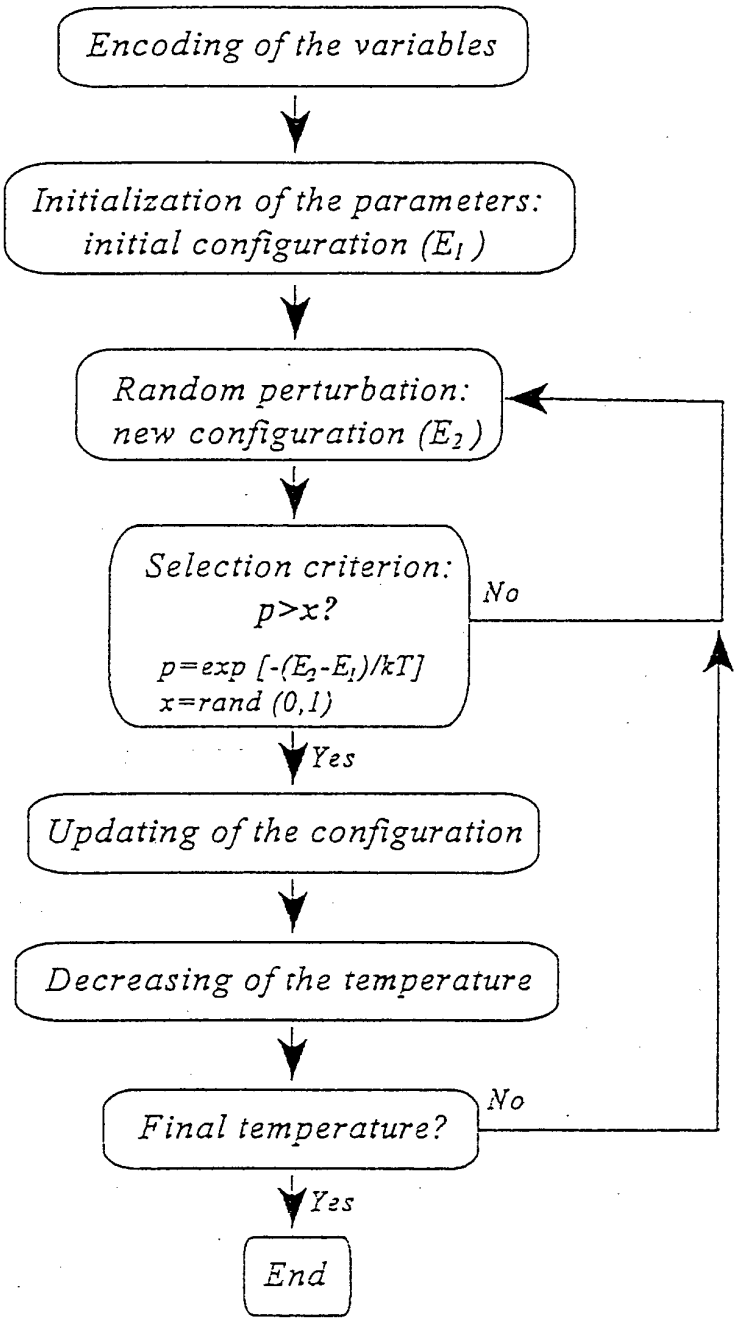

Figure 1. Flowchart of the simulated annealing algorithm.

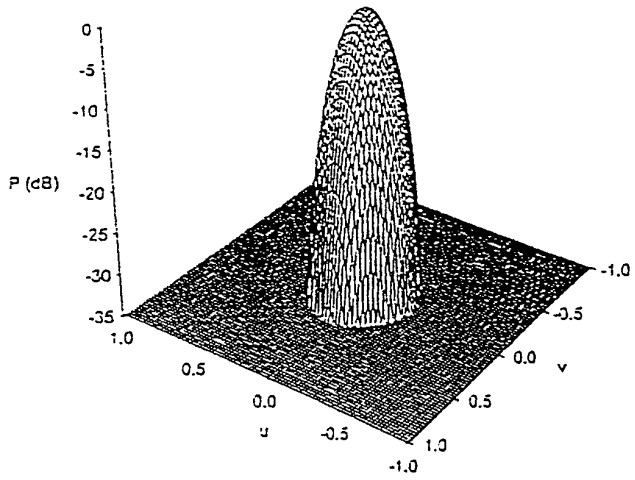

Figure 2. Sum power pattern obtained by sampling a circular Taylor distribution, SLL= -35 dB and $\overline{n} = \hat{6}$.

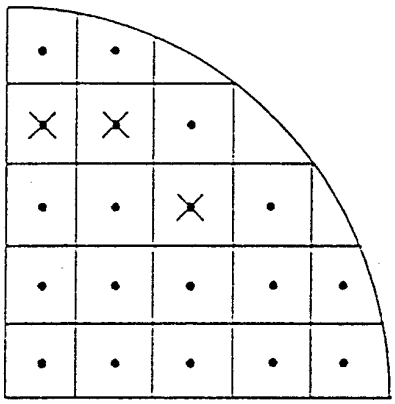

Figure 3. Location of the failed elements in the 10×10 element planar array.

in a rectangular grid and circular boundary with $\lambda/2$ interelement spacing. The corresponding aperture distribution was obtained by sampling a circular Taylor distribution [10] with a sidelobe level of -35 dB and $\overline{n} = 6$. The sum power pattern without element failures has a peak sidelobe level of -34.5 dB and is plotted in Figure 2, where $u = \sin\theta \cdot \cos\phi$ and $v = \sin\theta \cdot \sin\phi$.

Without loss of generality, let us assume that the array has three defective elements located in the first quadrant, as is shown in Figure 3. When these elements fail, the peak sidelobe level rises up to -29.3 dB. This degraded pattern is plotted in Figure 4.

In the first case, the optimization of the pattern has been performed calculating a new set of amplitudes for the non-defective elements. Hence, the number of unknowns to be solved by the simulated annealing technique is 73. The obtained pattern has a peak sidelobe level of -34.8 dB and is shown in Figure 5. The results indicate that it was possible to reduce the sidelobe level of the array with failed elements down to the design level. However, as it happened in [5], this reduction in the sidelobe level produces a corresponding increase in the beamwidth of the pattern, that has an elliptical cross section, yielding a drop in gain. This result could be improved by including the directivity in the cost function, at the expense of substantially increasing of the computational time.

In a second approach, a excitation phase for each non-defective element is calculated while keeping the original amplitude distribution. The obtained pattern using this technique has a peak sidelobe level of -30.5 dB and is shown in Figure 6. This yields an improvement of only 1.2 dB over the degraded pattern, which may not justify the use of the phase distribution required. However, it has been found that these results can be substantially improved if we fix asymmetric lobes in the optimization. This allows to recover almost the original sidelobe level in one half of the pattern at the expense of increasing the sidelobes in the other half. Using this asymmetry in our example, it was possible to reduce the peak sidelobe level to -33.5 dB in the ϕ-range $(0°–180°)$, since the desired level was -35 dB, and -27.3 dB in the ϕ-range $(180°–360°)$, in order to reach -28 dB. The obtained pattern is shown in Figure 7. Note that the pattern does not show a significant increase in the beamwidth, unlike the amplitude only synthesis.

The technique can be also applied to shaped beam patterns at only minor changes. In this case, the cost function (4) must include a new term to take into account the ripple level of the shaped region. To obtain optimal results, each ripple peak must be individually controlled as well as the peak sidelobe level. In our example, we have used a 16×16 element planar array, with rectangular grid, circular boundary, and a $\lambda/2$ interelement spacing. The

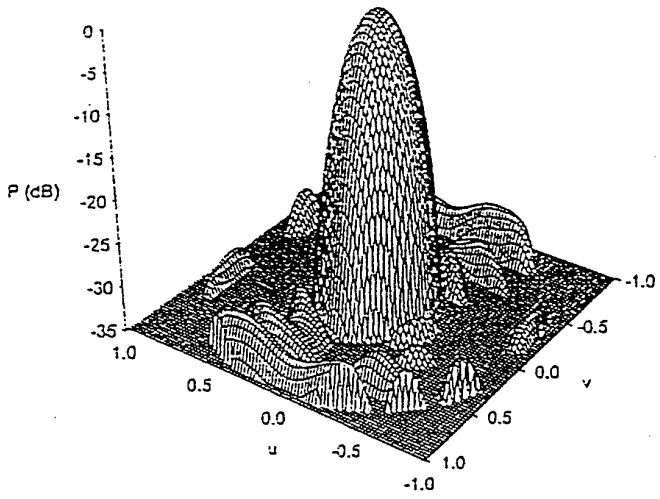

Figure 4. Sum power pattern with three element failures.

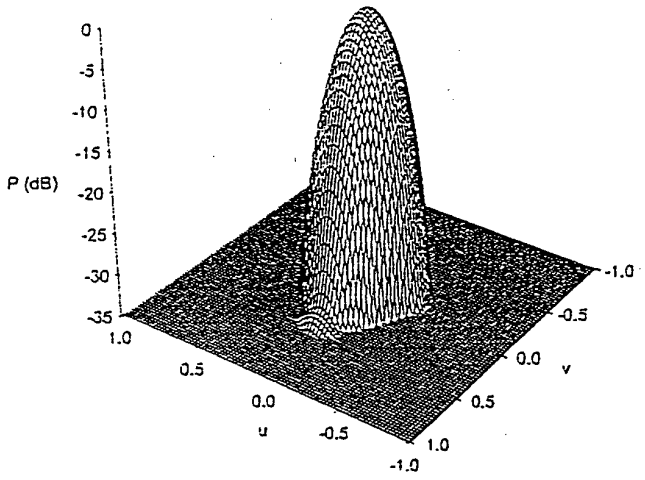

Figure 5. Synthesized sum power pattern with three element failures using amplitude-only changes.

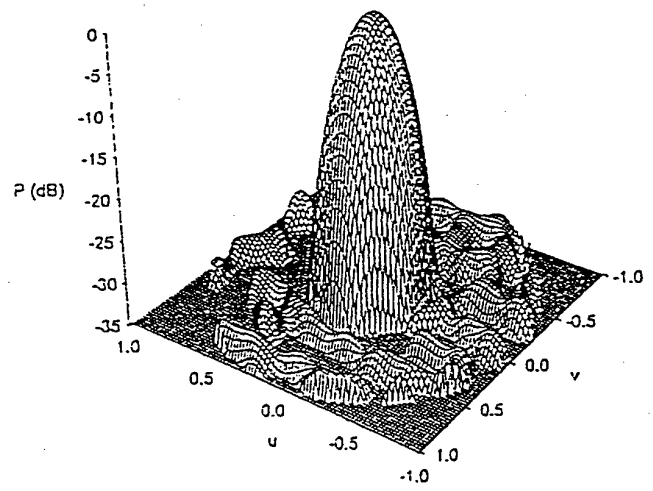

Figure 6. Synthesized sum power pattern with three element failures using phase-only control. Sidelobes lowered in the whole ϕ-range (0°–360°).

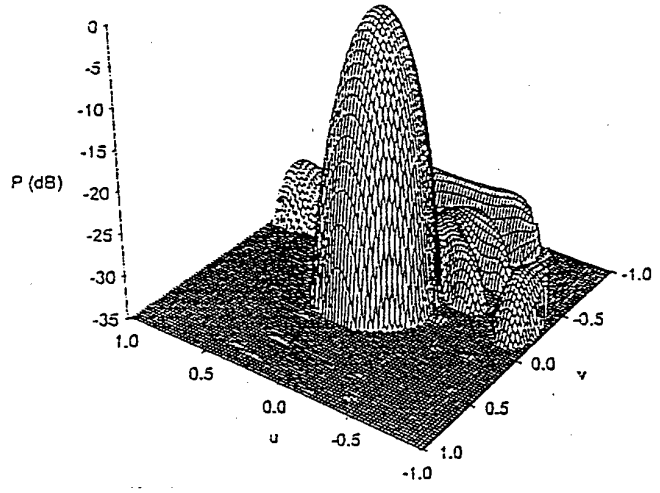

Figure 7. Synthesized sum power pattern with three element failures using phase-only control. Sidelobes lowered in the ϕ-range (0°–180°) but slightly increased in the ϕ-range (180°–360°).

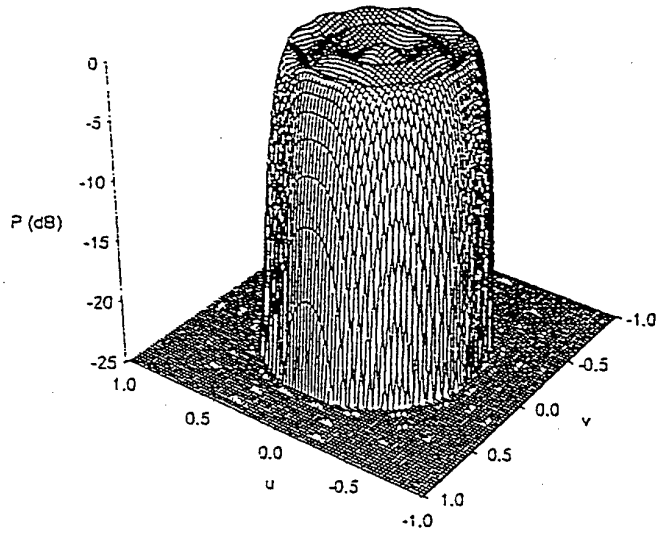

Figure 8. Power pattern obtained by sampling a ϕ-symmetric pure real aperture distribution corresponding to a ϕ-symmetric flat-topped beam (SLL$=-25$ dB, ripple ± 0.5 dB).

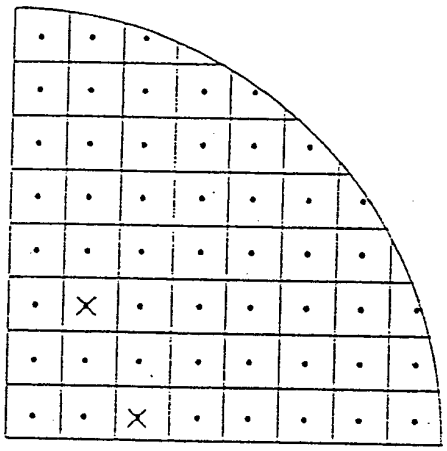

Figure 9. Location of the failed elements in the 16×16 element planar array.

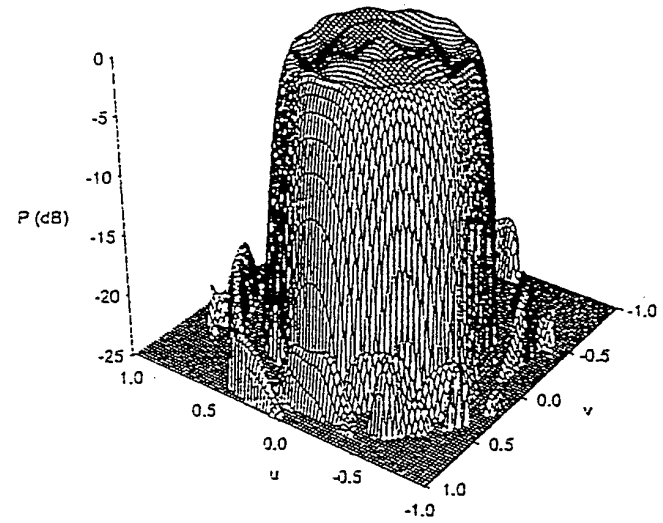

Figure 10. Shaped beam power pattern with two element failures.

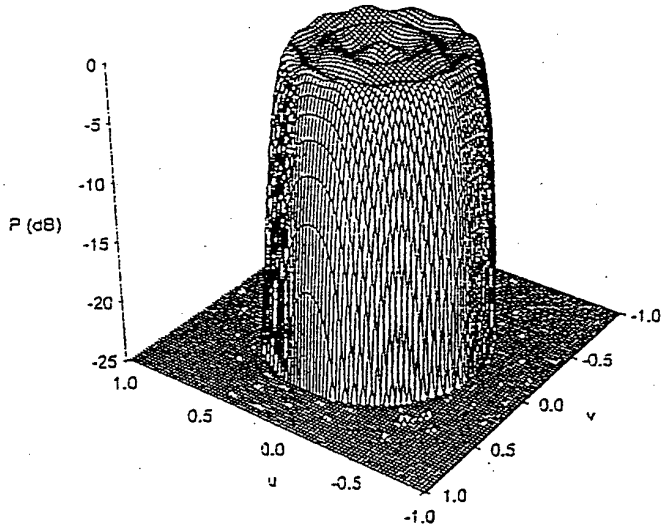

Figure 11. Synthesized shaped beam power pattern with two element failures using amplitude-only changes.

initial pattern was obtained by sampling a ϕ-symmetric pure real aperture distribution corresponding to a ϕ-symmetric flat-topped beam with a peak sidelobe level of -25 dB, ripple ± 0.5 dB [11], and is shown in Figure 8. We have simulated two null elements located in the first quadrant as Figure 9 shows. The pattern obtained after nulling these two elements has a peak a sidelobe level of -18.7 dB, ripple ± 1.1 dB and is plotted in Figure 10. Using the amplitude-only synthesis we could reduce the sidelobes to -24.5 dB and the ripple level to ± 0.5 dB. The synthesized pattern is shown in Figure 11. Again, we have found that the amplitude only synthesis allows to reduce the sidelobe level as well as the ripple level down to near the design level. Regarding to phase-only synthesis, we could not obtain so good results as modifying the amplitude weights because a reduction of the sidelobes yielded an increasing of the ripple level.

CONCLUSIONS

A method of array failure correction for planar arrays has been proposed. The optimization performed to the degraded pattern does not require to modify both the amplitude and phase weights of the non-defective elements, but only the amplitude or the phase aperture distribution. This reduces the hardware complexity required, specially in the case of the phase synthesis which has found to yield optimal results for asymmetric sidelobes. This method is applicable to planar arrays of a wide variety of grid structures, to non-uniformly spaced arrays, and even to antennas made up of non-identical elements.

ACKNOWLEDGMENT

The authors are grateful to Professor Sembiam R. Rengarajan of the University of California, Northridge for many discussions on this topic. We would also like to acknowledge the support from the European Office of Aerospace Research and Development (EOARD), and from the Air Force Office of Scientific Research (AFOSR).

REFERENCES

1. Mailloux, R. J., "Array failure correction with a digitally beamformed array," *IEEE Trans. Antennas Propagat.*, Vol. 44, 1542–1550, 1996.
2. Simmers, J., H. L. Southall, and T. O'Donnell, "Advances in neural beamforming," in *Proc. '93 Antennas Appl. Symp., Univ. Illinois, Urbana-Champaign*, 206–219, 1993.
3. Sim, S. L.,and M. H. Er, "Sidelobe suppression for general arrays in

presence of element failures," *Electronics Letters*, Vol. 33, No. 15, 1278–1280, 1997.
4. Yeo, B. B. K.,and Y. Lu, "Array failure correction with a genetic algorithm," *ACES-98, Monterey, CA*, 1087–1094, 1998.
5. Peters, T. J., "A conjugate gradient-based algorithm to minimize the sidelobe level of planar arrays with element failures," *IEEE Trans. Antennas Propagat.*, Vol. 39, pp. 1497–1504, 1981.
6. DeFord, J. F.,and O. P. Gandhi, "Phase-only synthesis of minimum peak sidelobe patterns for linear and planar arrays," *IEEE Trans. Antennas Propagat.*, Vol. 36, 191–201, 1988.
7. Bucci, O. M., G. Mazzarella, and G. Panariello, "Reconfigurable arrays by phase-only control," *IEEE Trans. Antennas Propagat.*, Vol. 39, 919–925, 1991.
8. Frey, J. R.,and R. S. Elliott, " Phase-only changes in aperture excitation to achieve sum patterns with asymmetric sidelobes," *Alta Frequenza*, Vol. 51, 31–35, 1982.
9. Press, W. H., W. T. Vetterling, S. A. Teukolsky, and B. P. Flannery, *Numerical Recipes in C*, Second Edition, Cambridge, 444–455, 1992.
10. Taylor, T. T., "Design of circular apertures for narrow beamwidth and low side lobes," *Trans. I. R. E.*, Vol. AP-8, 17–22, 1960.
11. Elliott, R. S.,and G. J. Stern, "Footprint patterns obtained by planar arrays," *IEEE Proc.*, Vol. 137, Pt. H, No. 2, 108–112, 1990.

Juan A. Rodriguez-Gonzalez was born in Orense, Spain in 1972. He received his B.S. and M. S. degrees in Physics from the University of Santiago de Compostela, Spain. He was also presenting several subjects related to electromagnetics at the Open National University Associated Centre in Pontevedra, Spain, for two years. At present, he is preparing his Ph.D. in Physics about antenna array pattern synthesis. His general research interests include numerical methods in solving electromagnetic problems and pattern synthesis. He is also interested in computer programming and software engineering.

Francisco J. Ares-Pena received the B.S. and M.S. degrees from the University of Santiago de Compostela, Spain, in 1986 and 1987 respectively, and the Ph.D. from the same institution in 1993, all in Physics. He is currently an Associate Professor in the Department of Applied Physics at the University of Santiago de Compostela, Spain. He has published more than 70 journal and conference papers. Dr. Ares is a Senior Member of IEEE and a member of the New York Academy of Sciences. His main research interests are antenna array pattern synthesis and design of slot arrays.

Date: Thu, 29 Oct 1998 20:47:07 -0800
From: Kai Chang <chang@ee.tamu.edu>
To: faares@usc.es
Subject: paper acceptance

No: 98353
Authors: J.A. Rodriguez and F. Ares
Title: Real Linear Array Excitations with ...

Dear Dr. Ares:

I am pleased to inform you that your paper has been accepted for publication in the Microwave and Optical Technology Letters and will appear in the March 20, 1999 issue.

I would like to emphasize that the editing of your manuscript is very light, and for this reason as well as time constraints, we will not show you any proof. If there are problems with your manuscript we will return it to you before typesetting.

There is no page charge, and the corresponding author will receive six copies of the issue in which this article appears without charge in 4-6 weeks after publication. Additional prints can be ordered on the form provided by Wiley later. If there is a problem in receiving the free copies, please contact: Mr. George Telecki, John Wiley & Sons, Inc., 605 Third Avenue, New York, NY 10158-0012, USA. Tel: 212-850-6317, Fax:212-850-6264. To keep current with new technologies and developments, please ask your library to subscribe this journal. For subscription information, please contact: Journal Subscription Department, John Wiley & Sons, Inc., 605 Third Avenue, New York, NY 10158-0012, USA. Email:subinfo@jwiley.com

Sincerely,

Kai Chang
Editor
Tel:409-845-5285
Fax:409-845-6259
Email:chang@ee.tamu.edu

REAL LINEAR ARRAY EXCITATIONS WITH NO EDGE BRIGHTENING FOR EFFICIENT SUM PATTERNS

J. A. Rodriguez, F. Ares

Grupo de Sistemas Radiantes,
Dpto. de Física Aplicada, Facultad de Física,
Universidad de Santiago de Compostela,
15706 Santiago de Compostela, Spain.
E-mail: faares@usc.es

Abstract

The authors report the application of the simulated annealing optimization technique to the synthesis of linear array sum patterns by highly efficient real aperture distributions with no edge brightening.

1. Introduction

Villeneuve [1] published a pattern synthesis method that is the equivalent, for linear arrays, of Taylor's method for synthesizing sum patterns of near-optimal peak directivity for linear antenna apertures [2]. Like Taylor's method, Villeneuve's affords excitation distributions with considerable edge brightening (i.e. a pronounced rise in amplitude at the ends of the array). To alleviate edge brightening (at the expense of efficiency), McNamara [3] modified Villeneuve's method by allowing the outer side lobe level to fall off more rapidly. Edge brightening can also be reduced by null filling, again at the expense of efficiency (and with the added complication of making the excitation distribution complex instead of real) [4].

We recently reported the use of a simulated annealing optimization method to synthesize radiation patterns approximating linear and circular Taylor sum pattern by means of highly

efficient real aperture distributions with smoothly varying amplitudes and no edge brightening [5]. We have now adapted this procedure to linear arrays producing patterns approximating Villeneuve sum patterns.

2. Method

Given the N roots b_i of a Villeneuve pattern [1], small perturbations δb_i are optimized by the simulated annealing method [6] using the cost function

$$C(\delta b_1, \delta b_2, \ldots, \delta b_N) = c_1 \cdot |I_{max}/I_{min}| + c_2 \cdot V + c_3/\eta + c_4 \sum_i f_i \qquad (1)$$

where $|I_{max}/I_{min}|$ is the dynamic range ratio of the aperture distribution, V is a measure of excitation distribution smoothness controlling edge brightening ($V = \max\{R_j\}$, where R_j is the ratio between the j-th excitation peak and the lesser of the flanking minima), η is the efficiency of the array (the ratio between its peak directivity and that of a uniformly excited array with the same number of elements), the f_i (which penalize side lobe levels SLL_i in excess of the desired levels $SLL_{i,d}$) are defined by

$$f_i = \begin{cases} (SLL_i - SLL_{i,d})^2 & \text{if } SLL_i \geq SLL_{i,d} \\ 0 & \text{otherwise} \end{cases} \qquad (2)$$

and the c_i are weights that can be varied by the designer in accordance with his or her design priorities.

3. Results

The dashed curve in Fig.1 shows a -20 dB Villeneuve pattern calculated for an array of 30 isotropic elements $\lambda/2$ apart ($\bar{n} = 6$, the value optimizing efficiency for $N = 30$ and

SLL = -20 dB). Fig.2 (dashed curve) shows the calculated excitation distribution, which exhibits marked edge brightening. The solid curves in Figs.1 and 2 show the radiation pattern and excitation distribution calculated by the method described in this letter. The new pattern respects the SLL specification (outer side lobes are in fact lower than in the Villeneuve pattern), and the excitation distribution shows no edge brightening. The excitation distribution also has a smaller dynamic range ratio and smaller $|I_n/I_{n\pm1}|_{max}$ than the Villeneuve distribution, and is even marginally more efficient (Table 1).

4. Conclusions

The method described in this letter allows edge brightening to be eliminated from Villeneuve excitation distributions with no increase in SLL or loss of efficiency while minimizing dynamic range ratio and $|I_n/I_{n\pm1}|_{max}$. It can also be applied with advantage to the synthesis difference patterns, shaped beams and sum patterns with inner side lobes that are depressed relative to outer side lobes.

Acknowledgments

This work was funded by the U.S. European Office of Aerospace Research and Development (EOARD) and the U.S. Air Force Office of Scientific Research (AFOSR).

References

[1] Villeneuve, A.T, "Taylor patterns for discrete arrays", *IEEE Trans. Antennas Propagat.*, 1984, AP-32, pp. 1089-1093.

[2] Taylor, T.T, "Design of line source antennas for narrow beamwidth and low side lobes",

Trans. IRE, Vol. AP-3, 1960, pp. 17-22.

[3] D.A. McNamara, "Generalised Villeneuve $\bar{n}$ distribution", *IEE Proc., Pt. H*, Vol. 136, 1989, pp. 245-249.

[4] F. Ares, S. R. Rengarajan, and E. Moreno, "Optimization of Aperture Distributions for sum patterns", *Electromagnetics*, Vol. 16, 1996, pp. 129-141.

[5] J. A. Rodriguez, and F. Ares, "Smooth, efficient real amplitude distributions with no edge brightening for linear and circular near-Taylor sum patterns", *Electronics Letters*, Vol. 34, 1998, pp. 611-612.

[6] W. H. Press, W. T. Teukolsky, S. A. Vetterling, and B. P. Flannery, Numerical Recipes in C, 2nd edn., Cambridge University Press, 1992, pp. 444-455.

LEGENDS FOR THE TABLE AND FIGURES

Table 1. Dynamic range ratio, adjacent excitation ratio and efficiency of the patterns of Fig.1.

Fig.1. Power plots of a Villeneuve pattern (SLL = -20 dB, $\bar{n}$ = 6; dashed curve) and the pattern achieved in this work taking the Villeneuve pattern as its starting point (solid curve).

Fig.2. Excitation distributions of the patterns of Fig.1 (dashed curve, Villeneuve pattern; solid curve, this work).

Table 1.

	$\lvert I_{max}/I_{min}\rvert$	$\lvert I_n/I_{n\pm1}\rvert_{max}$	η
Villeneuve pattern	1.75	1.13	0.966
Final pattern	1.55	1.09	0.967

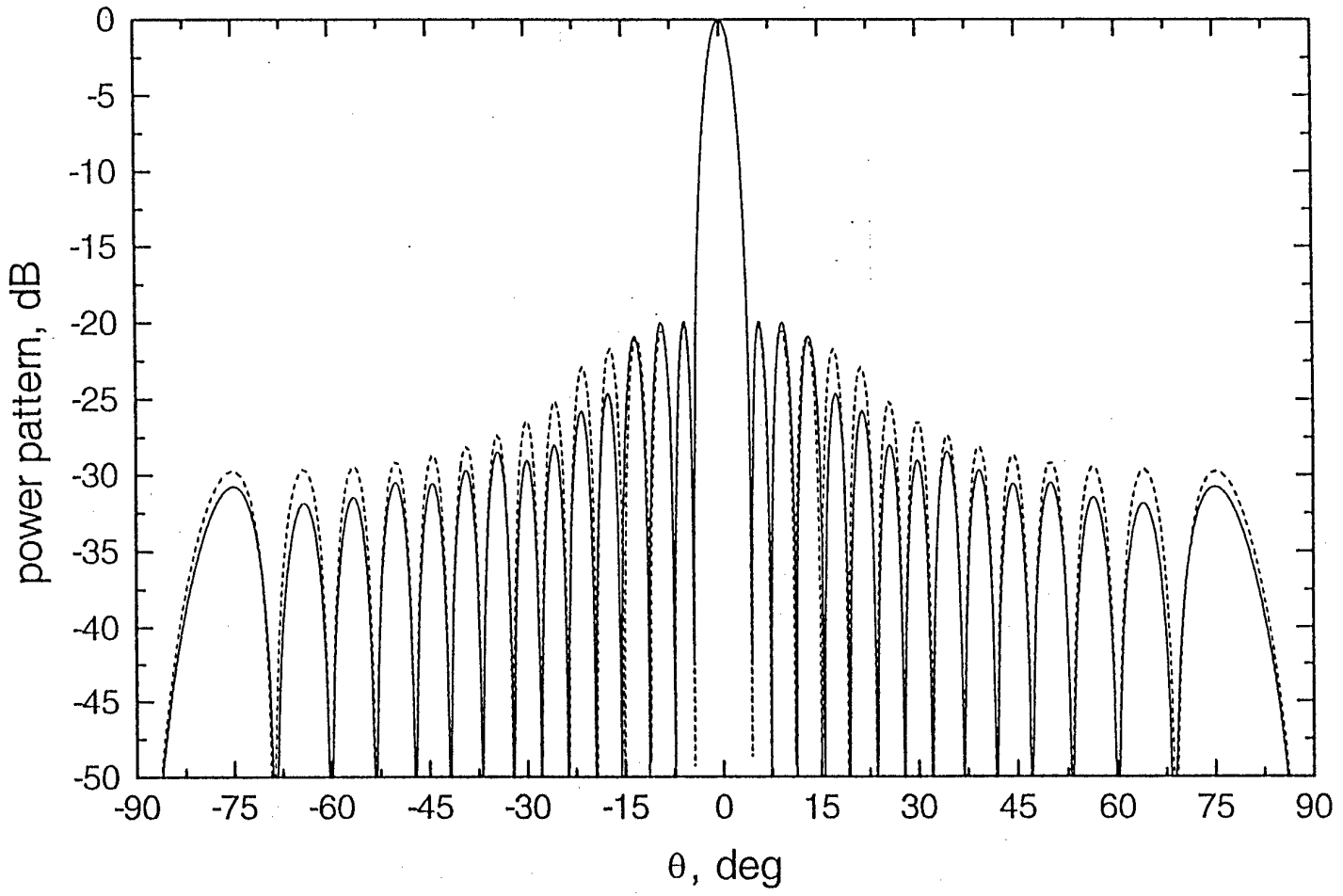
0
-5
-10
-15
-20
-25
-30
-35
-40
-45
-50
power pattern, dB
-90
-75
-60
-45
-30
-15
0
15
30
45
60
75
90
θ, deg

Fig. 1.

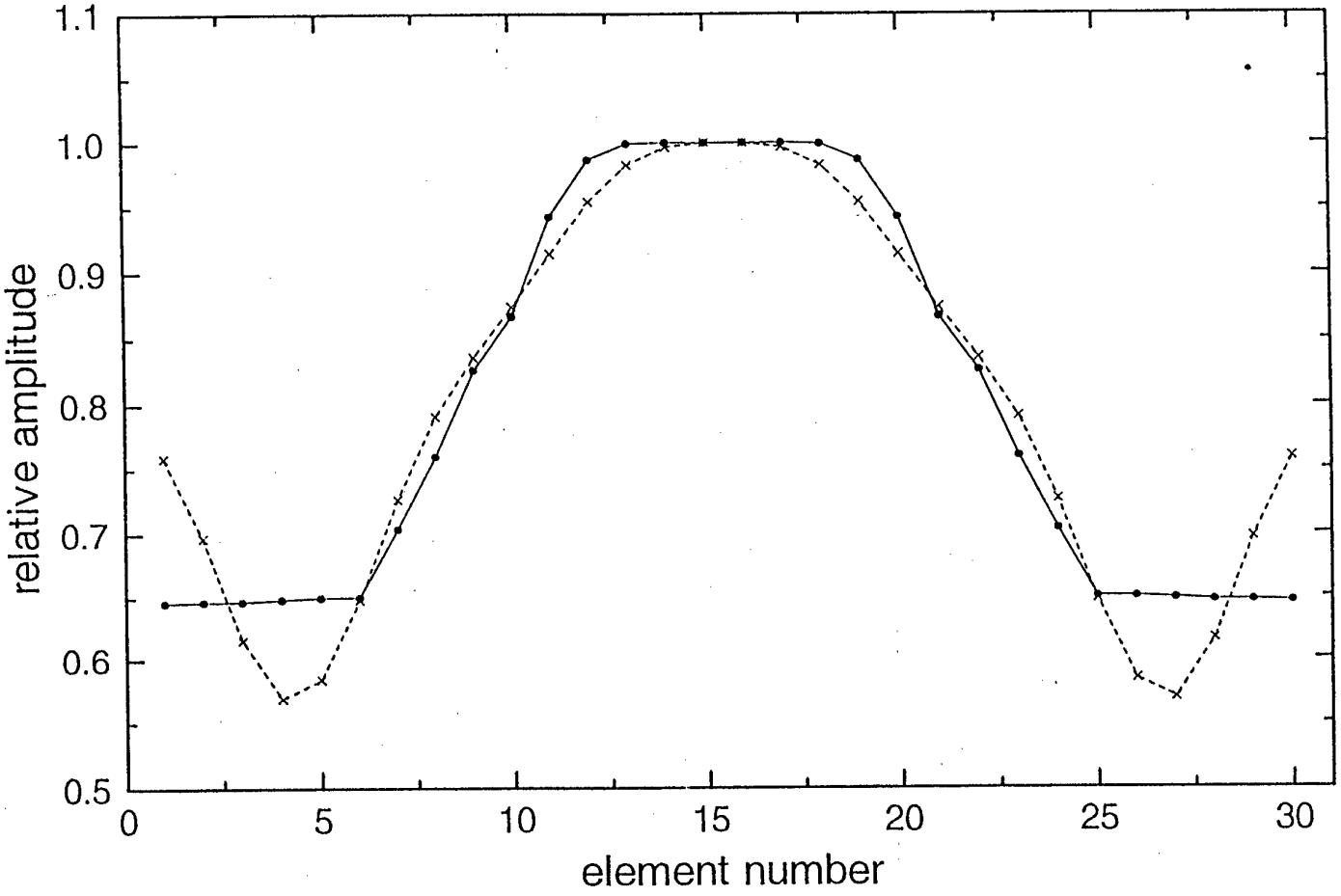
1.1
1.0
0.9
0.8
0.7
0.6
0.5
relative amplitude
0
5
10
15
20
25
30
element number

Fig. 2.

IBERDROLA
INSTITUTO
TECNOLOGICO

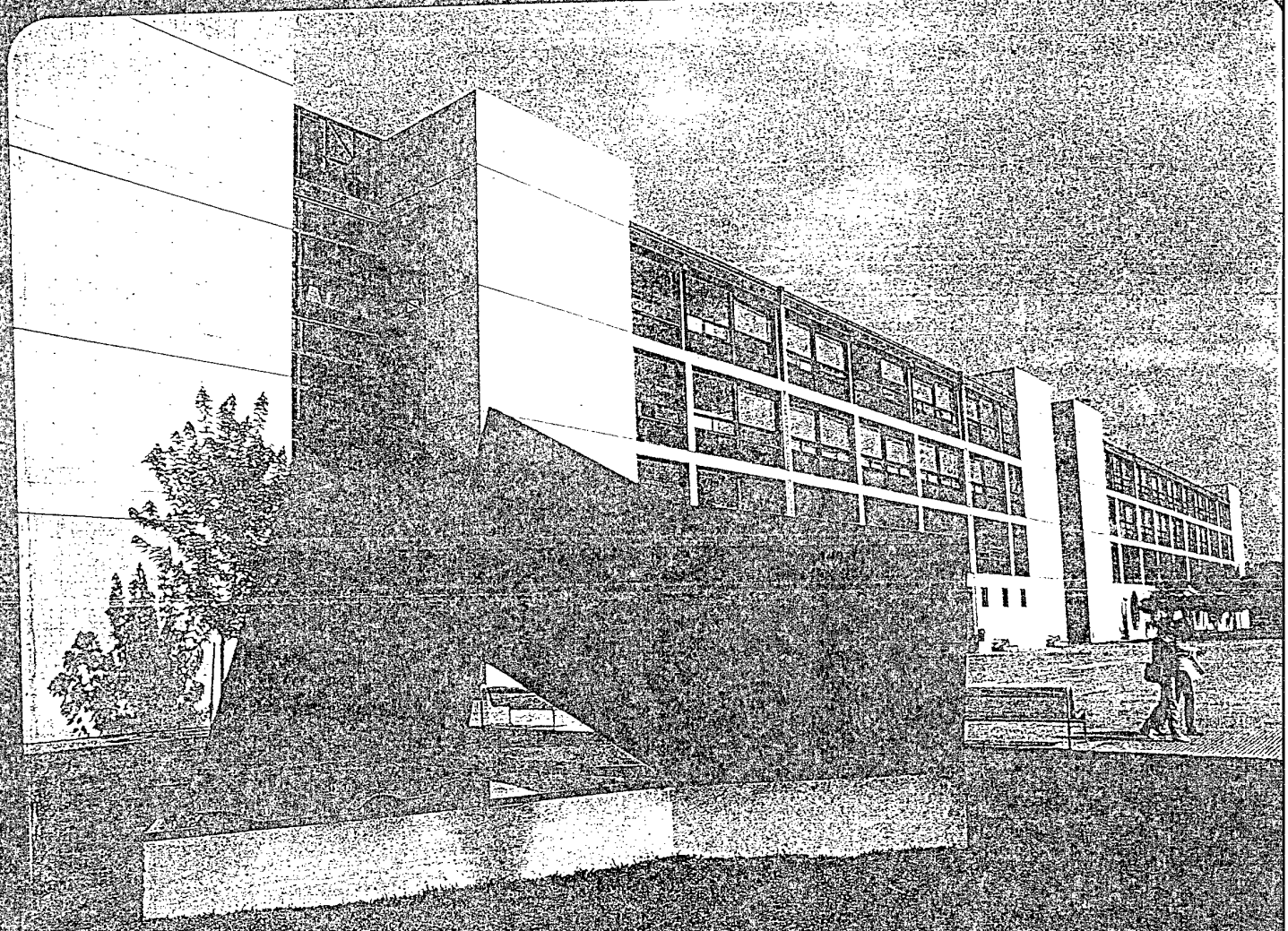

URSI'98

Unión Científica Internacional de Radio

XIII Simposium Nacional

Pamplona, 16-18 Septiembre

Síntesis de diagramas de radiación de tipo suma en arrays lineales mediante distribuciones de abertura reales que no presentan "edge brightening"

J. A. Rodriguez, F. Ares Pena
Departamento de Física Aplicada, Grupo de Sistemas Radiantes
Facultad de Física, Universidad de Santiago de Compostela
15706 Santiago de Compostela
e-mail: faares@usc.es

Abstract: The authors report the application of the simulated annealing optimization technique to the synthesis of sum patterns in linear arrays by means of high efficient real aperture distributions that show no edge brightening.

1. Introducción

En la literatura previa, Taylor [1] introdujo una técnica, aplicable a distribuciones lineales, que permitía generar diagramas de tipo suma de alta eficiencia con un nivel de lóbulos laterales deseado. Esta técnica ha sido muy utilizada en la determinación de las excitaciones de arrays lineales, mediante el muestreo de la distribución de abertura continua en aquellas posiciones en las que se encuentran localizados los elementos del array. El mayor problema que presentan estas distribuciones de Taylor es que sus amplitudes de excitación, en muchos casos, varían muy rápidamente en los extremos de la abertura, efecto que se conoce como "edge brigthening" y que puede hacer inviable la implementación física de la antena. Recientemente, se ha aplicado la técnica de "simulated annealing" para conseguir una topografía óptima de lóbulos laterales de modo que se eliminase el "edge brightening" manteniendo una alta eficiencia en la abertura [2].

Para arrays discretos, Villeneuve introdujo una técnica que permitía sintetizar directamente diagramas muy similares a los de Taylor [3]. Aunque las distribuciones de amplitud resultantes son muy eficientes, siguen presentando el efecto de "edge brightening". Posteriormente, McNamara [4] introdujo una generalización de esta técnica que, introduciendo un nuevo parámetro relacionado con la velocidad de caída de los lóbulos exteriores, permitía reducir el "edge brightening" a costa de disminuir la eficiencia de la abertura. En un trabajo posterior, se demostró que también era posible aliviar este efecto mediante el relleno de los ceros de los diagramas de radiación [5]. Sin embargo, esta técnica conlleva el uso de una distribución de abertura compleja y lleva asociada una pérdida en la eficiencia de la abertura.

Este trabajo, que es una extensión de [2] a arrays discretos, permite sintetizar diagramas de tipo suma mediante distribuciones de abertura reales que no presentan "edge brightening", manteniendo una alta eficiencia. La técnica perturba ligeramente las raíces de las distribuciones de Villeneuve de forma que se minimice una función de costo que tenga en cuenta el nivel de lóbulos laterales, la variabilidad de las excitaciones y todos los demás parámetros de interés en el diseño.

2. Descripción del método

El proceso parte de una distribución inicial de raíces dadas por b_i (como por ejemplo, las correspondientes a una distribución de Villeneuve [3]) y las va perturbando ligeramente de forma iterativa. Dichas perturbaciones δb_i se calculan mediante la técnica de "simulated annealing" a través de la minimización de una función de costo dada por la siguiente expresión:

$$C(\delta b_1,\delta b_2,...,\delta b_N)=c_1\cdot|I_{máx}/I_{mín}|+c_2\cdot V+ +c_3/\eta+c_4\sum_i f_i \qquad (1)$$

en donde f_i, que penaliza el incremento de los lóbulos laterales por encima del nivel de diseño, se define como

$$f_i=\begin{cases}(SLL_{i,o}-SLL_{i,d})^2 & \text{si } SLL_{i,o}\geq SLL_{i,d}\\ 0 & \text{en otro caso}\end{cases} \qquad (2)$$

en donde $SLL_{i,o}$ y $SLL_{i,d}$ es el nivel obtenido y deseado del lóbulo i-ésimo respectivamente; $|I_{máx}/I_{mín}|$ es el rango dinámico de la distribución de abertura; V, una medida de la suavidad de dicha distribución, controla el "edge brightening" ($V=máx\{R_j\}$, en donde R_j es la razón entre el máximo j y el menor de los mínimos adyacentes de la abertura); η es la eficiencia de la abertura, definida como la razón entre la directividad pico del diagrama obtenido y la directividad pico de un array uniforme con el mismo número de elementos. Finalmente c_i son los factores de peso que pueden ser ajustados en función de las especificaciones del diseño.

3. Resultados

Para ilustrar el método se ha utilizado un array lineal de 30 elementos isotrópicos equiespaciados $\lambda/2$. Se ha partido de una distribución de Villeneuve con un nivel de lóbulos laterales de -20 dB y un índice de

transición $\bar{n}$=6 (se ha elegido este valor puesto que optimiza la eficiencia de la distribución para el SLL y número de elementos considerado). El diagrama resultante se muestra en la fig. 1, mientras que en la fig. 2 se muestra la distribución de abertura correspondiente, la cual presenta "edge brightening". El diagrama obtenido tras la optimización y su distribución de abertura se representan en trazo continuo en dichas figuras. Tal y como se observa, se ha encontrado la topografía óptima de lóbulos laterales (manteniendo el nivel máximo de diseño de -20 dB) que permite eliminar el "edge brightening" de la distribución de abertura. En la tabla I se muestran los parámetros de ambos diagramas. Se observa que la distribución de abertura obtenida presenta un menor rango dinámico así como una menor variabilidad de las excitaciones entre elementos colindantes que la inicial, manteniendo una elevada eficiencia.

	$\lvert I_{máx}/I_{min}\rvert$	$\lvert I_n/I_{n\pm1}\rvert$	η
Villeneuve	1.75	1.13	0.966
Optimizado	1.55	1.09	0.967

Tabla I. Comparación del rango dinámico, variabilidad de las excitaciones y eficiencia del diagrama inicial y el obtenido tras la optimización.

4. Conclusiones

Se ha introducido una técnica que permite eliminar el efecto de "edge brightening" en las distribuciones de abertura correspondientes a los diagramas de radiación de tipo Villeneuve. La solución obtenida también optimiza el rango dinámico y la variabilidad de las excitaciones, además de mantener una alta eficiencia. El método también permite eliminar el "edge brightening" en patrones con lóbulos deprimidos, siendo también aplicable a diagramas diferencia y de haz perfilado.

5. Agradecimientos

Los autores quieren agradecer la ayuda económica ofrecida por la European Office of Aerospace Research and Development (EOARD) y la Air Force Office of Scientific Research (AFOSR).

Referencias:

[1] T. T. Taylor, "Design of line source antennas for narrow beamwidth and low side lobes", *Trans. IRE,* AP-3, pp. 17-22, 1955.

[2] J. A. Rodriguez and F. Ares, "Smooth, efficient real amplitude distributions with no edge brightening for linear and circular near-Taylor sum patterns", *Electronics Letters*, Vol. 34, N° 7, pp. 611-612, April 1998.

[3] A. T. Villeneuve, "Taylor patterns for discrete arrays", *IEEE Trans*, AP-32, pp. 1089-1093, 1984.

[4] D. A. McNamara, "Generalised Villeneuve $\bar{n}$ distribution", *IEE Proc.*, Vol. 136, Pt. H, N° 3, June 1989.

[5] F. Ares, S. R. Rengarajan, and E. Moreno, "Optimization of Aperture Distributions for sum patterns", *Electromagnetics*, Vol. 16, N° 2, pp. 129-141, March-April 1996.

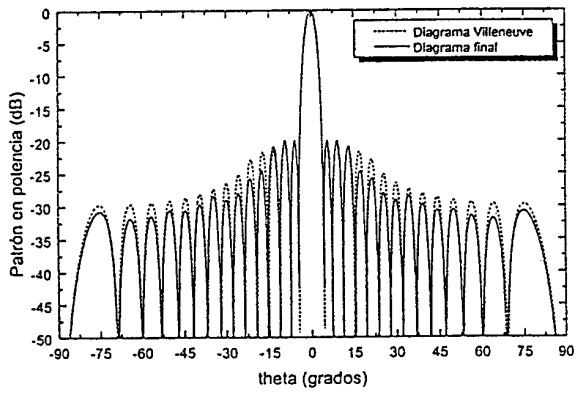

Fig. 1. Diagrama de radiación correspondiente a la distribución de Villeneuve (SLL=-20, $\bar{n}$=6) y el obtenido tras la optimización.

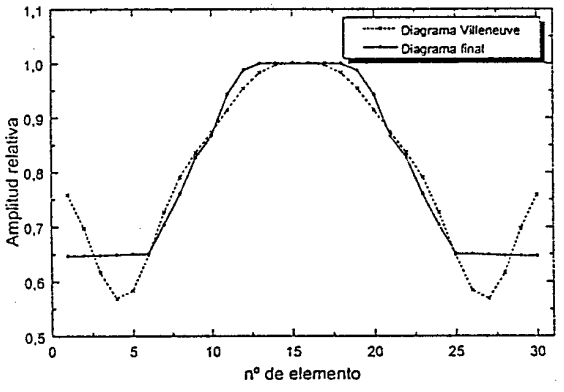

Fig. 2. Distribución de abertura de Villeneuve (SLL=-20, $\bar{n}$=6) y la obtenida tras la optimización.

ELECTRONICS LETTERS

AN INTERNATIONAL PUBLICATION

CONTENTS

pages 1273-1364

25th June 1998 Vol. 34 No. 13

(continued on back cover)

metallic sides. The element is fed by means of coaxial probes at the centre of the lower edge of one or more of the vertical sides. A single feed is sufficient for linear polarisation and feeds excited in phase quadrature on two adjacent sides may be used for circular polarisation. The circularly polarised (CP) element in the Figure has four-quadrant symmetry; however, other CP implementations which have only two vertical faces have been tested, and linearly polarised elements with a single vertical face have also been evaluated. In these other cases the element pattern is less symmetrical, with the beam peak occurring off broadside. This beam squint has been found to be useful in some array applications [1].

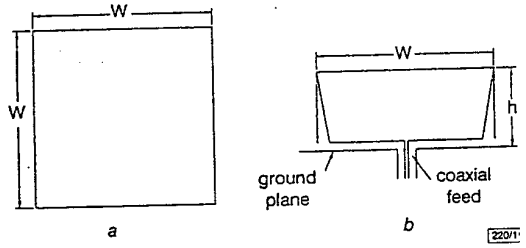

Fig. 1 *Radiator geometry*

a Top view
b Side view

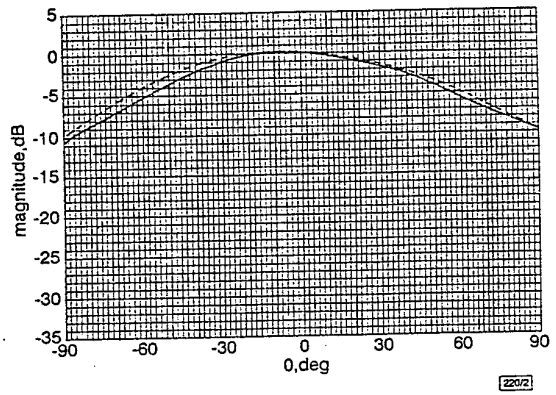

Fig. 2 *Measured and predicted RHCP radiation patterns at 1.65GHz*

——— measured
– – – – predicted

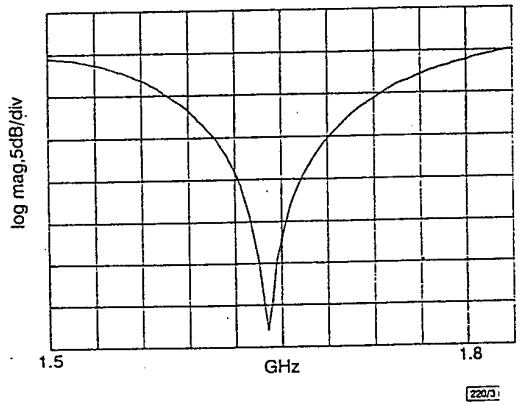

Fig. 3 *Measured return loss*

Experimental and analytical results: A circularly polarised version of the new radiator has been analysed using the WIPL software package [3], which implements a method of moments solution to the integral equation problem. In this case, the element has two vertical faces with one feed probe exciting each face. The probes are fed with equal current magnitudes and relative phases of 90°. The element, which has width w = 3.8cm and height h = 2.54cm, has been positioned at the centre of a 22cm square ground plane. The predicted RHCP radiation pattern at 1.65GHz and the corresponding measured pattern are given in Fig. 2. The prototype element was excited by a microstrip circuit incorporating a Wilkinson hybrid, followed by transmission lines differing in phase length by 90° and microstrip transformers matching to the 240Ω element resonant impedance. The return loss, which is plotted in Fig. 3, was measured without the hybrid, at the input to one of the matching transformers. The hybrid absorbs reflections from the element input ports, and consequently the return loss at the hybrid input port is not a good measure of the element performance.

Conclusion: The compact radiator described here has been used in a number of successful antenna development programs [1, 2] and has been found to be a useful alternative to microstrip patches and other low profile elements. The radiator has a footprint of only 0.04 square wavelengths while achieving a bandwidth of > 17% with 6dB return loss and a –6dB CP beamwidth of > 120°.

30 April 1998
Electronics Letters Online No: 19980938

P.C. Strickland (*CAL Corporation, 1725 Woodward Drive, Ottawa, Ontario, K2C OP9, Canada*)

E-mail: strickland@calcorp.com

References

1 STRICKLAND, P.C.: 'Compact, low profile antennas for MSAT and mini-M land mobile satellite communications'. Int. Mobile Satellite Conf., Ottawa, 1995, pp. 340–344
2 U.S. Patent No. 5,633,646
3 KOLUNDZIJA, B.M., OGNJANOVIC, J.S., SARKAR, T.K., and HARRINGTON R.F.: 'WIPL: Electromagnetic modelling of composite wire and plate structures' (Artech House, Boston, 1995)

Design of efficient, easily feed-matched array antennas by joint optimisation of excitations and element geometry: pencil beam example

J.A. Rodriguez, F. Ares and G. Franceschetti

By using simulated annealing for simultaneous optimisation of the geometries and excitations of the array elements, it is often possible to design array antennas that generate specified radiation power patterns, have elements with real active impedances, and are easily feed-matched. The example of a twelve-element pencil beam antenna fed by coaxial cables of practical dimensions with no additional circuitry is described.

Introduction: The efficiency, and indeed the realisability, of a given array antenna distribution of excitations depends on the mutual coupling among the array elements. Most available methods of array antenna power pattern synthesis make no attempt to take mutual coupling explicitly into account during the calculation of an excitation distribution attaining the desired power pattern. Coupling is minimised by reducing the dynamic range of the excitations or the ratio between the excitations of adjacent elements [1 – 4]. However, to design an efficiently fed antenna that also radiates the desired pattern efficiently, it is not sufficient to ensure that the excitation distribution has small dynamic range; even excitation distributions with quite small dynamic ranges can be very costly or impossible to implement efficiently because of coupling problems [5, 9]. This is because the active impedances of the array elements and the impedances presented to the main feed line by the branch lines to the array elements depend on both the excitation distribution and the geometry of the elements and/or array. In general, both excitations and geometry must be varied to find a combination which achieves the desired radiation pattern and antenna properties.

In the past, it has been common to follow a three-stage procedure. First, under the assumption that all the radiating elements are identical, and with fixed geometry, an excitation distribution attaining the desired radiation pattern is obtained. Next, with the excitation distribution fixed, the element geometry is calculated to ensure efficient radiation (this results in pattern degradation, but the degradation is often negligible except for extreme angles). Finally, feed matching is ensured by calculating feed network parameters.

In this Letter we describe how an efficient, easily feed-matched array producing a specified radiation power pattern can be synthesised by optimising element geometry and in-phase excitations simultaneously. We take as our example a linear array of twelve centre-fed dipoles that generates a pencil beam and is fed by coaxial cables with no additional circuitry; the method is readily generalisable to planar arrays and to arrays with other types of radiating elements (e.g. microstrip dipoles and waveguide slots, the design of which raises the same difficulty [6 – 9]).

Theory: Consider a linear array of N centre-fed dipoles located a distance h from a ground plane and connected to the main coaxial feed line by coaxial branch lines. For practical values of h ($h \leq \lambda/4$, where λ is the radiation wavelength), the image principle is applicable even for a finite ground plane, which may thus be replaced, for the purposes of analysis, by a parallel, identical virtual array excited 180° out of phase with respect to the real array. The active impedance of the ith dipole, Z_i^a, is therefore given by

$$Z_i^a = \sum_{j=1}^{N} (I_j/I_i) Z_{ij} \qquad (1)$$

where I_α is the current in the αth dipole and Z_{ij} is the mutual impedance between dipoles i and j minus the mutual impedance between dipole i and the virtual image of dipole j (Z_{ij} is the self-impedance of dipole i minus its mutual impedance with its image) [5]. Z_{ij} depends on the geometry of the dipoles and their mutual geometric relations.

If the array element excitations are all in phase, then for efficient radiation the active impedances Z_i^a should all be real (and are hereafter denoted by R_i^a). This additional constraint requires the simultaneous optimisation of the currents I_i and the array and/or dipole geometry. This can be done by using simulated annealing [10] to minimise a cost function including terms for deviation from the desired pattern and for the imaginary parts of the active impedances. In addition, easy feed matching can be ensured if the cost function also includes appropriate terms for feed network parameters. Note that the variation of element geometry means that the radiation pattern cannot be factorised as the product of an array factor and a single element factor, but must be calculated from the individual patterns of each dipole.

Example: Consider the synthesis of a pencil beam pattern by a linear array of twelve centre-fed dipoles of radius 0.0048 λ laid out in the x-y plane with a distance $\lambda/2$ from each other with their centres on the y axis. The array centre is at the origin, and a ground plane lies at $z = -h = -\lambda/4$. In the y-z plane ($\phi = \pi/2$), the radiation pattern is to have a maximum sidelobe level of –18dB (this maximises the peak directivity of the twelve-element Dolph-Chebyshev solution we assume as our starting point). The dipoles are to be fed in phase from a single 10Ω main transmission line via quarter-wave coaxial cables with no extra circuitry. We assume that the radiation patterns of the dipoles are given in terms of their lengths $2l_i$ by

$$F_i(\theta,\phi) = \sin(kh\cos\theta)\frac{\cos(kl_i\sin\theta\cos\phi) - \cos(kl_i)}{\sqrt{1-\sin^2\theta\cos^2\phi}} \qquad (2)$$

where $k = 2\pi/\lambda$, and that their self and mutual impedances are as given in [5] (this implies that dipole lengths can be varied only in the interval $[1.3/k, 1.7/k]$ in which the assumed expression for self-impedance is valid).

To verify pattern specification when optimising element currents and/or geometry, the cost function to be minimised can include the terms $c_1\Sigma_s(\Delta S_s)^2$ and c_2/D_p, where ΔS_s is the difference between the calculated level of the side lobe s and the maximum tolerated level, if this difference is positive, and $\Delta S_s = 0$ otherwise, and D_p is the peak directivity of the pattern (c_1 and c_2 are appropriate weights). To ensure that the array elements have real active impedances, the cost function can include the term $c_3\Sigma_i(X_i^a)^2$, where X_i^a is the imaginary part of Z_i^a (again, c_3 is an appropriate weight). Finally, the feed specification means that the feed network is determined by the characteristic resistances R_i^{BL} of the quarter-wave branch lines. We have $R_i^{BL} = (R_i^a R_i)^{1/2}$, where R_i are the resistances presented to the main feed line by the branch lines and are calculated by solving the equations [5]

$$R_i/R_j = (I_j^2 R_j^a)/(I_i^2 R_i^a) \qquad (3)$$

together with the feed matching condition

$$\sum_i (1/R_i) = 1/R^{ML} \qquad (4)$$

To meet the requirement that the R_i^{BL} have realistic values, e.g. < 140Ω, the cost function can include the term $c_4\Sigma_i g_i$, where $g_i = R_i^{BL} - 140$, if this is positive, and $g_i = 0$ otherwise, with c_4 an appropriate weight. If l_i are all given the fixed value $\lambda/4$, the radiation pattern specification is satisfied by the Dolph-Chebyshev solution [5] listed in Table 1. This solution is inefficient because of the coupling indicated by the complex active impedances of the dipoles (also listed in Table 1).

Table 1: Excitations, lengths and active impedances of elements of 12-dipole array when dipole length is kept uniform (= $\lambda/2$) and excitations are optimised to generate Dolph-Chebyshev pattern with –18dB side lobes

i	I_i	$2l/\lambda$	z_i^a
			Ω
1; 12	1.000	0.500	89.7 + 55.4j
2; 11	0.665	0.500	110.1 – 4.1j
3; 10	0.826	0.500	91.6 + 28.1j
4; 9	0.964	0.500	101.2 + 20.8j
5; 8	1.064	0.500	97.0 +23.2j
6; 7	1.117	0.500	98.6 + 22.5j

Peak directivity = 57.9

Table 2: Excitations, lengths and active impedances of elements of 12-dipole array after perturbation of dipole lengths of Table 1 to afford real active impedances and best possible set of branch line characteristic impedances, keeping excitations fixed

i	I_i	$2l/\lambda$	z_i^a	R_i^{BL}
			Ω	Ω
1; 12	1.000	0.461	70.9	96.6
2; 11	0.665	0.498	107.0	145.2
3; 10	0.826	0.479	81.7	117.0
4; 9	0.964	0.482	90.4	100.3
5; 8	1.064	0.481	86.9	90.8
6; 7	1.117	0.481	88.2	86.4

Peak directivity = 57.5, computation time = 1.2 min
Computation time refers to calculations on a Pentium II running at 266MHz

Table 3: As for Table 2, but with simultaneous optimisation of dipole lengths and excitations

i	I_i	$2l/\lambda$	z_i^a	R_i^{BL}
			Ω	Ω
1; 12	1.403	0.466	74.7	119.1
2; 11	1.426	0.485	95.4	117.2
3; 10	1.456	0.479	82.7	114.8
4; 9	1.444	0.490	95.7	115.8
5; 8	2.092	0.475	83.1	79.9
6; 7	1.875	0.484	90.1	89.1

Peak directivity = 57.0, computation time = 2.1 min

A solution with the same current set that radiates efficiently and maintains the directivity can be found by perturbing l_i with the currents fixed. The cost function $C = c_1\Sigma_s(\Delta S_s)^2 + c_2/D_p + c_3\Sigma_i(X_i^a)^2$ is used, to move to zero the imaginary part of the active impedances while penalising directivity loss. However, if simultaneous satisfaction of the feed specification is attempted by using the cost function $C = c_1\Sigma_s(\Delta S_s)^2 + c_2/D_p + c_3\Sigma_i(X_i^a)^2 + +c_4\Sigma_i g_i$ with $g_i = R_i^{BL} - 140$, no solution is attainable. To obtain the solution given in Table 2, it is necessary to raise the limiting values of R_i^{BL} to 145Ω (i.e. $g_i = R_i^{BL} - 145$), which provides characteristic impedances associated with coaxial cables which are difficult to manufacture.

In contrast, if the lengths $2l_i$ and currents I_i are simultaneously varied by using the same cost function (with $g_i = R_i^{BL} - 140$), then

the desired power pattern, real active impedances and more reasonable R_i^{BL} values can all be achieved together (Table 3).

Acknowledgments: This work was supported by the the U.S. European Office of Aerospace Research and Development (EOARD) and the U.S. Air Force Office of Scientific Research (AFOSR).

13 May 1998
Electronics Letters Online No: 19980912

J.A. Rodriguez and F. Ares (*Grupo de Sistemas Radiantes, Departamento de Fisica Aplicada, Facultad de Fisica, Universidad de Santiago de Compostela, 15706 Santiago de Compostela, Spain*)

E-mail: faares@usc.es

G. Franceschetti (*Dipartimento di Ingegneria Elettronica, Università di Napoli 'Federico II', Via Claudio 21, 80125 Napoli, Italy*)

References

1 HANSEN, R.C.: 'Array pattern control and synthesis', *Proc. IEEE*, 1992, **80**, pp. 141–151
2 ORCHARD, H.J., ELLIOTT, R.S., and STERN, G.J.: 'Optimising the synthesis of shaped beam antenna patterns', *IEE Proc., Microw. Opt. Antennas*, 1985, **132**, (1), pp. 63–68
3 ARES, F., RENGARAJAN, S.R., and MORENO, E.: 'Optimization of aperture distributions for sum patterns', *Electromagnetics*, 1996, **16**, (2), pp. 129–143
4 BUCCI, O.M., FRANCESCHETTI, G., MAZZARELLA, G., and PANARIELLO, G.: 'Intersection approach to array pattern synthesis', *IEE Proc., Microw. Antennas Propag.*, 1990, **137**, (6), pp. 349–357
5 ELLIOTT, R.S.: 'Antenna theory and design' (Prentice-Hall Inc., Englewood Cliffs, NJ, 1981)
6 ELLIOTT, R.S.: 'An improved design procedure for small arrays of shunt slots', *IEEE Trans. Antennas Propag.*, 1983, **AP-31**, pp. 48–53
7 ELLIOTT, R.S., and STERN, G.J.: 'The design of microstrip dipole arrays including mutual coupling, Part I: Theory', *IEEE Trans. Antennas Propag.*, 1981, **AP-29**, (9), pp. 757–760
8 STERN, G.J., and ELLIOTT, R.S.: 'The design of microstrip dipole arrays including mutual coupling, Part II: Experiment', *IEEE Trans. Antennas Propag.*, 1981, **AP-29**, (9), pp. 761–765
9 YANG, H., ALEXOPOULOS, N.G., LEPELTIER, P.M., and STERN, G.J.: 'Design of transversely fed EMC microstrip dipole arrays including mutual coupling', *IEEE Trans. Antennas Propag.*, 1990, **38**, (2), pp. 145–151
10 PRESS, W.H., TEUKOLSKY, S.A., VETTERLING, W.T., and FLANNERY, B.P.: 'Numerical recipes' (Cambridge University Press, 1992), 2nd edn., pp. 444–455

Two-dimensional beam-scanning phase-shifterless technique using linear active leaky-wave antenna array

Cheng-Chi Hu, C.F. Jou and Jin-Jei Wu

A novel two-dimensional electronic beam scanning technique using a linear leaky-wave antenna array with coupled oscillators is introduced, eliminating the need for phase shifters. The measured H-plane main beam can be continuously scanned from 70 to 40° as the frequency varies from 7.9 to 9.05GHz. By detuning the free running frequencies of the end elements, the measured E-plane main beam can be continuously scanned from –22 to –26°.

Introduction: The complexity usually associated with the two-dimensional (2D) scanning array offers a special challenge for the planar active phase array design. In 1990, Oliner [1] proposed a 2D scanning array using a one-dimensional (1D) phased array of leaky-wave line-source antennas. A pencil beam can scan in both elevation and azimuth planes, however, phase shifters are required in this design. These phase shifters usually require complicated control circuitry which it may also be difficult to achieve in the limited space. In 1994, Liao and York [2] proposed a new phase-shifterless 1D beam-scanning technique using a patch antenna array with coupled oscillators. By controlling the free running frequencies of the end elements of the array, the main beam can scan in the azimuth plane. In this Letter, we extend the work to encompass the phase control technique [2] and leaky-wave antenna characteristic [1, 3, 4], leading to a novel method for phase-shifterless 2D electronic beam scanning.

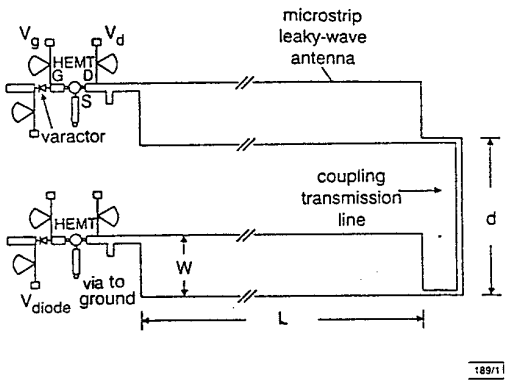

Fig. 1 *Configuration of active microstrip leaky-wave antenna array*
$w = 12\text{mm}$, $L = 100\text{mm}$, $d = 1\,\lambda_0$

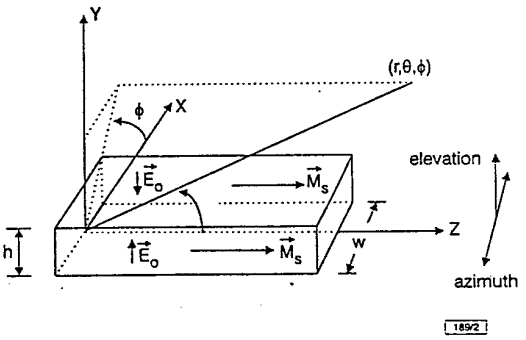

Fig. 2 *Geometry and coordinate system for microstrip leaky-wave antenna*

Design and measurement results: Fig. 1 shows the microstrip realisation of a two-element phase-shifterless active leaky-wave antenna array structure. The varactor-tuned oscillator is based on that we previously designed in [4]. Coupling circuits are designed to provide in-phase coupling, which ensures a stable in-phase mode of operation. The elements within the array are coupled to one another using one wavelength long transmission lines. To excite the first higher order mode, the microstrip leaky-wave antenna is fed asymmetrically [5]. The circuit is designed and fabricated on an RT/Duroid substrate with a dielectric constant of 2.2 and a thickness of 20mils. An NEC NE42484 low noise HEMT is used, and the drain is biased at 2.0V with a drain current of 10mA. The GaAs varactor (M/A-COM MA46410) is used as a tuning varactor, which has a capacitance ratio of 10:1 and a capacitance of 0.5pF at 4V.

Elevation plane scanning: To understand the radiation properties of such a microstrip leaky-wave antenna [1], we obtained its complex propagation constants $\beta - j\alpha$ of the first higher microstrip mode in its leaky range, where β is the phase constant, and α is the attenuation constant. Such complex propagation constants represent a forward leaky-wave radiating into the space at an angle $\theta_m = \cos^{-1}(\beta/k_0)$, where θ_m is the angle of the beam maximum measured from the z-axis, and k_0 is the free-space wave number. In addition, the scanning angle θ_m can be varied with frequency.

For a tuning voltage of 1.0 to 10V, our active leaky-wave antenna array exhibits a tuning bandwidth of 7.9 to 9.05GHz corresponding to a measured main beam position from 70 to 40°. Fig. 3 shows the experimental results of the radiating patterns scaned in the elevation plane. The maximum effective radiated power (ERP) of this active antenna array is ~ 20dBm ± 2dBm throughout the frequency tuning range. The difference in the power level of the main beam is caused mainly by the varied impedance of the microstrip leaky-wave antenna as function of frequency.

France Telecom

IEEE

U.R.S.I.

UNIVERSITE DE NICE SOPHIA ANTIPOLIS

9th EESC'98

see

JIA'98

ISSN 1168-3848

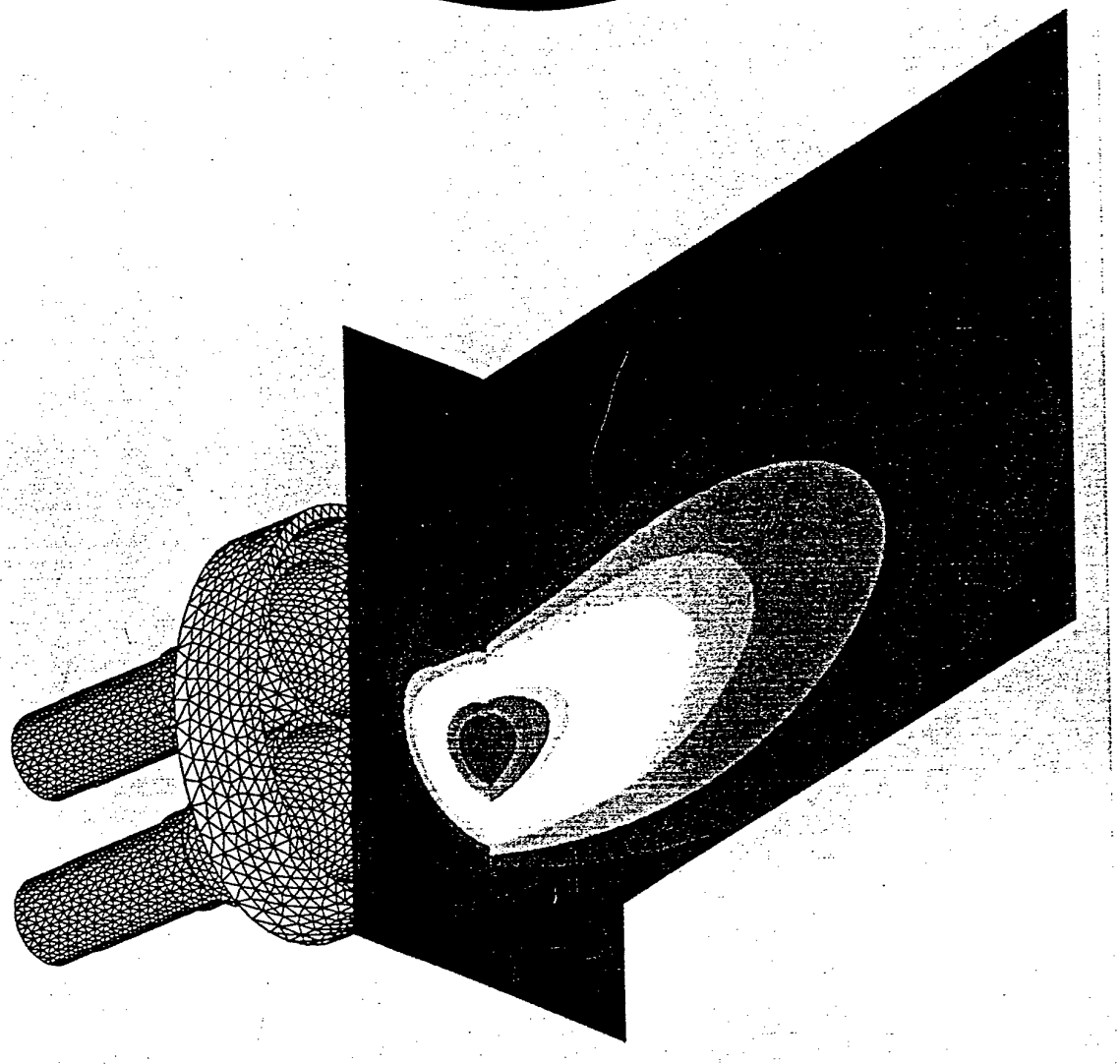

Champ proche par SR3D - dessin par TG

Near field by SR3D & TG graphics

10e JOURNÉES INTERNATIONALES DE NICE SUR LES ANTENNES

NICE

17-19 NOVEMBRE 1998

CONFÉRENCES

II.22

DESIGN OF EFFICIENT, EASILY FEED-MATCHED ARRAY ANTENNAS BY JOINT OPTIMIZATION OF EXCITATIONS AND ELEMENT GEOMETRY: A PENCIL BEAM EXAMPLE

J. A. Rodriguez[†], F. Ares[†], G. Franceschetti[††]

[†] Grupo de Sistemas Radiantes,
Dpto. de Física Aplicada, Facultad de Física,
Universidad de Santiago de Compostela,
15706 Santiago de Compostela, Spain.
E-mail: faares@usc.es

[††] Dipartimento di Ingegneria Elettronica,
Universitá di Napoli 'Federico II'
Via Claudio 21, 80125 Napoli, Italy.

Abstract

By using simulated annealing for simultaneous optimization of the geometries and excitations of the array elements, it is often possible to design array antennas that generate specified radiation power patterns, have elements with real active impedances, and are easily feed-matched. The example of a twelve-element pencil beam antenna fed by coaxial cables of practical dimensions with no additional circuitry is described.

1. Introduction

The efficiency, and indeed the realizability, of a given array antenna distribution of excitations depends on the mutual coupling among the array elements. Most available methods of array antenna power pattern synthesis make no attempt to take mutual coupling explicitly into account during calculation of an excitation distribution attaining the desired power pattern. Coupling is minimized by reducing the dynamic range of the excitations or the ratio between the excitations of adjacent elements [1-4]. However, to design an efficiently fed antenna that also radiates the desired pattern efficiently, it is not sufficient to ensure that the excitation distribution has small dynamic range; even excitation distributions with quite small dynamic ranges can be very costly or impossible to implement efficiently because of coupling problems [5,9]. This is because the active impedances of the array elements and the impedances presented to the main feed line by the branch lines to the array elements depend on both the excitation distribution and the geometry of the elements and/or array. In general, both excitations and geometry must be varied in order to find a combination attaining the desired radiation pattern and antenna properties.

In the past, it has been common to follow a three-stage procedure. First, under the assumption that all the radiating elements are identical, and with fixed geometry, an excitation distribution attaining the desired radiation pattern is obtained. Next, with the excitation distribution fixed, the element geometry is calculated to ensure efficient radiation (this results in pattern degradation, but the degradation is often negligible except for extreme angles). Finally, feed matching is ensured by calculating feed network parameters.

In this communication we describe how an efficient, easily feed-matched array producing a specified radiation

power pattern can be synthesized by optimizing element geometry and in-phase excitations simultaneously. We take as our example a linear array of twelve centre-fed dipoles that generates a pencil beam and is fed by coaxial cables with no additional circuitry, the method is readily generalizable to planar arrays and to arrays with other types of radiating elements (e.g., microstrip dipoles and waveguide slots, whose design meets the same difficulty [6-9]).

2. Theory

Consider a linear array of N centre-fed dipoles located a distance h from a ground plane and connected to the main coaxial feed line by coaxial branch lines. For practical values of h ($h \leq \lambda/4$, where λ is the radiation wavelength), the image principle is applicable even for a finite ground plane, which may thus be replaced, for the purposes of analysis, by a parallel, identical virtual array excited 180° out of phase with respect to the real array. The active impedance of the i-th dipole, Z_i^a, is therefore given by

$$Z_i^a = \sum_{j=1}^{N} (I_j / I_i) Z_{ij} \tag{1}$$

where I_α is the current in the α-th dipole and Z_{ij} is the mutual impedance between dipoles i and j minus the mutual impedance between dipole i and the virtual image of dipole j (Z_{ii} is the self-impedance of dipole i minus its mutual impedance with its image) [5]. The Z_{ij} depend on the geometry of the dipoles and their mutual geometric relations.

If the array element excitations are all in phase, then for efficient radiation the active impedances Z_i^a should all be real (and are hereafter denoted by R_i^a). This additional constraint requires the simultaneous optimization of the currents I_i and the array and/or dipole geometry. This can be done by using simulated annealing [10] to minimize a cost function including terms for deviation from the desired pattern and for the imaginary parts of the active impedances. In addition, easy feed matching can be ensured if the cost function also includes appropriate terms for feed network parameters. Note that the variation of element geometry means that the radiation pattern cannot be factorized as the product of an array factor and a single element factor, but must be calculated from the individual patterns of each dipole.

3. Example

Consider the synthesis of a pencil beam pattern by a linear array of twelve centre-fed dipoles of radius 0.0048λ laid out in the x-y plane with a distance $\lambda/2$ one from another with their centres on the y axis. The array centre is at the origin, and a ground plane lies at $z = -h = -\lambda/4$. In the y-z plane ($\phi = \pi/2$), the radiation pattern is to have a maximum sidelobe level of -18 dB (this maximizes the peak directivity of the twelve-element Dolph-Chebyshev solution we assume as our starting point). The dipoles are to be fed in phase from a single 10 Ω main transmission line via quarter-wave coaxial cables and no extra circuitry. We assume that the radiation patterns of the dipoles are given in terms of their lengths $2l_i$ by

$$F_i(\theta,\phi)=\sin(kh\cos\theta)\cdot\frac{\cos(kl_i\sin\theta\cos\phi)-\cos(kl_i)}{\sqrt{1-\sin^2\theta\cos^2\phi}} \tag{2}$$

where $k = 2\pi/\lambda$; and that their self and mutual impedances are as given in [5] (this implies that dipole lengths can be varied only in the interval $[1.3/k, 1.7/k]$ in which the assumed expression for self-impedance is valid).

To verify pattern specification when optimizing element currents and/or geometry, the cost function to be minimized can include the terms $c_1\sum_s(\Delta S_s)^2$ and c_2/D_p, where ΔS_s is the difference between the calculated level of the side lobe s and the maximum tolerated level, if this difference is positive and $\Delta S_s=0$ otherwise, and D_p is the peak directivity of the pattern (c_1 and c_2 are appropriate weights). To ensure that the array elements have real active impedances, the cost function can include the term $c_3\sum_i(X_i^a)^2$, where X_i^a is the imaginary part of Z_i^a (again, c_3 is an appropriate weight). Finally, the feed specification means that the feed network is determined by the characteristic resistances R_i^{BL} of the quarter-wave branch lines. We have $R_i^{BL}=(R_i^aR_i)^{1/2}$, where R_i are the resistances presented to the main feed line by the branch lines and are calculated by solving the equations [5]

$$R_i/R_j=(I_j^2R_j^a)/(I_i^2R_i^a) \tag{3}$$

together with the feed matching condition

$$\sum_i(1/R_i)=1/R^{ML} \tag{4}$$

To meet the requirement that the R_i^{BL} have realistic values, say < 140 Ω, the cost function can include the term $c_4\sum_i g_i$, where $g_i=R_i^{BL}-140$, if this is positive, and $g_i = 0$ otherwise, with c_4 an appropriate weight. If the l_i are all given the fixed value $\lambda/4$, the radiation pattern specification is satisfied by the Dolph-Chebyshev solution [5] listed in Table 1. This solution is inefficient because of the coupling indicated by the complex active impedances of the dipoles (also listed in Table 1).

A solution with the same current set that radiates efficiently and maintains the directivity can be found by perturbing the l_i with the currents fixed. The cost function $C=c_1\sum_s(\Delta S_s)^2+c_2/D_p+c_3\sum_i(X_i^a)^2$ is used, to move to zero the imaginary part of the active impedances while penalizing directivity loss. However, if simultaneous satisfaction of the feed specification is attempted by using the cost function $C=c_1\sum_s(\Delta S_s)^2+c_2/D_p+c_3\sum_i(X_i^a)^2+c_4\sum_i g_i$ with $g_i=R_i^{BL}-140$, no solution is attainable. To obtain the solution given in Table 2, it is necessary to raise the limiting values of the R_i^{BL} to 145 Ω (i.e., $g_i=R_i^{BL}-145$), which provides characteristic impedances associated with coaxial cables difficult to manufacture.

By contrast, if the lengths $2l_i$ and currents I_i are simultaneously varied by using the same cost function (with $g_i=R_i^{BL}-140$), then the desired power pattern, real active impedances and more reasonable R_i^{BL} values can all be achieved together (Table 3).

i	I_i	$2l_i/\lambda$	$Z_i^a\ (\Omega)$
1;12	1.000	0.500	89.7+55.4j
2;11	0.665	0.500	110.1-4.1j
3;10	0.826	0.500	91.6+28.1j
4;9	0.964	0.500	101.2+20.8j
5;8	1.064	0.500	97.0+23.2j
6;7	1.117	0.500	98.6+22.5j
Peak directivity: 57.9			

Table 1. Excitations, lengths and active impedances of the elements of a 12-dipole array when the dipole length is kept uniform ($=\lambda/2$) and the excitations are optimized to generate a Dolph-Chebyshev pattern with -18 dB side lobes. Peak directivity and branch line characteristic impedances are also shown.

i	I_i	$2l_i/\lambda$	$Z_i^a\ (\Omega)$	$R_i^{BL}\ (\Omega)$
1;12	1.000	0.461	70.9	96.6
2;11	0.665	0.498	107.0	145.2
3;10	0.826	0.479	81.7	117.0
4;9	0.964	0.482	90.4	100.3
5;8	1.064	0.481	86.9	90.8
6;7	1.117	0.481	88.2	86.4
Peak directivity: 57.5 Computation time: 1.2 min.				

Table 2. Excitations, lengths and active impedances of the elements of a 12-dipole array after perturbation of the dipole lengths of Table 1 to afford real active impedances and the best possible set of branch line characteristic impedances, keeping excitations fixed. Computation time refers to calculations on a Pentium II running at 266 Mhz.

i	I_i	$2l_i/\lambda$	$Z_i^a\ (\Omega)$	$R_i^{BL}\ (\Omega)$
1;12	1.403	0.466	74.7	119.1
2;11	1.426	0.485	95.4	117.2
3;10	1.456	0.479	82.7	114.8
4;9	1.444	0.490	95.7	115.8
5;8	2.092	0.475	83.1	79.9
6;7	1.875	0.484	90.1	89.1
Peak directivity: 57.0 Computation time: 2.1 min				

Table 3. As for Table 2, but with simultaneous optimization of dipole lengths and excitations.

Acknowledgments

This work was supported by the the U.S. European Office of Aerospace Research and Development (EOARD) and the U.S. Air Force Office of Scientific Research (AFOSR).

References

[1] R. C. Hansen, "Array pattern control and synthesis", *Proc. IEEE*, 1992, vol. 80, pp. 141-151.

[2] H. J. Orchard, R. S. Elliott, and G. J. Stern, "Optimising the synthesis of shaped beam antenna patterns", *Proc. IEE, Pt. H,* 1985, vol. 132, 1, pp. 63-68.

[3] F. Ares, S. R. Rengarajan, and E. Moreno, "Optimization of aperture distributions for sum patterns", *Electromagnetics*, 1996, vol. 16, 2, pp. 129-141.

[4] O. M. Bucci, G. Franceschetti, G. Mazzarella, G. Panariello, "Intersection approach to array pattern synthesis", *Proc. IEE, Pt. H,* 1990, vol. 137, 6, pp. 349-357.

[5] R. S. Elliott, Antenna Theory and Design, Englewood Cliffs, N. J.: Prentice-Hall Inc, 1981.

[6] R. S. Elliott, "An improved design procedure for small arrays of shunt slots", *IEEE Trans. Antennas Propagat.*, 1983, vol. AP-31, pp. 48-54.

[7] R. S. Elliott and G. J. Stern, "The design of microstrip dipole arrays including mutual coupling, Part I: Theory", *IEEE Trans. Antennas Propagat.*, 1981, vol. AP-29, 9, pp. 757-760.

[8] G. J. Stern and R. S. Elliott, "The design of microstrip dipole arrays including mutual coupling, Part II: Experiment", *IEEE Trans. Antennas Propagat.*, 1981, vol. AP-29, 9, pp. 761-765.

[9] H. Yang, N. G. Alexopoulos, P. M. Lepeltier, and G. J. Stern, "Design of transversely fed EMC microstrip dipole arrays including mutual coupling", *IEEE Trans. Antennas Propagat.*, 1990, vol. 38, 2, pp. 145-151.

[10] W. H. Press, S. A. Teukolsky, W. T. Vetterling, and B. P. Flannery, Numerical Recipes, 2nd Ed., Cambridge University Press, 1992, pp. 444-455.

JOURNAL OF ELECTROMAGNETIC WAVES AND APPLICATIONS

PROGRESS IN ELECTROMAGNETICS RESEARCH

Professor J. A. Kong
Room 26-305
77 Massachusetts Avenue
Cambridge, MA 02139, USA

September 17, 1998

Dr. F. Ares
Dpto. Fisica Aplicada
Grupo de Sistemas Radiantes
Facultad de Fisica
Universidad de Santiagode Compostela
15706 Santiago de Compostela
Spain

Dear Dr. Ares:

9808101.LR.Ares: RECALCULATING LINEAR ARRAY ANTENNAS TO COMPENSATE FOR FAILED ELEMENTS WHILE MAINTAINING FIXED NULLS
by M. V. Lozano, J. A. Rodriguez, and F. Ares

Enclosed please find a preprint of the above article, which has been scheduled for publication in the Journal of Electromagnetic Waves and Applications. It contains the information of the year of publication, and issue and page numbers.

Thank you very much for your contribution and with my best regards.

Sincerely yours,

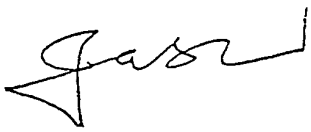

J. A. Kong
Chief Editor

Journal of Electromagnetic Waves and Applications, Vol. 13, 397–412, 1999

RECALCULATING LINEAR ARRAY ANTENNAS TO COMPENSATE FOR FAILED ELEMENTS WHILE MAINTAINING FIXED NULLS

M. V. Lozano, J. A. Rodríguez, and F. Ares

Departamento de Física Aplicada,
Grupo de Sistemas Radiantes
Facultad de Física
Universidad de Santiago de Compostela
15706 Santiago de Compostela, SPAIN

Abstract–A new technique for the synthesis of linear array antenna patterns is presented. This technique allows to fix nulls in prescribed directions, to simulate the presence of failed elements and to obtain power patterns when both situations occur at the same time. These patterns are synthesized by finding the optimal configuration of the array factor roots using the simulated annealing technique. Examples of fixing nulls and/or failed elements in both sum and flat-topped beam patterns are presented.

1. INTRODUCTION

Given a linear array antenna, there exist well-known analytic techniques that can be used to find a radiation pattern with specific requirements about beamwidth and sidelobe level. However, if some elements fail, no analytic means exist to obtain an aperture distribution that compensates for the degradation of the pattern. The defective elements destroy the symmetry and cause sharp variations in the field intensity across the array aperture, increasing the side lobe level of the power pattern. In the literature, there exist some solutions for this problem: in the case of receiving antennas the degradation can be offset by transforming the received pattern [1], another approach uses neural networks to produce a new array transfer function and offers advantages in direction finding in a single signal environment [2]. In

the case of transmitting antennas, the currents of the non-defective elements can often be adjusted to produce a pattern with minimal loss of quality with respect of the original pattern [3–5]. This compensation for the defective elements can be achieved by numerically finding the excitation of each non-defective element that optimizes some objective function.

As far as we know, however, pattern recovery techniques have not hitherto been developed for or applied to the problem of recovering patterns in which nulls have been fixed in certain specific directions. The synthesis of array patterns to obtain nulls in prescribed directions while also having some other generally desirable pattern features (like low sidelobe level, beamwidth, etc.) has received considerable attention [6–9], but not the problem of maintaining fixed nulls in the presence of failed elements.

In this paper, we have used the simulated annealing technique [10] to minimize an objective function in order to obtain a desired linear array power pattern with some defective elements and/or with some fixed nulls. The objective function used takes into account several specifications such as side lobe level, directivity, dynamic range ratio ($|I_{max}/I_{min}|$) and beamwidth.

2. THEORY

The array factor of a linear array of $N+1$ radiating elements laid out at equal intervals d along the z axis with its center at the origin is:

$$F(w) = \sum_{n=0}^{N} I_n w^n = I_N \prod_{n=1}^{N} (w - w_n) \tag{1}$$

where I_n is the complex excitation of the n-th element, $w = e^{j\psi}$ with $\psi = kd\cos(\theta)$, where k is the wavenumber and θ is the angle from endfire, and the roots w_n may be written in the form:

$$w_n = e^{a_n \pm jb_n} \tag{2}$$

Fixing nulls in certain directions means fixing a subset W_o of roots of $F(w)$; for each root w_i in W_o, a_i is left in its initial value (a_i^o) and b_i depends on the angular position of the corresponding null. The failure of element n means that $|I_n| = 0$. We denote the set of defective elements by H.

Given a set W_o of null-fixing roots, a set of defective elements H and a desired side lobe level SLL_d, it is often possible to calculate, for the non-defective elements, excitations producing a pattern with the desired side lobe level and nulls, good peak directivity D, low dynamic range ratio $|I_{max}/I_{min}|$ and also to control the beamwidth. This can be achieved by using the simulated annealing technique to minimize the following objective function:

$$\begin{aligned} C =& c_1|SLL - SLL_d|^2 + c_2|I_{max}/I_{min}|^2 \\ &+ \frac{c_3}{D} + c_4 \sum_{k\in H} |I_k|^2 + c_5|BW - BW_d|^2 \end{aligned} \tag{3}$$

where SLL is the side lobe level, and BW and BW_d are the current beamwidth in the optimization and the desired beamwidth respectively. The coefficients c_i are weights controlling the optimization process. These coefficients must be selected according to the required specifications, i.e., presence of defective elements, fixed nulls or both situations at the same time. Among all the weights, c_1 is one of the most important ones because the final pattern must have a desired side lobe level that is usually the most difficult specification to achieve. However, all the weights are closely connected.

In the following sections we analyze all the cases that the presented algorithm can simulate: null fixing in prescribed directions, element failure simulation and the case in which both situations occur together.

2.1 Fixed Nulls

The nulls in a power pattern are related with the roots of the array factor $F(w)$ since their angular positions are determined by the b_n factors. Then, it is possible to fix nulls in a desired directions (angular positions) associated to specific b_i's. Therefore in the optimization process it is necessary to specify previously both the location of the fixed nulls (which root will contain each fixed root) and their angular positions. The values of a_n are left in their original values to avoid unwanted null-filling. The mathematical expression for the roots variation is:

$$\begin{aligned} b_n &= b_n^f & \forall w_n \in W_o \\ b_n &= b_n^o + \delta b_n & \forall w_n \notin W_o \\ a_n &= a_n^o & \forall n \in \{1, 2, \ldots, N\} \end{aligned} \tag{4}$$

where the superscript o indicates the original value of a_n and b_n,

the superscript f the pre-fixed value of b_n and δb_n the perturbation introduced to b_n^o.

With this perturbation of the roots, the minimization of the objective function (3) is performed in order to obtain the desired power pattern. In the general objective function we set the weight $c_4 = 0$ since the simulation of failed elements is not needed in this case.

2.2 Failed Elements

To simulate failed elements no restrictions are imposed to the variation of the roots, i.e., all the roots are moved and therefore both a_n and b_n for each root are perturbed. This is necessary because, in general, there will be some roots off the Schelkunoff circle when the power pattern has failed elements [11]. Therefore, the variation of the roots is given by:

$$\left.\begin{aligned} a_n &= a_n^o + \delta a_n \\ b_n &= b_n^o + \delta b_n \end{aligned}\right\} \quad \forall n \in \{1, \ldots, N\} \tag{5}$$

In the objective function (3) the weight c_4 must be chosen large enough to ensure small values of the excitations associated to the failed simulated elements (represented in the H set). The other weights are chosen according to the desired specifications of side lobe levels, dynamic range ratio, directivity and beamwidth.

2.3 Fixed Nulls and Failed Elements

With the presented algorithm it is possible to obtain power patterns with failed elements while maintaining fixed nulls. To search the solution eq. (5) is used, maintaining invariable the set of roots associated with fixed nulls. The minimization of the objective function (3) is performed using a high value for the weight c_4 as in the previous subsection.

3. RESULTS

In this section we present some results chosen between all the examples performed to test the method proposed. The method was applied to a sum pattern and to a flat-topped beam pattern and the tests include fixing of nulls, failed elements and failed elements with fixed nulls. At the end of each power pattern analysis we present a table summarizing the results about the desired parameters to optimize, and the computation time required for this optimization. This time has

been measured in a personal computer with a Pentium II processor running at 266 MHz.

3.1 Sum Power Pattern

As a first example we considered a 40-element $(\lambda/2)$-spaced linear array producing a Dolph-Chebyshev sum pattern with a side lobe level of -25 dB [12]. Other parameters of interest are the beamwidth at -3 dB, $9.5°$ (in ψ), the dynamic range ratio, 3.16, and the peak directivity 36.58.

3.1.1 Fixing Nulls

The first operation performed was to fix nulls in certain directions. The selected directions were $\psi = 14°$ and $\psi = 15°$ which are nearby the main lobe. In Figure 1 it is shown the resulting power pattern after the optimization process. The arrow indicates the fixed nulls. The corresponding excitations are shown in Table 1.

3.1.2 Failed Elements

Starting from the initial power pattern, we simulated the presence of defective elements trying to decrease as much as possible the excitations associated with the "failed" elements while maintaining other factors of interest in the design, such as sidelobe level and beamwidth, the most invariable as possible. As an example we simulated the failure of the elements 6^{th} and 32^{nd}. These elements had normalized amplitude excitations of 0.51 and 0.66 respectively in the initial Dolph-Chebyshev power pattern. If the excitations of these elements are directly set to zero the pattern suffers important degradations, as it is shown in dashed line in Figure 2, with an increase of the sidelobe level of about 5 dB. However, if we start from the initial pattern and optimize the objective function, we obtain the power pattern shown in solid line in Figure 2. In Table 2 the final currents (amplitude and phase) of this optimization are shown.

Other examples were performed with successful results, for instance we obtained a good solution for the problem of simulating the presence of a failure in the 20^{th} element which is the most excited one. The final sidelobe level obtained was -24.3 dB.

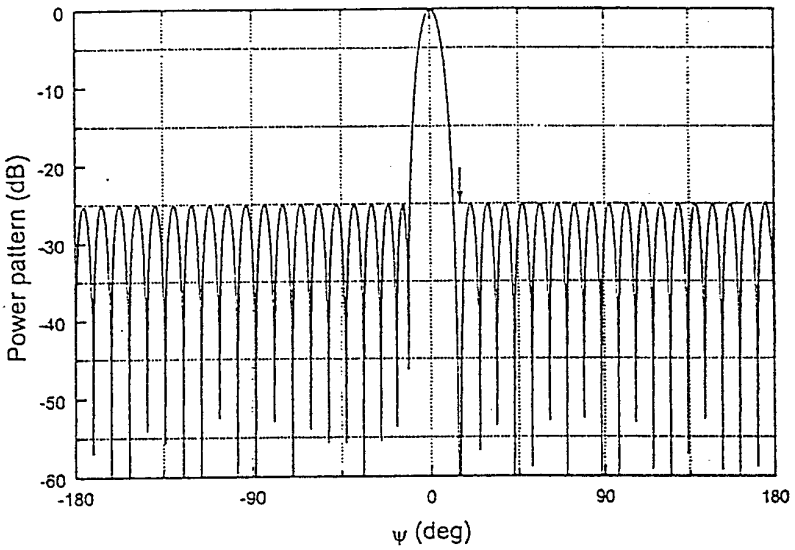

Figure 1. Sum power pattern with two fixed nulls at $\psi = 14°$ and $\psi = 15°$.

Table 1. Excitations associated to a sum power pattern with two fixed nulls in $\psi = 14°$ and $\psi = 15°$.

n	Amplitude	Phase (deg)	n	Amplitude	Phase (deg)
1	0.911	−2.156	21	1.000	−0.228
2	0.279	−1.453	22	0.994	−1.054
3	0.315	0.435	23	0.979	−1.496
4	0.359	0.983	24	0.957	−2.276
5	0.406	2.372	25	0.929	−2.629
6	0.454	2.738	26	0.895	−3.322
7	0.505	3.741	27	0.856	−3.545
8	0.557	3.848	28	0.812	−4.119
9	0.610	4.425	29	0.764	−4.138
10	0.662	4.260	30	0.714	−4.516
11	0.714	4.516	31	0.662	−4.260
12	0.764	4.138	32	0.610	−4.425
13	0.812	4.119	33	0.557	−3.848
14	0.856	3.545	34	0.505	−3.741
15	0.895	3.322	35	0.454	−2.738
16	0.929	2.629	36	0.406	−2.372
17	0.957	2.276	37	0.359	−0.982
18	0.979	1.496	38	0.315	−0.435
19	0.994	1.054	39	0.279	1.452
20	1.000	0.228	40	0.911	2.156

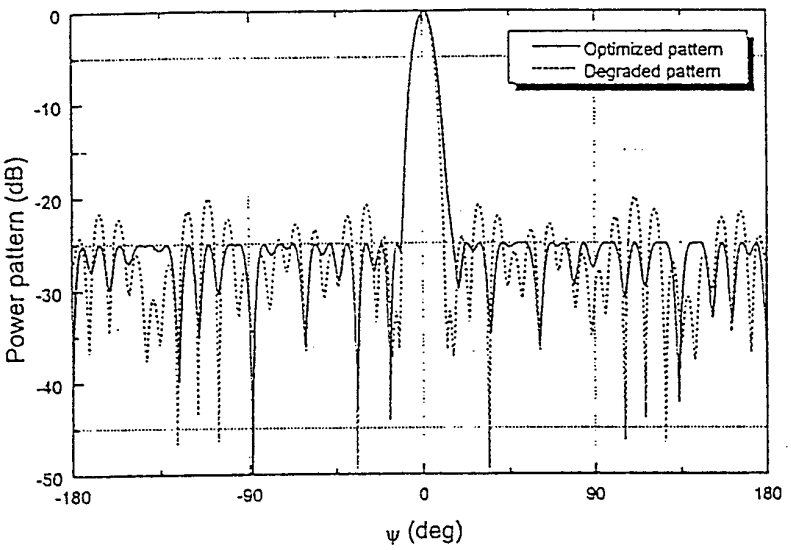

Figure 2. Degraded and recovered power patterns when the radiating elements 6^{th} and the 32^{nd} are failed.

Table 2. Excitations for a sum power pattern with two failed elements, the 6^{th} and the 32^{nd}.

n	Amplitude	Phase (deg)	n	Amplitude	Phase (deg)
1	0.568	4.145	21	0.809	−8.769
2	0.246	−8.735	22	0.926	−8.151
3	0.225	16.198	23	0.840	−9.554
4	0.408	11.693	24	0.918	−5.120
5	0.484	11.452	25	0.882	−18.051
6	0.000	0.000	26	0.801	−11.969
7	0.582	14.874	27	0.544	−21.964
8	0.724	2.577	28	0.698	−14.679
9	0.803	3.958	29	0.436	−12.113
10	0.759	5.193	30	0.695	−18.080
11	0.717	−0.172	31	0.488	−13.497
12	0.793	5.516	32	0.000	0.000
13	0.800	6.499	33	0.392	−19.388
14	0.685	−4.622	34	0.367	−15.202
15	0.959	1.197	35	0.610	−6.802
16	1.000	3.553	36	0.368	−19.754
17	0.916	−7.369	37	0.225	−24.634
18	0.999	−4.382	38	0.349	−14.446
19	0.823	−5.293	39	0.225	−40.717
20	0.982	−7.991	40	0.487	0.000

3.1.3 Fixed Nulls Together with Failed Elements

In the following example four elements were considered as failed elements: the 34^{th}, 35^{th}, 36^{th} and the 37^{th} (their initial normalized amplitude excitations were 0.57, 0.51, 0.46 and 0.41 respectively). Furthermore we fixed two nulls in $\psi = -83.6°$ and $\psi = -82.6°$. The degraded and the optimized power patterns are shown in Figure 3 and the obtained excitations in Table 3.

The information about the optimized parameters for each example performed, sidelobe level, dynamic range ratio, peak directivity, beamwidth and computation time is shown in Table 4.

3.2 Flat-Topped Beam Power Pattern

In this example we used a 40-element $(\lambda/2)$-spaced linear array producing a starting flat-topped beam pattern with -30 dB side lobes and four filled nulls with ± 0.5 dB ripple. The beamwidth at -3 dB is $52°$ (in ψ) and $|I_{max}/I_{min}|$ is 3.35. This initial pattern was obtained by the Orchard-Elliott method [13].

3.2.1 Fixing Nulls

The first example performed in this subsection consists in fixing two nulls in the positions $-37°$ and $-35°$ (ψ values), nearby the main lobe. The roots that contain these nulls are the 16^{th} and the 17^{th}. After the optimization process the pattern obtained is shown in Figure 4 where the resulting dip is indicated with an arrow. In Table 5 the excitations of the resulting pattern are shown.

3.2.2 Failed Elements Simulation

In this case we simulated the presence of three defective elements in the positions 3, 4, and 5 that had an initial normalized amplitude excitations of 0.40, 0.48 and 0.53 respectively. The degraded power pattern with these failed elements is shown in dashed line in Figure 5. It can be seen that the sidelobe level has increased up to -20 dB, 10 dB above the initial sidelobe level. After performing the optimization process a new power pattern was obtained, plotted with solid line in Figure 5, that has again a sidelobe level of -30 dB. The corresponding excitations (amplitude and phase) are shown in Table 6.

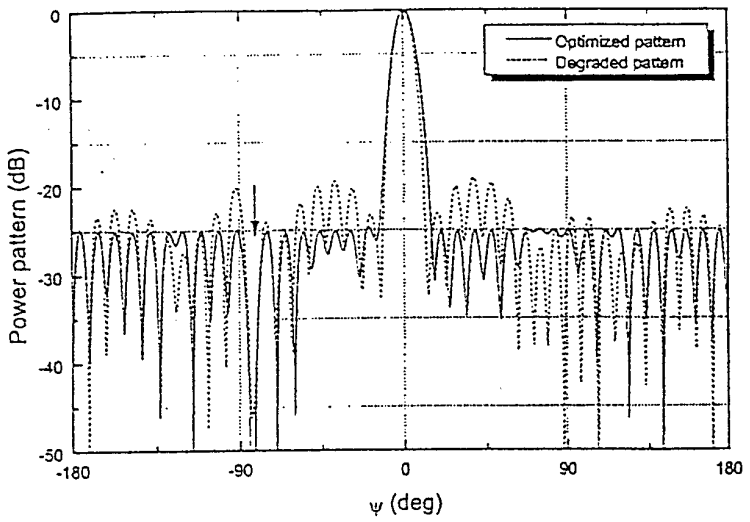

Figure 3. Degraded and optimized power patterns with four defective elements (34,35,36,37) and two fixed nulls in $\psi = -83.6°$ and $\psi = -82.6°$.

Table 3. Excitations for a sum power pattern with 4 defective elements: the 34^{th}, 35^{th}, 36^{th}, and 37^{th}, and two fixed nulls in $\psi = -83.6°$ and $\psi = -82.6°$.

n	Amplitude	Phase (deg)	n	Amplitude	Phase (deg)
1	0.721	6.291	21	0.864	−27.435
2	0.335	−42.504	22	0.760	−24.732
3	0.286	−46.772	23	0.752	−31.932
4	0.376	−0.277	24	0.817	−34.487
5	0.573	−10.571	25	0.619	−28.572
6	0.682	−21.344	26	0.665	−25.658
7	0.813	−14.724	27	0.577	−35.536
8	0.660	−21.723	28	0.495	−32.826
9	0.800	−16.424	29	0.564	−31.294
10	0.836	−19.785	30	0.488	−23.517
11	0.907	−19.432	31	0.350	−31.270
12	0.995	−20.388	32	0.320	−48.453
13	0.939	−15.962	33	0.341	−16.468
14	0.969	−20.619	34	0.000	0.000
15	1.000	−27.772	35	0.000	0.000
16	0.963	−20.886	36	0.000	0.000
17	0.968	−24.631	37	0.000	0.000
18	0.914	−25.816	38	0.250	−25.224
19	0.831	−25.430	39	0.250	−89.240
20	0.927	−24.892	40	0.506	0.000

Table 4. Resulting dynamic range ratio, peak directivity, beamwidth and computation time in the sum power pattern examples.

Failed elements	Fixed nulls position (ψ)	$\left\|\frac{I_{max}}{I_{min}}\right\|$	Peak directivity	Beamwidth at -3 dB	Comp. time
—	$14°, 15°$	3.58	35.76	9.50°	1'24"
$6^{th}, 32^{nd}$	—	4.45	33.43	9.75°	7'11"
20^{th}	—	6.09	33.47	10.00°	6'42"
$34^{th}, 35^{th}$, $36^{th}, 37^{th}$	$-83.6°$, $-82.6°$	4.00	31.93	10.75°	7'46"

3.2.3 Fixed Nulls and Failed Elements

The example performed consisted on fixing a null in $\psi = -36.2°$ and simulate the 11^{th} element as defective (that had a normalized excitation amplitude of 0.88). The degraded power pattern with the 11^{th} element as defective and the recovered pattern with the presence of the fixed null are shown with dashed and solid lines respectively in Figure 6. In this Figure it can be observed that the failed element causes an initial degradation in the power pattern in such a way that the fixing null, in spite of being located in the desired direction, it cannot be seen in the degraded pattern. In the optimized pattern, also showed in Figure 6, the fixed null is indicated with an arrow. The excitations of this recovered flat-topped beam power pattern are shown in Table 7.

Finally, the results about the sidelobe level, dynamic range ratio, beamwidth and computation times for these flat-topped beam examples are shown in Table 8.

4. CONCLUSIONS

The simulated annealing technique, along with an appropriate way of varying the roots of the array factor, allows to obtain power patterns with fixed nulls, defective elements and power patterns with fixed nulls in presence of defective elements. Furthermore, the obtained patterns have suitable properties about sidelobe level, beamwidth, dynamic range ratio and peak directivity.

It can be observed that the recovery of the patterns with clustered failed elements is better than if they are distributed more uniformly along the array. This is related to the fact that the pattern distortion

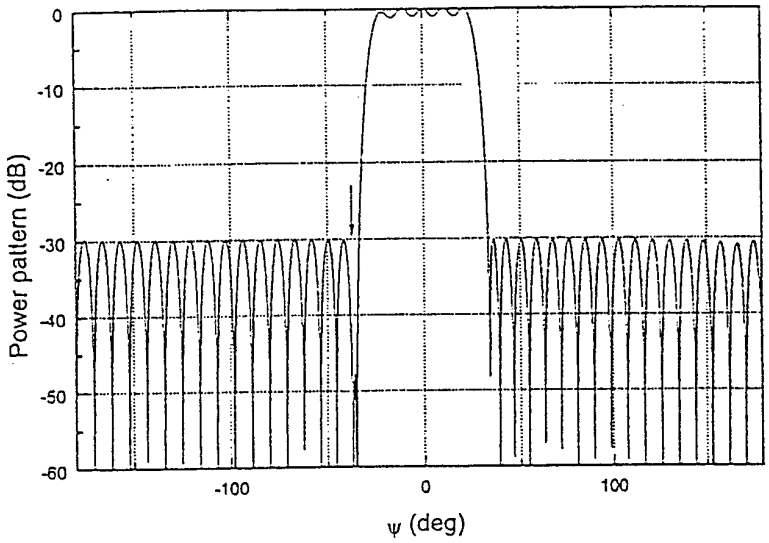

Figure 4. Flat-topped beam power pattern with two fixed nulls in $\psi = -35°$ and $\psi = -37°$.

Table 5. Optimized excitations for a flat-topped beam pattern with fixed nulls in $\psi = -35°$ and $\psi = -37°$.

n	Amplitude	Phase (deg)	n	Amplitude	Phase (deg)
1	0.298	11.044	21	0.499	119.740
2	0.293	7.588	22	0.466	130.797
3	0.390	1.358	23	0.456	153.676
4	0.474	−4.608	24	0.534	179.546
5	0.532	−13.306	25	0.687	198.322
6	0.557	−24.259	26	0.845	210.306
7	0.556	−39.665	27	0.960	218.955
8	0.580	−59.086	28	1.000	226.461
9	0.640	−80.064	29	0.965	234.379
10	0.741	261.430	30	0.864	244.094
11	0.861	247.430	31	0.737	257.153
12	0.955	236.516	32	0.619	−85.021
13	0.991	227.808	33	0.554	−63.882
14	0.954	219.577	34	0.536	−43.665
15	0.846	210.537	35	0.537	−28.756
16	0.693	198.277	36	0.518	−18.153
17	0.544	149.814	37	0.469	−11.576
18	0.465	154.400	38	0.387	−6.363
19	0.470	131.626	39	0.293	−3.811
20	0.500	120.021	40	0.298	0.000

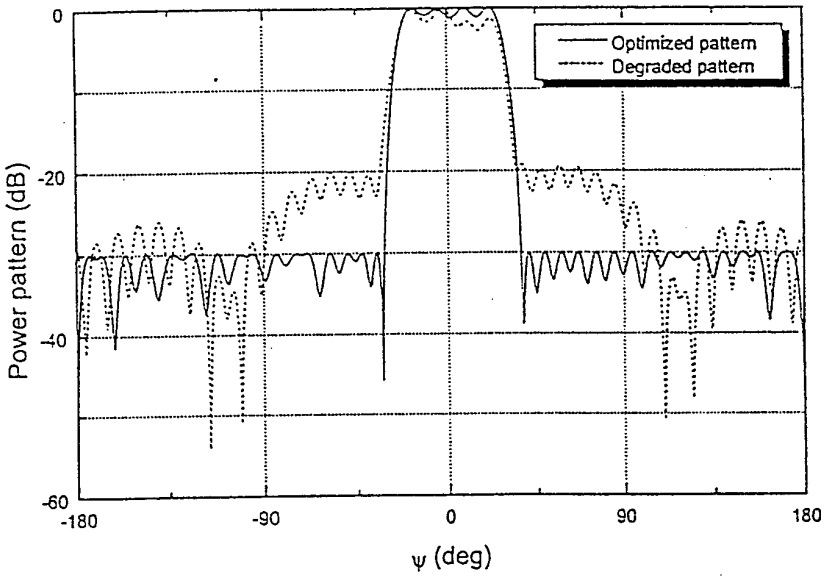

Figure 5. Degraded and optimized flat-topped beam pattern with three failed elements (3^{rd}, 4^{th}, and 5^{th}).

Table 6. Excitations to produce a desired flat-topped beam pattern with three defective elements: the 3^{rd}, 4^{th}, and 5^{th}.

n	Amplitude	Phase (deg)	n	Amplitude	Phase (deg)
1	0.142	8.960	21	0.870	128.794
2	0.135	41.624	22	0.738	138.155
3	0.000	0.000	23	0.515	152.119
4	0.000	0.000	24	0.479	181.265
5	0.000	0.000	25	0.546	212.264
6	0.135	−52.532	26	0.685	227.222
7	0.190	−76.041	27	0.733	235.591
8	0.355	261.166	28	0.769	240.794
9	0.477	261.685	29	0.720	244.654
10	0.595	253.814	30	0.564	255.071
11	0.723	244.549	31	0.423	265.840
12	0.778	236.431	32	0.309	−67.611
13	0.761	227.068	33	0.250	−33.803
14	0.735	210.007	34	0.337	−1.845
15	0.742	193.874	35	0.324	2.357
16	0.765	168.706	36	0.334	12.156
17	0.849	152.288	37	0.337	20.932
18	0.983	140.509	38	0.221	0.993
19	0.999	133.627	39	0.159	38.323
20	1.000	128.888	40	0.135	0.000

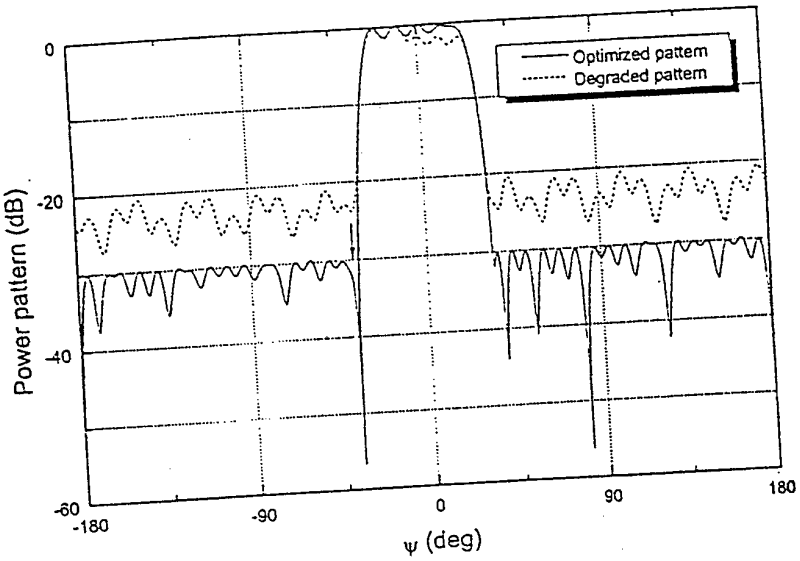

Figure 6. Degraded and recovered flat-topped beam power pattern with the 11^{th} element defective and a fixed null in $\psi = -36.2°$.

Table 7. Excitations for a flat-topped beam pattern with a failure in the 11^{th} element and a fixed null in $\psi = -36.2°$.

n	Amplitude	Phase (deg)	n	Amplitude	Phase (deg)
1	0.169	1.679	21	0.471	260.652
2	0.163	−1.406	22	0.572	240.361
3	0.202	5.157	23	0.763	222.910
4	0.218	−1.198	24	0.933	217.417
5	0.195	−0.207	25	0.999	216.068
6	0.195	−0.179	26	1.000	213.511
7	0.116	−8.830	27	0.933	219.719
8	0.100	−0.268	28	0.807	225.816
9	0.100	37.996	29	0.625	236.879
10	0.100	161.857	30	0.431	258.433
11	0.000	0.000	31	0.422	−58.620
12	0.100	−79.839	32	0.447	−31.628
13	0.141	−57.684	33	0.552	−18.230
14	0.222	−41.112	34	0.633	−7.728
15	0.372	−36.489	35	0.579	−1.220
16	0.526	−35.529	36	0.529	2.904
17	0.533	−35.649	37	0.410	5.021
18	0.573	−38.280	38	0.324	11.632
19	0.508	−50.727	39	0.199	7.576
20	0.458	−68.774	40	0.151	0.000

Table 8. Resulting dynamic range ratio, peak directivity, beamwidth and computation time in the flat-topped beam power pattern examples.

Failed elements	Fixed nulls position (ψ)	$\left\|\frac{I_{max}}{I_{min}}\right\|$	Beamwidth at -3 dB	Computation time
—	$-37°, -35°$	3.41	52°	2'33"
$3^{rd}, 4^{th}, 5^{th}$	—	7.39	51°	9'17"
11^{th}	$-36.2°$	10.03	52°	10'17"

caused if all the defective elements are close together consists largely in a relatively localized increase in side lobe level, whereas the increase is general if there are defective elements throughout the array.

Fixing nulls in the power pattern also has effects on the convergence of the algorithm, but not as important as simulating elements failure. The examples presented demonstrate the capability of the algorithm of fixing nulls very close to the main lobe or the shaped region, which is a considerable advantage for some applications.

Finally, with slight changes in the algorithm it is possible to obtain power patterns with symmetric fixed nulls, and the computation time decreases drastically. The key factor is to optimize the pattern in a symmetric way, i.e., only taking into account half of the array factor roots. Nevertheless, if failed elements are introduced, the results are worse than in the presented algorithm because the simulated annealing uses fewer variables to find the optimal solution.

ACKNOWLEDGEMENT

This work was supported by the European Office of the US Aerospace Research and Development Board (EOARD) and the US Air Force Office of Scientific Research (AFOSR).

REFERENCES

1. Mailloux, R. J., "Array failure correction with a digitally beamformed array," *IEEE Transactions on Antennas and Propagation*, Vol. 44, 1543–1550, 1996.
2. Simmers, J., H. L. Southall, and T. O'Donnell, "Advances in neural beamforming," in *Proc. '93 Antennas Appl. Symp.*, Univ. Illinois, Urbana-Champaign, 206–219, 1993.
3. Sim, S. L., and M. H. Er, "Sidelobe suppression for general arrays

in the presence of element failures," *Electronics Letters,* Vol. 33, 1278–1280, 1996.
4. Peters, T. J., "Conjugate gradient-based algorithm to minimize de sidelobe level of planar arrays with element failures," *IEEE Transactions on Antennas and Propagation,* Vol. 39, 1497–1504, 1991.
5. Rodríguez, J. A., and F. Ares, "Optimization of the performance of arrays with failed elements using the simulated annealing technique," *Journal of Electromagnetic Waves and Applications,* Vol. 12, 1625–1637, 1998.
6. Trastoy, A., and F. Ares, "Linear array pattern synthesis with minimum sidelobe level and null control," *Microwave and Optical Technology Letters,* Vol. 16, 322–325, 1997.
7. Ares, F., A. Vieiro, E. Moreno, and S. R. Rengarajan, "Extension of Orchard's pattern synthesis technique for overdetermined systems," *Electromagnetics,* Vol. 17, 15–23, 1997.
8. Steyskal, H., R. A. Shore, and R. L. Haupt, "Methods for null control and their effects on the radiation pattern," *IEEE Transactions on Antennas and Propagation,* Vol. 34, 404–409, 1986.
9. Haupt, R. L., "Phase-only adaptive nulling with a genetic algorithm," *IEEE Transactions on Antennas and Propagation,* Vol. 45, 1009–1014, 1997.
10. Press, W. H., W. T. Vetterling, S. A. Teukolsky, and B. P. Flannery, *Numerical Recipes in C,* Second Edition, Cambridge, 444–455, 1992.
11. Haupt, R. L., "Unit circle representation of aperiodic arrays," *IEEE Transacations on Antennas and Propagation,* Vol. 43, 1152–1156, 1995.
12. Dolph, C. L., "A current distribution for broadside arrays which optimizes the relationship between beamwidth and side lobe level," *Proc. IRE,* 34, 335–48, 1946.
13. Orchard, H. J., R. S. Elliott, and G. J. Stern, "Optimising the synthesis of shaped beam antenna patterns," *Proc., IEE. Pt. H.,* Vol. 132, 63–67, 1985.

Manuel Vicente-Lozano was born in Madrid, Spain, in 1972. He received his B.S. and M.S. degrees in Physics from the University of Santiago de Compostela, Spain. Nowadays he is a Ph.D. student in Physics. His main research activities are focused in microwave circuits and antenna array pattern synthesis. Other activities or interests are programming languages and computer science.

Juan A. Rodríguez-Gonzalez was born in Orense, Spain, in 1972. He received his B.S. and M.S. degrees in Physics from the University of Santiago de Compostela, Spain. He was also presenting several subjects related to electromagnetics at the Open National University Associated Centre in Pontevedra, Spain, for two years. At present, he is preparing his Ph.D. in Physics about antenna array pattern synthesis. His general research interests include numerical methods in solving electromagnetic problems and pattern synthesis. He is also interested in computer programming and software engineering.

Francisco J. Ares-Pena received the B.S. and M.S. degrees from the University of Santiago de Compostela, Spain, in 1986 and 1987 respectively, and the Ph.D. from the same institution in 1993, all in Physics. He is currently an Associate Professor in the Department of Applied Physics at the University of Santiago de Compostela, Spain. He has published more than 70 journal and conference papers. Dr. Ares is a Senior Member of IEEE and a member of the New York Academy of Sciences. His main research interests are antenna array pattern synthesis and design of slot arrays.

RECALCULATING LINEAR ARRAY ANTENNAS TO COMPENSATE FOR FAILED ELEMENTS WHILE MAINTAINING FIXED NULLS

M. V. Lozano, J. A. Rodríguez, F. Ares*
Departamento de Física Aplicada, Grupo de Sistemas Radiantes
Facultad de Física, Universidad de Santiago de Compostela
15706 Santiago de Compostela, SPAIN
E-mail: faares@usc.es
Fax: +34 981 520676

Abstract
Given the failure of one or more elements of an array antenna designed to produce a radiation pattern including nulls in arbitrarily fixed directions, a pattern with the desired side lobe level and nulls can often be recovered by modifying the excitations of the non-defective elements. The modified excitations can be calculated by simulated annealing using an appropriate cost function.

1. INTRODUCTION

The radiation pattern produced by an array antenna is in general severely degraded by the failure of even a very small number of the array elements. In the case of receiving antennas, the degradation can be offset by transforming the received pattern [1]. In the case of transmitting antennas, the excitations of the non-defective elements can often be adjusted to produce a pattern with minimal loss of quality with respect to the original pattern [2-4]. As far as we know, however, pattern recovery techniques have not hitherto been developed for or applied to the problem of recovering patterns in which nulls have been fixed in certain specific directions. The problem of null-fixing itself has received considerable attention [5-8], but not the problem of maintaining fixed nulls in the presence of element failure. In this paper we report that, for linear arrays, fixed nulls and side lobe levels can both be recovered, with minimal increase in beamwidth and in the dynamic range ratio of the element excitations, if the excitations of non-defective elements are recalculated by simulated annealing using an appropriate cost function.

2. THEORY

The array factor of a linear array of N+1 radiating elements laid out at equal intervals d along the z axis with its centre at the origin is

$$F(w) = \sum_{n=0}^{N} I_n w^n = I_N \prod_{n=1}^{N} (w - w_n) \qquad (1)$$

where I_n is the complex excitation of the n-th element, $w = \exp(j\psi)$ ($\psi = kd\cos(\theta)$, where k is the wavenumber and θ the angle from endfire), and the roots w_n may be written in the form $w_n = \exp(a_n + jb_n)$. Fixing nulls in certain

directions means fixing a subset W_0 of roots of $F(w)$; for $w_i \in W_0$, $a_i = 0$ and b_i depends on the angular position of the corresponding null. The failure of element n means that $I_n = 0$; we denote the set of defective elements by H.

Given a set W_0 of null-fixing roots, a set of defective elements H and a desired side lobe level SLL_d, it is often possible to calculate, for the non-defective elements, excitations producing a pattern with the desired side lobe level and nulls, good peak directivity D and low dynamic range ratio $|I_{max}/I_{min}|$. This can be achieved using simulated annealing to minimize the cost function

$$C = c_1\left|SLL - SLL_d\right|^2 + c_2\left|I_{max} / I_{min}\right|^2 + \frac{c_3}{D} + c_4 \sum_{k \in H}\left|I_k\right| \qquad (2)$$

where SLL is side lobe level and the c_i are weights controlling the optimization process (c_4 must be large to ensure that the "optimized excitations" of the defective elements are effectively zero); the optimization is carried out by introducing slight perturbations in the values of a_n and b_n for non-fixed roots.

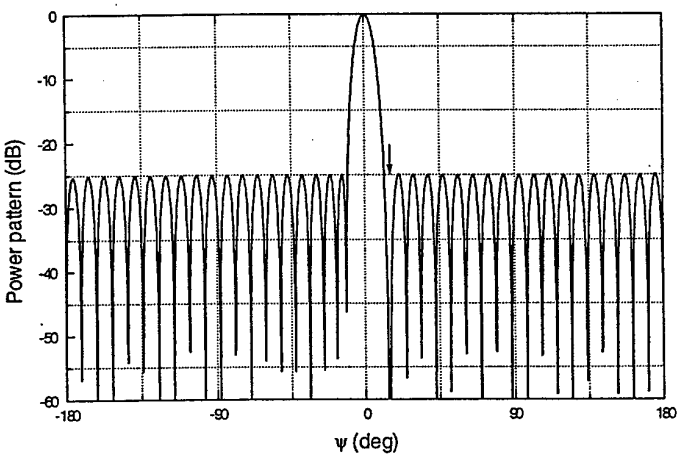

Fig.1. Sum power pattern with two fixed nulls at $\psi = 14°$ and $\psi = 15°$.

3. EXAMPLES

As a first example, we consider a 40-element ($\lambda/2$)-spaced linear array required to produce an initial sum power pattern with -25 dB side lobe level. In this array two nulls in $\psi = 14°$ and $\psi = 15°$ were fixed. The final obtained pattern is shown in Figure 1. Other examples including fixed nulls together with failed elements (to be shown in the symposium) were performed using the initial sum power pattern. Table 1 summarises the obtained results about the sidelobe level, dynamic range ratio, beamwidth and computation times, measured in a

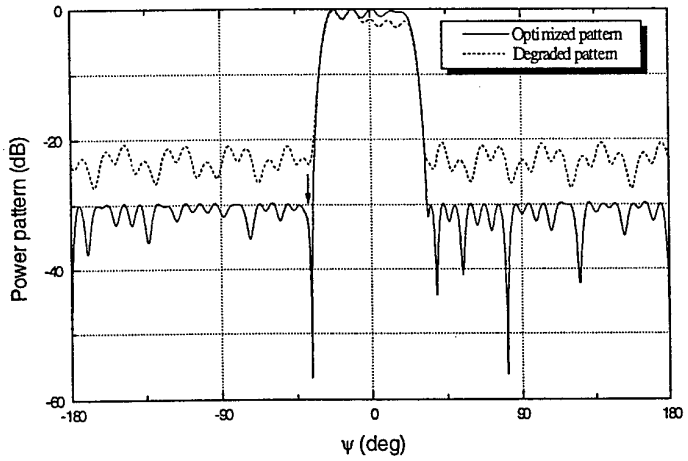

Fig. 2. Degraded and recovered flat-topped beam power pattern with the 11^{th} element defective and a fixed null in ψ=-36.2°

Pentium II at 266Mhz, for this and other sum power pattern examples performed.

Another example consisted in using the same linear array, but producing a starting flat-topped beam pattern with –30dB side lobes and four filled nulls with ±0.5 dB ripple. In Figure 2 it is shown the degraded and the recovered power pattern when the 11^{th} element is simulated as defective and a null is fixed in ψ = -36.2°. In Table 2, there are shown the results about this and other flat-topped beam power pattern examples.

Failed elements	Fixed nulls position (ψ)	$\lvert I_{max}/I_{min}\rvert$	Peak directivity	Beamwidth at –3dB	Computation time
----	14°,15°	3.58	35.76	9.50°	1' 24''
6^{th} ,32^{nd}	----	4.45	33.43	9.75°	7' 11''
20^{th}	----	6.09	33.47	10.00°	6' 42''
34^{th},35^{th},36^{th},37^{h}	-83.6°, -82.6°	4.00	31.93	10.75°	7' 46''

Table 1. Dynamic range ratio, peak directivity, beamwidth and computation time in several sum power pattern examples.

Failed elements	Fixed nulls position (ψ)	$\lvert I_{max}/I_{min}\rvert$	Beamwidth at -3dB	Computation time
----	-37°,-35°	3.41	52°	2' 33''
3^{th} ,4^{th},5^{th}	----	7.39	51°	9' 17''
11^{th}	-36.2°	10.03	52°	10' 17''

Table 2. Dynamic range ratio, peak directivity, beamwidth and computation time in some flat-topped beam power pattern examples.

4. FINAL REMARKS

1) As was done in synthesizing the pattern of Fig.1, the method described in Section 2 can be used to fix nulls in the patterns of non-defective antennas. This approach to null-fixing can fix nulls very close to the main beam.
2) When more than one element fails, the pattern recovered by the method described in this communication is generally better if the defective elements form a cluster than if they are distributed more uniformly along the array (see Tables 1 and 2). This is related to the fact that the pattern distortion caused if all the defective elements are close together consists largely in a relatively localized increase in side lobe level, whereas the increase is general if there are defective elements throughout the array.

Acknowledgements

This work was supported by the European Office of the US Aerospace Research and Development Board (EOARD) and the US Air Force Office of Scientific Research (AFOSR).

References

[1] R. J. Mailloux, "Array failure correction with a digitally beamformed Array", IEEE *Transactions on Antennas and Propagation*, Vol. 44, 12, pp. 1543-1550,1996.

[2] S. L. Sim and M. H. Er, "Sidelobe suppression for general arrays in the presence of element failures", *Electronics Letters*, Vol. 33, 15, pp. 1278-1280, 1997.

[3] T. J. Peters, "Conjugate gradient-based algorithm to minimize de sidelobe level of planar arrays with element failures", *IEEE Transactions on Antennas and Propagation*, Vol. 39, 10, pp. 1497-1504, 1991.

[4] J.A. Rodríguez and F. Ares, "Optimization of the perfomance of arrays with failed elements using the simulated annealing technique", Journal of Electromagnetic Waves and Applications, Vol. 12, pp. 1625-1637, 1998.

[5] A. Trastoy and F. Ares, "Linear array pattern synthesis with minimum sidelobe level and null control", *Microwave and Optical Technology Letters*, Vol. 16, 15, pp. 322-325, 1997.

[6] F. Ares, A. Vieiro, E. Moreno, and S. R. Rengarajan,. "Extension of Orchard's pattern synthesis technique for overdetermined systems", *Electromagnetics*, Vol. 17, 1, pp. 15-23, 1997.

[7] H. Steyskal, R. A. Shore and R. L. Haupt, "Methods for null control and their effects on the radiation pattern", *IEEE Transactions on Antennas and Propagation*, Vol. 34, 3, pp. 404-409, 1986.

[8] R. L. Haupt, "Phase-only adaptive nulling with a genetic algorithm", *IEEE Transactions on Antennas and Propagation,* Vol. 45, 6, pp. 1009-1014, 1997.

JOURNAL OF ELECTROMAGNETIC WAVES AND APPLICATIONS

PROGRESS IN ELECTROMAGNETICS RESEARCH

Professor J. A. Kong
Room 26-305
77 Massachusetts Avenue
Cambridge, MA 02139, USA

October 12, 1998

Dr. F. Ares
Dpto. Fisica Aplicada
Grupo de Sistemas Radiantes
Facultad de Fisica
Universidad de Santiagode Compostela
15706 Santiago de Compostela
Spain

Dear Dr. Ares:

9809121.R.Ares: OPTIMAL COMPROMISE BETWEEN SUM AND DIFFERENCE PATTERNS WHILE FIXING QUASI-NULLS IN BOTH by J. A. Rodriguez, and F. Ares

Enclosed please find a preprint of the above article, which has been scheduled for publication in the Journal of Electromagnetic Waves and Applications. It contains the information of the year of publication, and issue and page numbers.

Thank you very much for your contribution and with my best regards.

Sincerely yours,

J. A. Kong
Chief Editor

Journal of Electromagnetic Waves and Applications, Vol. 13, 655–664, 1999

OPTIMAL COMPROMISE BETWEEN SUM AND DIFFERENCE PATTERNS WHILE FIXING QUASI-NULLS IN BOTH

J. A. Rodriguez and F. Ares

Departmento de Física Aplicada
Grupo de Sistemas Radiantes
Facultad de Física
Universidad de Santiago de Compostela
15706 Santiago de Compostela
SPAIN

Abstract–Methods previously developed for designing linear array monopulse antennas with relatively simple feed network requirements are extended to allow the suppression of jamming signals in both sum and difference modes.

1. INTRODUCTION

High-performance monopulse array antennas must generate both sum and difference patterns with low side lobes, high directivity and narrow beamwidth. They are also often required to operate in situations in which intentional or unintentional jamming signals are being received from certain directions. To counteract such interferences, both the sum and difference patterns of the antenna must feature nulls or quasi-nulls (highly depressed responses) in these directions. Although this can certainly be achieved by synthesizing the sum and difference patterns by means of excitation distributions that are mutually independent [1], this approach maximizes the complexity and cost of feed networks. Haupt [2] showed how nulls can be introduced into given sum and difference patterns with minimal modification requirements by assigning each element a phase shift or complex factor modifying both its sum and difference excitations, but assumed that for high pattern quality the original sum and difference patterns would have to be generated

by independent excitation distributions. For linear arrays with $2N$ elements it is possible to synthesize sum and difference patterns with common arbitrary nulls using a sum distribution that is periodic with period N and a difference distribution that is the same as the sum distribution except for a phase inversion affecting half the elements, but the resulting pattern quality can be rather poor [3]. Lee [4] sought a compromise between pattern quality and feed network simplicity by modifying Chebyshev and Bayliss distributions so that the outer elements have the same excitations for both sum and difference modes (except for the phase inversion affecting one side of the distribution) while the sum and difference excitations of the inner elements are obtained by phase-shifting the original Chebyshev and Bayliss excitations respectively; however, this compromise clearly favours pattern quality more than feed network simplicity.

In previous work [5, 6] we developed synthesis methods that, without tackling the jammer neutralization problem, significantly reduced the feed network complexity of monopulse array antennas by forcing certain excitation parameters to be shared among elements or between modes. Specifically, we showed that by using simulated annealing [7] to optimize appropriate objective functions, high-quality patterns can be synthesized in which either the excitation amplitude of each element is the same for both the sum and difference patterns ("phase-only control") or the difference pattern is obtained by multiplying the sum excitations of all the elements in each of a series of subarrays by a single subarray weight (Fig. 1). In this paper we report the extension of these methods to allow the introduction of arbitrary quasi-nulls common to the sum and difference patterns.

2. METHODS

2.1 Phase-Only Control

We assume that the phase-only control method described in [5] for planar arrays has been used to calculate the amplitudes A_i, sum pattern phases α_i and difference pattern phases β_i of compromise excitation distributions for a linear array of $2N$ elements, and that the sum and difference distributions are respectively symmetric and antisymmetric about the centre of the array so as to generate symmetric sum and dif-

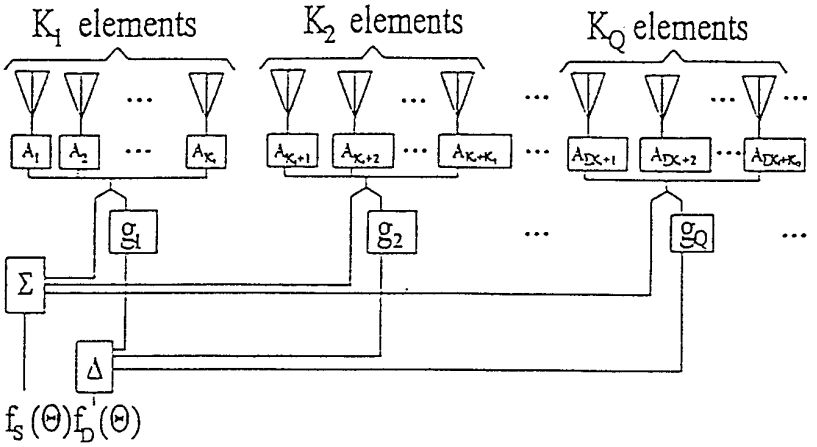

Figure 1. Subarray method: configuration of the element and subarray weighting devices of one side of a monopulse linear array antenna.

ference patterns. We wish to introduce quasi-nulls in given directions θ_j (measured from broadside). In keeping with the "phase-only" philosophy, we do so by altering the phases α_i and β_i by increments $\delta\alpha_i$ and $\delta\beta_i$ respectively, and we maintain the symmetry or antisymmetry of the distributions. The increments $\delta\alpha_i$ and $\delta\beta_i$ are calculated by using simulated annealing to optimize the cost function

$$C(\delta\alpha,\delta\beta) = c_1 \cdot \left\{ [SLL_{\Sigma o} - SLL_{\Sigma d}]^2 + [SLL_{\Delta o} - SLL_{\Delta d}]^2 \right\} + c_2 \cdot \sum_j \left\{ [F(\theta_j)_{\Sigma o} - F(\theta_j)_{\Sigma d}]^2 + [F(\theta_j)_{\Delta o} - F(\theta_j)_{\Delta d}]^2 \right\} \tag{1}$$

where $\delta\alpha$ and $\delta\beta$ are the vectors of $\delta\alpha_i$ and $\delta\beta_i$, SLL indicates a side lobe level and $F(\theta_j)$ the value of the power pattern in the direction θ_j, subscript Σ indicates the sum distribution or pattern and subscript Δ the difference distribution or pattern, subscript d indicates the desired value of a variable or parameter and subscript o the value obtained with the current arguments $\delta\alpha$ and $\delta\beta$, and c_1 and c_2 are weighting factors controlling the balance between maintenance of desired side lobe levels and suppression of interferences in the directions θ_j. A broad quasi-null extending over a finite angular

interval $[\theta_{\text{start}}, \theta_{\text{end}}]$ can be obtained by specifying a large number of point quasi-nulls θ_j within this interval.

2.2 Subarraying

In the subarray method for linear arrays described previously [5, 6] the sum pattern is generated by a Taylor or Dolph-Chebyshev distribution and the real subarray weights g_q are optimized to make the difference pattern as good as possible using a cost function involving only difference pattern characteristics. This approach, which leaves the original sum pattern unchanged, is not possible when nulls or quasi-nulls are to be imposed in both the difference and sum patterns. In this situation, for a $2N$-element array the cost function must also optimize the sum excitations A_i (constrained to be real and symmetric about the centre of the array) and control the characteristics of both the sum and difference patterns. A suitable cost function is

$$\begin{aligned} C(A,g) = {} & c_1 \cdot \left\{ [SLL_{\Sigma o} - SLL_{\Sigma d}]^2 + [SLL_{\Delta o} - SLL_{\Delta d}]^2 \right\} \\ & + c_2 \cdot \sum_j \left\{ \left[F(\theta_j)_{\Sigma o} - F(\theta_j)_{\Sigma d}\right]^2 + \left[F(\theta_j)_{\Delta o} - F(\theta_j)_{\Delta d}\right]^2 \right\} \\ & + c_3 \cdot \{ |A_{\max}/A_{\min}| + |B_{\max}/B_{\min}| \} \end{aligned} \tag{2}$$

where $A = (A_1, \cdots, A_N)'$, $g = (g_1, \cdots, g_Q)'$ (Q is the number of subarrays on each side of the array centre, about which the difference excitation distribution is constrained to be antisymmetric), $A_{\max}$ and $A_{\min}$ are respectively the greatest and least of the A_i, $B_{\max}$ and $B_{\min}$ are respectively the greatest and least of the $B_i = A_i g_{q(i)}$, and c_3 is a weight analogous to c_1 and c_2. The optimization method is, as usual, simulated annealing.

3. EXAMPLES

In this section we illustrate the above techniques by applying them to a linear array of 50 equispaced elements one half wavelength apart. In all cases, the desired power level specified for quasi-nulls was -60 dB, which is in most situations sufficient to neutralize jammers. The sum and difference patterns plotted in Figs. 2–6 have been normalized to their respective peak directivities. None of the calculations took more than 5 min on a personal computer with a Pentium II running at 266 MHz.

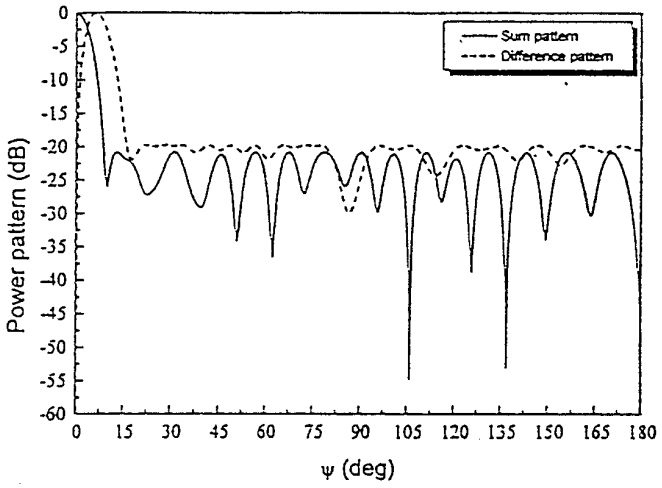

Figure 2. Sum and difference patterns of a 50-element antenna obtained by the phase-only control method [5] specifying −20 dB side lobes but no fixed quasi-nulls.

3.1 Phase-Only Control

Fig. 2 shows, as functions of $\psi = \pi \sin\theta$, the compromise sum and difference patterns that were obtained, without specification of nulls or quasi-nulls, by the phase-only control design method previously described for planar arrays [5]. The side lobe levels of the sum and difference patterns are −20.8 and −19.7 dB respectively, and the dynamic range ratio $|A_{\max}/A_{\min}|$ is 1.29.

Fig. 3 and Fig. 4 show the results of using the method of Section 2.1 to modify the excitation distributions corresponding to the patterns of Fig. 2 so as to introduce quasi-nulls at $\psi = 40°$, 80° and 120° (Fig. 3) or throughout the interval $[50°, 60°]$ (Fig. 4). The side lobe levels of the sum and difference patterns are now −19.6 and −17.0 dB respectively in the former case, and respectively −17.7 and −14.4 dB in the latter.

3.2 Subarraying

For best results, application of the subarraying technique to the 50-

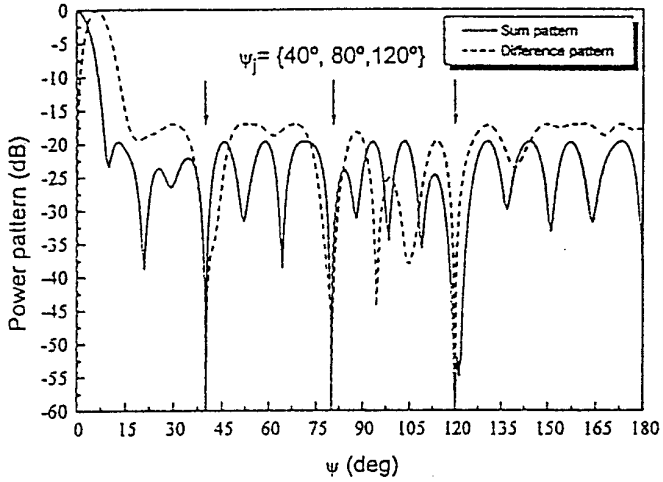

Figure 3. Sum and difference patterns obtained by using the phase-only method to introduce quasi-nulls at $\psi = 40°$, 80° and 120° in the patterns of Fig. 2.

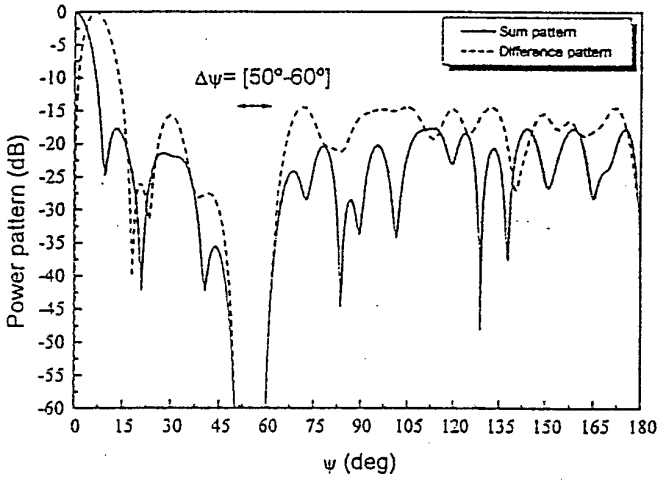

Figure 4. Sum and difference patterns obtained by using the phase-only method to introduce a broad quasi-null over the interval $50° \leq \psi \leq 60°$ in the patterns of Fig. 2.

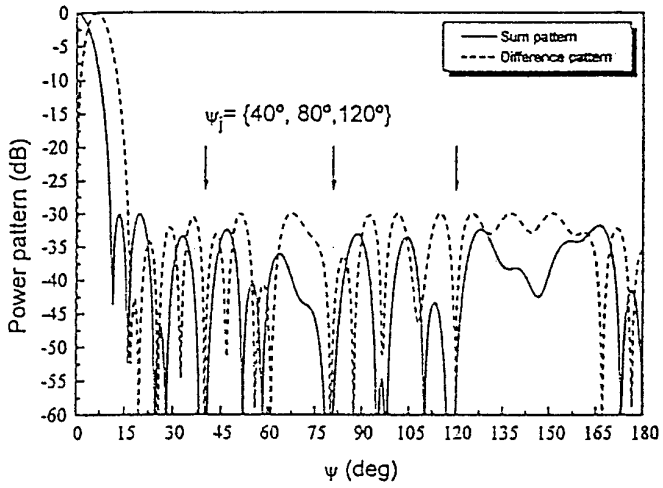

Figure 5. Sum and difference patterns obtained using the subarray method to fix quasi-nulls at $\psi = 40°$, $80°$ and $120°$ while ensuring side lobe levels of -30 dB.

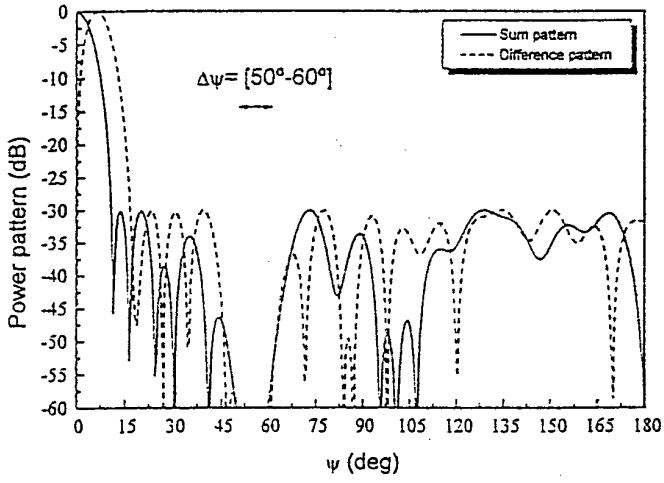

Figure 6. Sum and difference patterns obtained using the subarray method to fix a broad quasi-null over the interval $50° \leq \psi \leq 60°$ while ensuring side lobe levels of -30 dB.

element array required the use of four subarrays in each half of the antenna: one comprising two elements and the other three comprising three each (the remaining fourteen elements on each side receive the same excitation for both sum and difference patterns). Fig. 5 shows the results obtained when quasi-nulls were specified at $\psi = 40°$, $80°$ and $120°$ and side lobe levels of -30 dB were required in both sum and difference patterns. The specified side lobe levels have been achieved for both patterns, with dynamic range ratios of 1.32 and 1.93 for the sum and difference patterns respectively.

Fig. 6 shows the results of subarraying to achieve a broad quasi-null covering the interval $50° \leq \psi \leq 60°$ together with side lobe levels of -30 dB in both patterns. Again, both these goals have been met, with dynamic range ratios of 1.56 and 1.87 for the sum and difference patterns respectively.

3.3 Addendum: Phase and Amplitude Perturbation

In view of the relatively large rise in side lobe levels when a broad quasi-null was introduced using phase-only control (Section 3.1), we resorted to perturbation of both phases and amplitudes, adding the term $c_4 \cdot (\nu - \max\{|\delta A_i|/A_i\})^2$ to the cost function so as to limit the relative magnitude of the perturbations. Table 1 lists the side lobe levels and dynamic range ratios achieved with various specified values of ν (the desired quasi-null was achieved in all cases). As might be expected, as ν increases the side lobe levels improve but the dynamic range ratio also increases.

$\nu = \max\{\|\delta A_i\|/A_i\}$	$SLL_{\Sigma o}$	$SLL_{\Delta o}$	$\|A_{\max}/A_{\min}\|$
10%	-18.6 dB	-15.4 dB	1.30
25%	-19.5 dB	-16.4 dB	1.36
50%	-19.9 dB	-17.7 dB	1.57

Table 1. Side lobe levels and dynamic range ratios achieved by perturbing both the phases and amplitudes of the distributions corresponding to Fig. 2 so as to introduce a broad quasi-null over the interval $50° \leq \psi \leq 60°$, for various values of ν in the cost function.

4. CONCLUSIONS

Of the two techniques extended in this paper to allow specification of common quasi-nulls in sum and difference patterns, the better appears to be the subarraying technique, at least as regards achievement of side lobe level specifications. This may be attributed to its reducing, by means of its subarray weights, the discontinuity present in the unweighted difference excitation distribution at the centre of the array. As regards ease of implementation for antennas that must be able to adapt to changing jamming environments, the phase-only control method requires $2N$ fixed amplitude attenuators calculated for the starting patterns, together with either $2N$ fixed phase-shifters and $2N$ variable phase-shifters, or $4N$ variable phase-shifters; the subarray method requires $2N + 2Q$ variable amplitude attenuators. Both methods appear to conserve pattern quality significantly better than do previously published methods using feed networks of comparable complexity. Both can be extended to planar arrays.

ACKNOWLEDGMENT

This work has been supported by the Xunta de Galicia under Project XUGA 20601B98 and by the U.S. European Office of Aerospace Research and Development (EOARD) and by the U.S. Air Force Office of Scientific Research (AFOSR).

REFERENCES

1. Steyskal, H., R. A. Shore, and R. L. Haupt, "Methods for null control and their effects on the radiation pattern," *IEEE Trans. Antennas Propagat.*, Vol. 34, 404–409, 1986.
2. Haupt, R. L., "Simultaneous nulling in the sum and difference patterns of a monopulse antenna," *IEEE Trans. Antennas Propagat.*, Vol. 32, 486–493, 1984.
3. Vu, T. B., "Simultaneous nulling in sum and difference patterns by amplitude control," *IEEE Trans. Antennas Propagat.*, Vol. 31, 163–166, 1986.
4. Lee, T., "Simultaneous nulling for monopulse array with partially adaptive weights," *IEEE Trans. Antennas Propagat.*, Vol. 42, 928–935, 1994.
5. Ares, F., S. R. Rengarajan, J. A. Rodriguez, and E. Moreno, "Optimal compromise among sum and difference patterns," *Journal*

of Electromagnetic Waves and Applications, Vol. 10, 1543–1555, 1996.

6. Ares, F., S. R. Rengarajan, J. A. Rodriguez, and E. Moreno, "Optimal compromise among sum and difference patterns through sub-arraying," *IEEE Antennas and Propagation Society International Symposium,* 1142–1146, Baltimore, Maryland, 1996.
7. Kirkpatrick, S., C. D. Gelatt, and M. P. Vecchi, "Optimization by simulated annealing," *Science,* Vol. 220, 4598, 671–679, 1983.

Juan A. Rodriguez-Gonzalez was born in Orense, Spain, in 1972. He received his B.S. and M.S. degrees in Physics from the University of Santiago de Compostela, Spain. He was also presenting several subjects related to electromagnetics at the Open National University Associated Centre in Pontevedra, Spain, for two years. At present, he is preparing his Ph.D. in Physics about antenna array pattern synthesis. His general research interests include numerical methods in solving electromagnetic problems and pattern synthesis. He is also interested in computer programming and software engineering.

Francisco J. Are-Pena received the B.S. and M.S. degrees from the University of Santiago de Compostela, Spain, in 1986 and 1987 respectively, and Ph.D. from the same institution in 1993, all at Physics. He is currently an Associate Professor in the Department of Applied Physics at the University of Santiago de Compostela, Spain. He has published more than 70 journal and conference papers. Dr. Ares is a Senior Member of IEEE and a member of the New York Academy of Sciences. His main research interests are antenna array pattern synthesis and design of slot arrays.

electromagnetics

EDITOR-IN-CHIEF
H.Y. David Yang, Ph.D.
1120 SEO, M/C 154
Department of EECS
University of Illinois at Chicago
Chicago, IL 60607-7053
(312) 996-0675 • Fax: (312) 413-0024
E-mail: hyang@eecs.uic.edu

December 15, 1998

Dr. F. Ares
Departamento de Fisica Aplicada
Universidad de Santiago de Compostela
15706 Santiago de Compostela, Spain

Dear Dr. Ares:

I am pleased to inform you that your paper "Placing quasi-nulls in planar and conformal arrays", has been found acceptable for publication in **Electromagnetics**.

I am enclosing the materials necessary for your manuscript's preparation. The issue your paper will apear depending on when you return the final, formatted version. I will inform when I know it for sure. Please remember to include the copyright form!

Since the journal does not request page charges, authors submitting papers to **Electromagnetics** are asked to subscribe to the journal. Enclosed please find a subscription form, in case you have not done so already. Another alternative is for your Library to be a subscriber member. The rates are: $260 (institution) and $99 (personal).

Thank you for your contribution to **Electromagnetics**!

Sincerely yours,

David Yang

H.Y. David Yang
Editor-in-Chief, **Electromagnetics**

enclosures: - copyright form
- subscription/information card - reprint order form
- instructions for preparing manuscript

Taylor&Francis
Publishers since 1798

PLACING QUASI-NULLS IN PLANAR AND CONFORMAL ARRAYS

A. Trastoy and F. Ares
Grupo de Sistemas Radiantes, Departamento de Física Aplicada
Universidad de Santiago de Compostela
15706 Santiago de Compostela, Spain

ABSTRACT

We describe the use of the simulated annealing optimization method to introduce minimal modifications in the excitations and/or geometries of planar and circular arc antenna arrays so as to depress the radiation pattern in arbitrary directions while maintaining side lobe levels and beamwidth.

1. INTRODUCTION

Given an array antenna, null fixing consists in modification of its parameters so that the radiated power is zero (null), or at least highly depressed (quasi-null), in certain specified directions. Most null-fixing methods have been developed for linear arrays (see, for example, (Trastoy and Ares, 1997)). (Vu, 1992) devised two methods for fixing nulls in planar arrays, but the first, based on the method of separable distributions, only controls pattern parameters in the two principal φ-cuts, while the second, which uses a cancelling beam as in some techniques developed for linear arrays, has only been applied to uniform excitation distributions; neither of these two methods exercises any control over the dynamic range ratio of the array excitation distribution, $|I_{max}/I_{min}|$, or is able to null a finite angular segment of the pattern rather than just a point or series of points. Nulls have also been fixed in the radiation patterns of circular arc arrays, both by perturbing the excitations of the array elements (Prasad and Charan, 1984), (Vescovo, 1996), (Ares *et al.*, 1996) and by perturbing their radial positions (Hejres and Richie, 1996). The excitation perturbation method of (Ares *et al.*, 1996) has the advantage over the others of minimizing dynamic range ratio and the extent of perturbation

at the same time as it fixes nulls.

In this article we extend to planar and circular arc arrays the null-fixing method described previously for linear arrays (Trastoy and Ares, 1997). Briefly, a simulated annealing technique based on the simplex method (Press *et al.*, 1992) is used to optimize perturbations of parameters characterizing the array (specifically, the amplitudes, phases and/or geometric positions of its elements) so as to introduce desired quasi-nulls while controlling other radiation pattern characteristics (side lobe levels, beamwidth, etc.) and minimizing the dynamic range ratio of the excitation distribution.

2. DESCRIPTION OF THE METHOD

We start with an antenna array of given geometry, composed of radiating elements with given excitations and positions. By perturbing these *array parameters*, i.e. the excitations and/or positions of the elements, the radiation pattern can be changed so that quasi-nulls appear in certain desired directions. In general, this can be achieved by an infinite number of perturbation combinations: the aim is to identify a combination of perturbations that not only fixes the required quasi-nulls, but also maintains or improves other pattern characteristics (side lobe levels, beamwidth, etc.) and facilitates implementation by minimizing both the dynamic range ratio of the excitation distribution and the absolute values of the perturbations. This can be achieved by using a suitably versatile optimization procedure such as simulated annealing (Press *et al.*, 1992) (see Section 3) to minimize a cost function containing a group of terms fixing pattern parameters (including quasi-nulls), a group of terms minimizing perturbations, and a term minimizing the dynamic range ratio:

$$C = \sum_{i=1}^{q} a_i (Dd_i - Do_i)^2 + b\,|I_{\max}/I_{\min}|^2 + c \sum_{n=1}^{N} |\delta A_n|^2 \qquad (1)$$

where Dd_i and Do_i denote respectively the desired value of radiation pattern parameter i (power level in the direction where the quasi-null is required, side lobe level, beamwidth, etc.) and the value afforded by the current array parameters; q indicates the number of these parameters that are used; δA_n is the current perturbation of the n-th array parameter; and the a_i, b and c are weighting factors controlling the relative priorities of the various terms in the cost function.

3. THE OPTIMIZATION METHOD

The cost function defined in equation 1 is a function of a large number of variables, upon which each of its terms depends in a complex fashion. Such functions generally have a large number of local minima, and it is not usually possible for them to be minimized by conventional optimization procedures based on their local topography; these methods will usually not find the global minimum, but the local minimum downhill from the starting point, i.e. the minimum of that local basin (of the hypersurface defined by the function) which contains the point used as the starting point of the optimization procedure. The optimization technique called simulated annealing overcomes this difficulty in a fashion inspired on the thermodynamical process it is named after. Broadly, the system (i.e. the current best estimate of the position of the minimum) is first allowed to roam randomly from one local basin to another, with a tendency - but not an absolute obligation - to occupy successively lower positions; then the "energy" of this motion is gradually reduced (by decreasing a "temperature" parameter) so that the system eventually settles into a single basin; and finally the lowest point of that basin is found, usually by a conventional optimization method. Like other "evolutionary" optimization procedures, simulated annealing cannot guarantee to find the global minimum of a function, but it will usually find a much better local minimum than any conventional method. Of the various forms of simulated annealing that have been proposed, the variant used to obtain the results reported below in Section 4 was the algorithm published by (Press *et al.*, 1992), which is based on the conventional deterministic optimization procedure known as the simplex method (Press *et al.*, 1992). In minimizing a function $f(\mathrm{x})$ of n variables, the simplex method does not start with just a single initial estimate of the point at which the minimum lies, but with $n+1$ estimates $\mathbf{x}_1,\ldots,\mathbf{x}_{n+1}$ which jointly define a simplex, the n-dimensional equivalent of a plane triangle. At each iteration, the procedure first identifies the $\mathbf{x}_i$ for which the value of the function is greatest, $\mathbf{x}_{max}$ say, and implicitly adopts the working hypothesis that the face of the simplex that is opposite to this point divides high values from low. It accordingly constructs a new estimate $\mathbf{x}_0$ lying on the prolongation of the line from $\mathbf{x}_{max}$ to the centre of the opposite face, and proceeds to test the validity of this estimate and to act in consequence. For example, if $f(\mathbf{x}_0)$ is less than all the other $f(\mathbf{x}_i)$ (suggesting that a good line of descent has been found), a new point $\mathbf{x}_{00}$ is constructed further along the same line as before, the simplex is re-defined (excluding $\mathbf{x}_{max}$ and including the better of $\mathbf{x}_0$ and $\mathbf{x}_{00}$), and the next iteration is begun. Depending on the results

of similar comparisons, the simplex thus changes in position, shape and volume. Eventually, it becomes smaller and smaller until all the function f has very similar values at all its vertices, at which point the least of these values is taken as the minimum.

When the simplex method is used for simulated annealing, the procedure is the same as above except that comparisons between points are biased in favour of acceptance of a new candidate for inclusion in the simplex. For example, the criterion for constructing $\mathbf{x}_{00}$ is no longer $f(\mathbf{x}_i) > f(\mathbf{x}_0)$ for all i, but $f(\mathbf{x}_i) + Y_i > f(\mathbf{x}_0)$ for all i, where Y_i is a random variable with a G(2,T) distribution, T being the temperature parameter. When T is large, then so, on average, are the Y_i, which means that $\mathbf{x}_{00}$ is almost always constructed (and then almost always accepted). The simplex thus grows until prevented from growing further by meeting high values of $f(\mathbf{x})$ as $|\mathbf{x}|$ grows. Lowering T every few tens of iterations reduces the probability of accepting $\mathbf{x}_{00}$ and increases the probability of the simplex becoming smaller and settling in a local basin. At $T = 0$ the Y_i are all zero and the procedure is exactly the standard simplex method.

4. RESULTS

4.1 Application to Planar Arrays

To establish notation, we recall that the far field $F(\theta,\varphi)$ of a planar array of N elements lying in the (x,y) plane is given by

$$F(\theta,\varphi) = \sum_{n=1}^{N} I_n e^{\alpha_n} e^{j\beta(x_n \sin\theta\cos\varphi + y_n \sin\theta\sin\varphi)} FE(\theta,\varphi) \qquad (2)$$

where x_n and y_n are the position coordinates of the n-th element, I_n and α_n are respectively the amplitude and phase of its excitation, β is the wavenumber and $FE(\theta,\varphi)$ is the element pattern. We take as an example the case of a 468-element array composed of 52 3x3-element subarrays of circular patches arranged on an 8x8-subarray grid with three subarrays omitted at each corner so as to form an approximately circular global array boundary. The power pattern of each circular patch is given by $FE(\theta)=10^{(-\theta/82.16)}$, which falls to -22 dB at $\theta = 90°$.

Starting from a uniform excitation distribution, a distribution with a dynamic range ratio $|I_{max}/I_{min}|$ of just 2.07 producing a power pattern with a side lobe level of -26.0 dB can be synthesized by perturbing the excitation amplitudes and phases and controlling side lobe level in φ-cuts taken every 5°. A quasi-

null with a radius of 1° centred on $(\theta,\varphi) = (20°,40°)$ can now be introduced in this power pattern by further perturbing the excitation amplitudes and phases while using a cost function that penalizes not only side lobe level and dynamic range but also departure from -60 dB at any of a series of points within the desired quasi-null sector. Fig.1, in which $u = \sin(\theta)\cos(\varphi)$ and $v = \sin(\theta)\sin(\varphi)$, shows the resulting power pattern, which has a side lobe level of -23.3 dB and a quasi-null in the desired direction (arrowed, at $u = 0.26$, $v = 0.23$) and is produced by an excitation distribution with a dynamic range ratio of 2.38. If only phases are perturbed in the second stage of this process, a distribution with a dynamic range ratio of 2.07 producing a power pattern with a side lobe level of -20.7 dB is obtained (Fig.2).

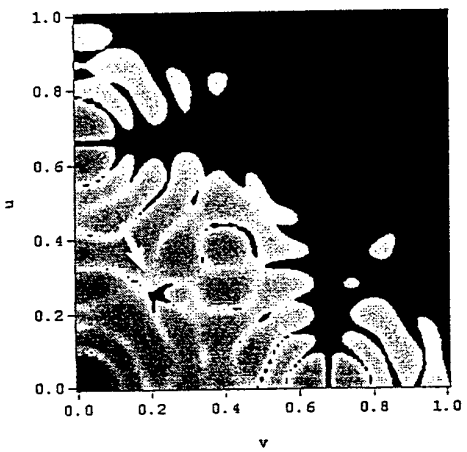

FIGURE 1. A broad (1°) null fixed at $(\theta_0, \varphi_0) = (20°,40°)$ in the power pattern of a planar array antenna by perturbing excitation amplitudes and phases.

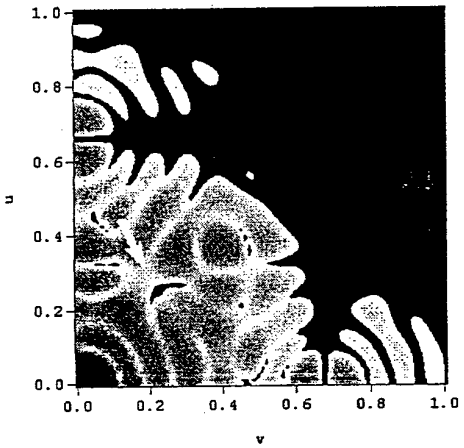

FIGURE 2. A broad (1°) null fixed at $(\theta_0, \varphi_0) = (20°,40°)$ in the power pattern of a planar array antenna by perturbing excitation phases only.

4.2. Application to Circular Arc Arrays

The far field of an array of N radiating elements lying on equispaced rays in a sector $(-\varphi,\varphi)$ of a circle is given in the plane of the circle by

$$F(\varphi) = \sum_{n=1}^{N} I_n \, e^{j\alpha_n} e^{j\beta R_n \cos(\varphi - \varphi_n)} \, FE(\varphi - \varphi_n) \qquad (3)$$

where R_n and φ_n are the polar coordinates of the n-th element and the other

notation is the same as for equation 2. Fig.3 shows the geometry when $R_n = R$ for all n.

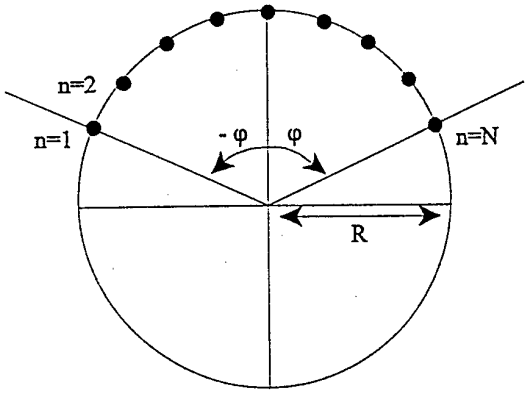

FIGURE 3. Geometry of a circular arc array

In this case, the element pattern cannot be factored out of the expression for $F(\varphi)$, leaving an array factor, because each element faces in a different direction. As an example, consider the case $N = 25$ and $\varphi = 60°$, with the elements initially at equal intervals of $\lambda/2$ along the arc ($R_n = 5.73\lambda$ for all n) and

$$FE(\theta,\varphi) = \frac{1}{3}\sin\theta\,[1 + 2\max(\cos\varphi, -\tfrac{1}{2})] \qquad (4)$$

(this is the element pattern used for ($\lambda/2$)-spaced elements by (Jiao *et al.*, 1993), who adapted the findings of (Herper *et al.*, 1985)).

Starting from the excitation distribution found by excitation perturbation in (Ares *et al.*, 1996), which has a dynamic range ratio of 7.54 and produces a pencil beam with a side lobe level of -40 dB, our aim is to perturb the excitations and/or positions of the elements so as to introduce quasi-nulls at φ = 20°, 22° and 24°, thereby creating a broad quasi-null centred on φ = 22°. Table 1 and Figs. 4-7 show the results obtained by varying a) excitation amplitudes and phases (Fig.4), b) excitation phases only (Fig.5), c) radial and angular element coordinates (Fig.6), and d) excitation phases and angular coordinates (Fig.7); in all cases, perturbations were symmetric with respect to φ = 0° so as to reduce the number of variables. Best results were achieved perturbing phases and position angles, which introduced the desired quasi-null sector at the expense of only a 2.64 dB rise

in side lobe level. Note that the position angle perturbations were small enough for equation 4 still to be a valid approximation for the element pattern.

TABLE 1. Results of Fixing a Broad Null at φ=22° in the Power Pattern of a Circular Arc Array by Perturbing Various Combinations of Array Parameters

Paramenters perturbed	SLL	$\lvert I_{max}/I_{min} \rvert$	Δ
Amplitudes and phases (Fig.4)	-36.38 dB	8.31	0.5λ
Phases (Fig.5)	-34.32 dB	7.54	0.5λ
Radial and angular positions (Fig.6)	-36.84 dB	7.54	0.48λ - 0.51λ
Phase and angular position (Fig.7)	-37.36 dB	7.54	0.47λ - 0.52λ

SLL=Side lobe level; Δ=distance between adjacent elements along the arc.

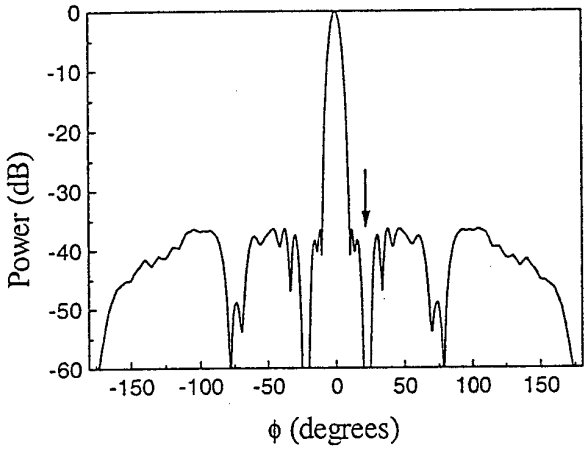

FIGURE 4. A broad (4°) null fixed at φ=22° in the power pattern of a circular arc array by perturbing excitation amplitudes and phases.

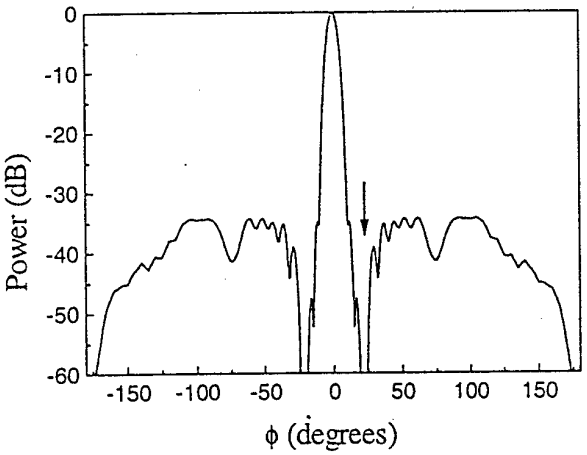

FIGURE 5. A broad (4°) null fixed at φ=22° in the power pattern of a circular arc array by perturbing excitation phases only.

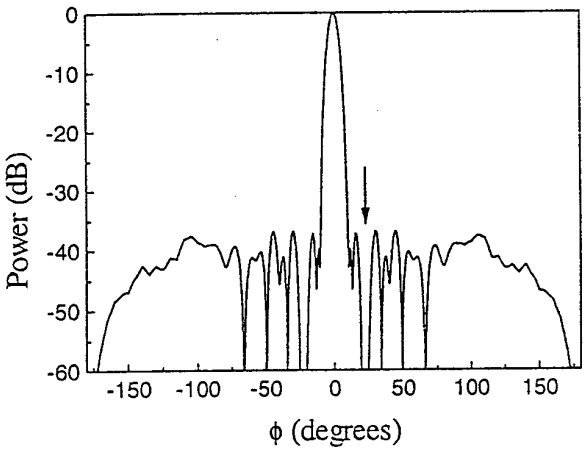

FIGURE 6. A broad (4°) null fixed at φ=22° in the power pattern of a circular arc array by perturbing radial and angular element coordinates.

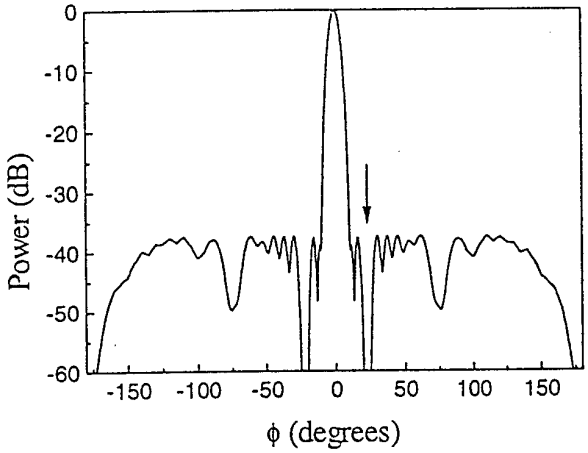

FIGURE 7. A broad (4°) null fixed at φ=22° in the power pattern of a circular arc array by perturbing excitation phases and angular element coordinates.

It was also found that quite good results could be obtained by perturbing the parameters of a relatively small number of array elements. Starting from the excitation distribution found in (Ares *et al.*, 1996) for the equispaced array with $R_n = 5.73\lambda$ for all n, perturbation of the phases of the eight elements whose phases were changed most in synthesizing the pattern of Fig.5 (four on each side of the array) afforded the pattern shown in Fig.8, which still has a side lobe level of -29.6 dB.

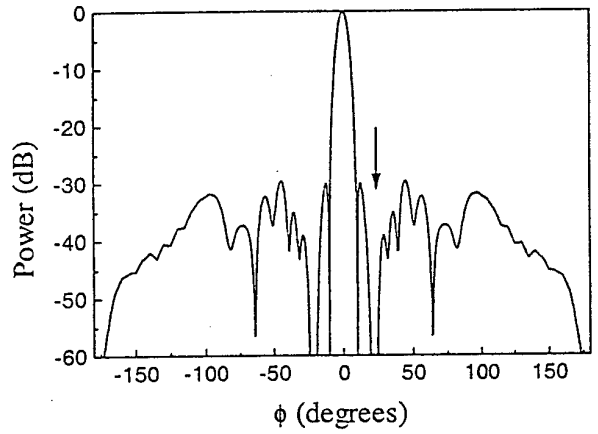

FIGURE 8. A broad (4°) null fixed at φ=22° in the power pattern of a circular arc array by perturbing the excitation phases of just 8 of its 25 elements.

5. CONCLUSIONS

By perturbing the excitations and/or positions of some or all of the radiating elements, the method described here is able to fix quasi-nulls over a finite sector of the power patterns of planar and circular arc array antennas while controlling other power pattern characteristics and minimizing the dynamic range ratio of the excitation distribution. Though not shown in this article, multiple point quasi-nulls can be fixed by the same method. Although the perturbation of element positions is of course more difficult to implement physically than perturbation of excitations, it shares with phase-only control the advantage of allowing no increase in dynamic range ratio, and for circular arcs affords better results than perturbation of excitations alone.

6. ACKNOWLEDGEMENTS

This work was supported by the European Office of the US Aerospace Research and Developement Board (EOARD) and the US Air Force Office of Scientific Research (AFOSR).

REFERENCES

Ares, F., Rengarajan, S. R., Lence, J. A. F., Trastoy, A., and Moreno, E., "Synthesis of antenna patterns of circular arc arrays", *Electronics Letters*, Vol. 32, N° 20, pp. 1845-1846, 1996.

Hejres, J. A., and Richie, J. E., "A simple method for null steering in a circular array by perturbations of the radial locations of the elements", *IEEE/AP-S International Symposium, Baltimore*, pp. 1138-1141, July 1996.

Herper, J. C., Hessel, A., and Tomasic, B., "Element pattern of an axial dipole in a cylindrical phased array, Part I: Theory", *IEEE Trans. Antennas Propagat.*, Vol. 33, pp. 259-272, March 1985.

Herper, J. C., Hessel, A., and Tomasic, B., "Element pattern of an axial dipole in a cylindrical phased array, Part II: Element design and experiments", *IEEE Trans. Antennas Propagat.*, Vol. 33, pp. 273-278, March 1985.

Jiao, Y. C., Wei, Y., Huang, L., and Wu, H. S., "A new low-side-lobe pattern synthesis technique for conformal arrays", *IEEE Trans. Antennas Propagat.*, Vol. 41, N° 6, pp. 824-831, June 1993.

Prasad, S., and Charan, R., "On the constrained synthesis of array patterns with applications to circular and arc arrays", *IEEE Trans. Antennas Propagat.*, Vol. AP-32, N° 7, pp. 725-730, July 1984.

Press, W. H., Teukolsky, S. A., Vetterling, W. T., and Flannery, B. P., "Numerical Recipes in C", *Cambridge University Press*, pp. 444-455, 1992.

Trastoy, A., and Ares, F., "Linear array pattern synthesis with minimum sidelobe level and null control", *Microwave and Optical Technology Letters*, Vol. 16, N°5, pp. 995-997, December 1997.

Vescovo, R., "Pattern synthesis with null constraints for circular arrays of equally spaced isotropic elements", *IEEE Proc.-Microw. Antennas Propagat.*, Vol. 143, N° 2, pp. 103-106, April 1996.

Vu, T. B., "On null steering in rectangular planar arrays", *IEEE Trans. Antennas Propagat.*, Vol. 40, N° 8, pp. 995-997, August 1992.

IBERDROLA
INSTITUTO
TECNOLOGICO

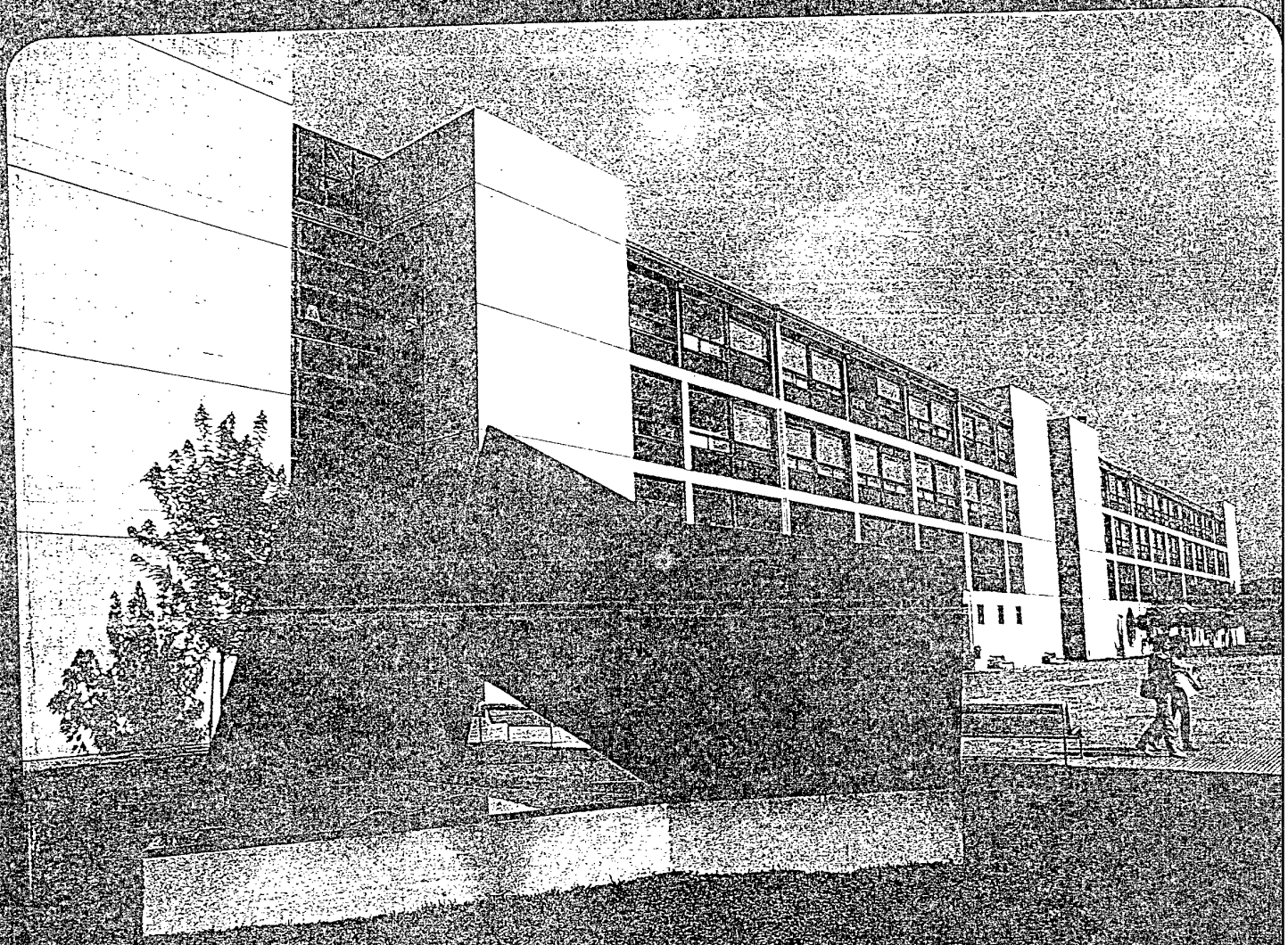

URSI'98

Unión Científica Internacional de Radio

XIII Simposium Nacional

Pamplona, 16-18 Septiembre

Sesión VI. 2 — Antenas III

Sesión VI. 3 — Circuitos Pasivos

Sesión VI. 4 — Análisis de Voz

Sesión VI. 5 — Dispositivos Fotónicos IV

Fijado de nulos en diagramas de radiación de arrays planos

A. Trastoy Ríos, F. Ares Pena
Departamento de Física Aplicada, Grupo de Sistemas Radiantes
Facultad de Física, Universidad de Santiago de Compostela
15706 Santiago de Compostela
E-mail: faares@usc.es

Abstract: A planar array design method of fixing nulls is presented. This method allows to fix narrow and broad nulls by varying amplitudes and phases or only phases of the excitations of the radiating elements. Besides, it is possible to control, at the same time, the sidelobe level and the dynamic range.

1. Introducción

Aunque las técnicas de fijado de nulos en arrays lineales han sido tratadas en gran número de artículos, no sucede lo mismo en arrays planos. Vu [1] presentó dos técnicas para ello. La primera de ellas, basada en la utilización de distribuciones separables, es una técnica no óptima, puesto que el control de los parámetros del diagrama se realiza sólo en los dos cortes ϕ principales. La segunda, que es similar a técnicas propuestas para arrays lineales, está basada en la formación de un haz de cancelación y presenta mejores resultados aunque es aplicada sólo a distribuciones de excitación uniforme (control sólo en fase). Sin embargo, ninguna de ellas permite el control del rango dinámico $|I_{max}/I_{min}|$ ni el fijado de nulos anchos.

La técnica aquí propuesta consiste en la extensión a arrays planos del método descrito en [2] para arrays lineales. Esta extensión permite la síntesis de diagramas de radiación de arrays planos mediante el control de las excitaciones de los elementos radiantes, bien variando conjuntamente la amplitud y la fase de dichas excitaciones, o bien modificando únicamente la fase. Aunque el objetivo primero de esta técnica es el fijado de nulos (tanto puntuales como en un cierto entorno de un punto deseado), este método permite la modificación de otros parámetros importantes del diagrama de radiación, como pueden ser el nivel de lóbulos laterales o el ancho angular del haz principal. Además, también permite la minimización del rango dinámico de las excitaciones, lo que favorece la realizabilidad del array resultante.

2. Descripción del método

La expresión del patrón de radiación en campo lejano, para un array plano de N elementos idénticos situados en un plano paralelo al plano XY, es la siguiente:

$$F(\theta,\phi)=\sum_{n=1}^{N} I_n\, e^{j\alpha_n} e^{j\beta x_n sen\theta\cos\phi}\, e^{j\beta y_n sen\theta sen\phi}\, FE(\theta,\phi)$$

donde I_n denota la amplitud de la excitación del elemento n-ésimo, α_n su fase, x_n, e y_n denotan su posición sobre el plano, $FE(\theta, \phi)$ el factor elemento y $\beta=2\pi/\lambda$.

Se parte de un diagrama inicial que es modificado con el fin de conseguir otro con nulos fijados en unas ciertas posiciones angulares y que posea, además, unas características deseadas. Para ello se varían las excitaciones de los elementos radiantes, bien sus amplitudes y sus fases:

$$I_n = I_n^0 + \delta I_n$$
$$\alpha_n = \alpha_n^0 + \delta\alpha_n$$

o bien sólo sus fases:

$$\alpha_n = \alpha_n^0 + \delta\alpha_n$$

Es importante que estas variaciones en las excitaciones sean mínimas, condición ésta que podemos poner en nuestra técnica, ya que esto permite una mayor simplicidad de la red de alimentación requerida para el sistema radiante. Este parámetro, junto con otros característicos del diagrama y/o de las excitaciones, se introduce en una función de coste que será minimizada mediante la técnica de optimización de "Simulated Annealing"[3]. Dicha función de coste incluye, entonces, un primer término para conseguir unas ciertas características en el diagrama de radiación tales como la posición angular y la profundidad de los nulos, el ancho de haz o el nivel de lóbulos laterales. Un segundo término permite minimizar el rango dinámico de las excitaciones, y un tercer sumando permite conseguir que las excitaciones de los elementos radiantes varíen lo menos posible con respecto a las del diagrama de partida. Es decir:

$$C=\sum_{i=1}^{P} a_i(Dd_i-Do_i)^2+b\,|I_{max}/I_{min}|^2+c\sum_{n=1}^{N}(Ef_n-Ei_n)^2$$

donde, por Dd_i y Do_i se denotan los valores deseado y obtenido de un cierto parámetro i del diagrama de radiación, p indica el número de estos parámetros que queremos controlar, Ef_n y Ei_n los valores final e inicial de las amplitudes y/o fases del elemento n-ésimo y a_i, b y c son los factores de peso que nos permiten dar prioridad a unos sumandos sobre los otros.

3. Resultados

Para ilustrar la técnica que se presenta, hemos escogido un array plano de 468 elementos radiantes equiespaciados $\lambda/2$, colocados según un enrejado rectangular de 8x8 subarrays eliminando tres subarrays en cada esquina para aproximar a un contorno circular. Cada subarray consta de 3x3 parches circulares cuyo factor elemento, dependiente de θ, puede aproximarse por la siguiente expresión:

$$FE(\theta) = 10^{(-\theta/82.16)}$$

Inicialmente se parte de un diagrama de radiación correspondiente a una distribución de excitaciones uniforme y, mediante la variación de las amplitudes y las fases de las excitaciones de cada uno de los elementos radiantes, se sintetiza un diagrama en el que se fijarán posteriormente los nulos y que presenta un nivel de lóbulos laterales SLL=-26.0 dB y un rango dinámico minimizado hasta $|I_{max}/I_{min}|$=2.07. Los nulos pueden ser tanto muy localizados en una posición angular deteminada, como nulos más anchos que se consiguen fijando varios de ellos en un entorno de la posición deseada. Los ejemplos que aquí se muestran son de este último tipo. En la figura 1 se presenta la proyección en el plano XY (primer cuadrante) de un diagrama con un nulo de banda ancha que ocupa un entorno de radio 1° alrededor de la posición (θ_0,ϕ_0)=(20°,40°), es decir, en u=0.26, v=0.23 (donde $u=sen\theta cos\phi$ y $v=sen\theta sen\phi$) y que se ha fijado mediante la variación de amplitudes y fases de las excitaciones. El diagrama obtenido presenta un nivel de lóbulos laterales de -23.3 dB y un rango dinámico de 2.38.

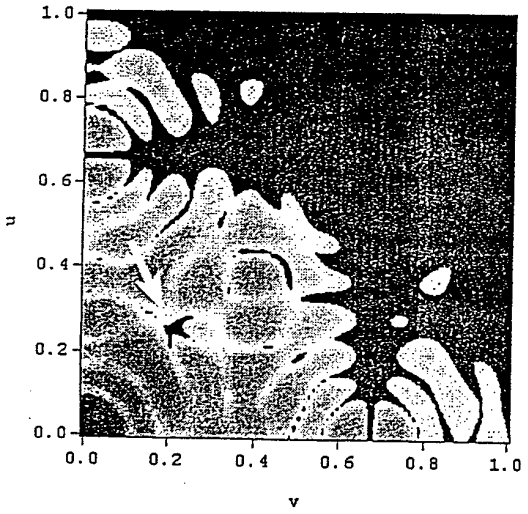

Figura 1. Nulo centrado en (θ_0,ϕ_0)=(20°,40°) obtenido mediante la variación de amplitudes y fases.

En la figura 2 se muestra ese mismo diagrama obtenido mediante solamente la variación de las fases de las excitaciones. Este diagrama de radiación presenta un nivel de lóbulos laterales de -20.7 dB y, obviamente, su rango dinámico es el mismo que en el patrón de partida: 2.07.

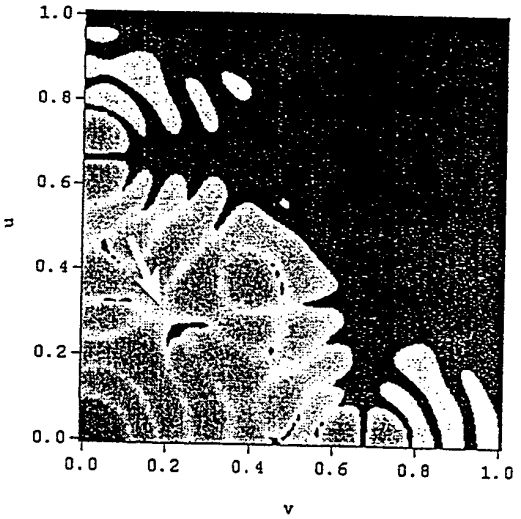

Figura 2. Nulo centrado en (θ_0,ϕ_0)=(20°,40°) obtenido mediante la variación de fases.

4. Conclusiones

Se ha presentado una técnica para el fijado de nulos, tanto sencillos como múltiples, en el diagrama de radiación de arrays planos. Además, posibilita el control del nivel de lóbulos laterales en todo el diagrama 3D, así como la minimización del rango dinámico de las excitaciones y de las variaciones de dichas excitaciones (en amplitud y fase) con respecto a las correspondientes al diagrama de partida.

5. Agradecimientos

Los autores quieren agradecer su ayuda económica a la European Office of Aerospace Research and Development (EOARD) y a la Air Force Office of Scientific Research (AFOSR).

Referencias:

[1] T. B. Vu, "On Null Steering in Rectangular Planar Array", *IEEE Trans. On Antennas and Propagat.*, Vol. 40, N° 8, pp. 995-997, August 1992.

[2] A. Trastoy, F. Ares, "Linear Array Pattern Synthesis with Minimum Sidelobe Level and Null Control", *Microwave and Optical Technology Letters*, Vol. 16, N° 5, pp. 322-325, Dec. 1997.

[3] W. H. Press, S. A. Teukolsky, W. T. Vetterling, B. P. Flannery, "Numerical Recipes in C", Cambridge University Press, pp. 444-455, 1002.

ELECTRONICS LETTERS

AN INTERNATIONAL PUBLICATION

CONTENTS

pages 1533 - 1620

6th August 1998 Vol. 34 No. 16

(continued on back cover)

and digitisers, sampling each element signal at four samples/bit (1.08MHz); a direction finding DSP subsystem which pre-processes and stores the digitised signals; a survey vehicle containing a standard DCS-1800 mobile station (MS) and a GPS receiver; and a DCS-1800 base station (BSS) to set up and maintain the call and to provide a timing reference for the location estimation subsystem. The experiments were carried out by driving the survey vehicle over a number of test routes with a standard call in progress between the MS in the vehicle and the BSS in the field trial system. The signals received at the antenna array were processed in real time to estimate H and R, which were time stamped and stored for later analysis.

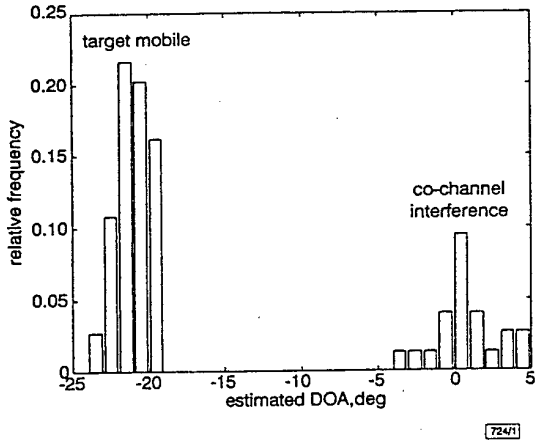

Fig. 1 *Histogram of DOA estimates over 2s period*

Raw DOA and range estimates were computed with the technique described under 'Polar location estimation'. The number of sources N_p was fixed to one. The mobile trajectory was estimated with the method based on the histogram maxima with time intervals of 2s and the threshold of reliability set to 40%. Averaging was then performed with a window of size 20s, or ten estimates. An example of the DOA histograms obtained from analysis of the experimental data is shown in Fig. 1. This example was obtained from an experiment in which a co-channel interference signal was present in addition to the target mobile.

Results: Since differential GPS equipment was not available, the GPS measurements were subject to a bias that varies between experiments. Knowing the exact routes, the measured OPS positions were overlaid onto an Ordnance Survey map and the corrected GPS trajectories were calculated.

Table 1: DOA error in degrees, range error in metres and r.m.s. position error in metres

(Ref.) scenario	DOA error		Range error		Position	P(err < Xm)		
	Mean	Std	Mean	Std	RMSE	X=50	X=125	X=250
	deg	deg	m	m	m	%	%	%
(039) moving MS	-0.4	0.6	-53	98	133	24.5	59.6	98.4
(045) moving MS stationary interferer	0.3	0.6	2	68	114	36.4	82.0	97.9

Last three columns represent probability that position error is < X, with X = 50, 125 and 250m, respectively

The position estimates derived from the mobile location algorithm are subject to a DOA bias (due to misalignment of the antenna array and phase and amplitude mismatch between the receiver channels) and a range bias (due to fixed delays in the eight receivers.) These bias terms were estimated using data from a 'calibration' experiment in which the mobile station was stationary at a location with line of sight to the base station. The resulting bias corrections were applied to the estimates derived from other experimental data sets. Performance was evaluated with the mean error and standard deviation on the DOA and range estimates, and the r.m.s position error. The accuracy of the location estimates was also assessed by counting the number of position estimates within circles of increasing radius centred on the true positions. Table 1 shows the results for two scenarios. In the first one, the mobile station is in a moving vehicle travelling at an average speed of 30mph. The duration of the test is ~ 5min and the distance from the base station is ~ 5km. The second scenario is the same except that a stationary co-channel interference signal is introduced.

In the first scenario, the estimated location is within 250m of the true location for 98% of the time, and within 50m for 24% of the time. The second scenario gives a larger percentage of estimates within 50m and comparable results for 250m.

Conclusion: This Letter has presented a technique for estimating the location of a mobile radio transmitter using an antenna array at a single receiving point. Experimental results from a DCS-1800 system have been presented which compare favourably with other published results. Of course, position accuracy is very dependent on the propagation environment and future experimental work will include the application of the technique to a wider range of propagation environments (including micro-cell environments), as well as the refinement of the location estimation algorithms.

Acknowledgments: The results presented in this Letter used data provided by the ACTS AC020 TSUNAMI (II) research project which is partly funded by the European Community. The authors would like to acknowledge the help of their TSUNAMI (II) colleagues. More information about TSUNAMI (II) is available at http://www.era.co.uk/div80/bc82/smartant/tsunami2.htm.

28 May 1998
Electronics Letters Online No: 19981090

F. Cesbron and R. Arnott (*ERA Technology Ltd, Cleeve Road, Leatherhead, Surrey, KT22 7SA, United Kingdom*)

E-mail: rarnott@era.co.uk

References

1 SAKAGAMI, S., AOYAMA, S., KUBOI, K., SHIROTA, S., and AKEYAMA, A.: 'Vehicle position estimates by multibeam antennas in multipath environments', *IEEE Trans. Vehic. Technol.*, 1992, 41, (1), pp. 63–68

2 MOULY, M., and PAUTET, M.: 'The GSM system for mobile communications' (Michel Mouly and Marie-Bernadette Pautet, 1992)

Pattern synthesis of array antennas with additional isolation of near field arbitrary objects

L. Landesa, F. Obelleiro, J.L. Rodríguez, J.A. Rodríguez, F. Ares and A.G. Pino

A new technique for synthesising array antennas in the presence of arbitrary obstacles in the near field region is presented. This technique allows a prescribed far field pattern to be synthesised, while trying to avoid coupling with near field obstacles through the constraint of minimising the radiated power over the obstacle surface. Some results have been obtained showing that the obstacles are finally isolated from the array antenna radiation.

Introduction: In recent works [1 – 3], the synthesis of array antennas with the presence of obstacles in the near field environment has been investigated. In [1], a solution based on a pattern synthesis procedure imposing near field nulls inside the obstacles was presented by Steyskal; this straightforward approach provides good results for small obstacles, although it may be inefficient when dealing with large objects. A new solution, presented in [2], tries to take into account the obstacles as parasitic elements, including them in a pattern synthesis algorithm, which allows us to take advantage of their scattering, even for large obstacles. Directivity optimisation is achieved in [3] following a similar coupling procedure to take into account the presence of the obstacles. These two last approaches [2, 3] need to calculate accurately the electromagnetic coupling of the obstacle in order to obtain the array excitations. This complicates the synthesis procedure and, besides, requires the use of an accurate numerical technique to

calculate this coupling matrix, mainly in complex and three-dimensional problems.

In this Letter, we present a new technique that generalises the approach presented in [1] for large objects. This technique allows us to synthesise a prescribed far field pattern while attempting to avoid the coupling with near field obstacles through the constraint of minimising the radiated power over the obstacle surface by a simple and straightforward procedure. This technique has been shown to be very efficient, providing results as good as those obtained with the previous techniques [2, 3] in which the scattering of the obstacle was used to improve the radiation pattern.

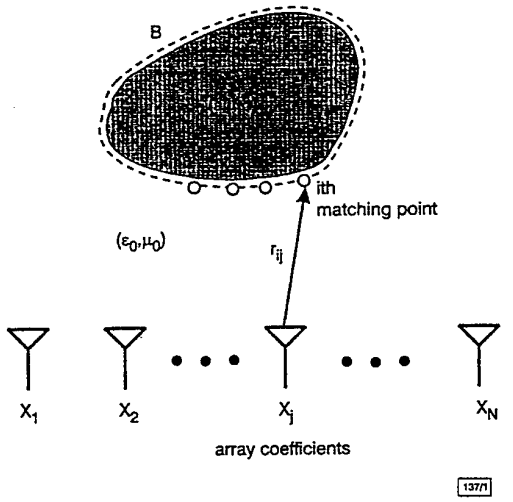

Fig. 1 *Linear array of isotropic sources in presence of arbitrary obstacle*

Pattern synthesis technique: In this pattern synthesis problem we attempt to obtain those array complex coefficients x_i that best approximate, in a mean least square sense, a desired far field pattern f_d, simultaneously minimising the near field radiated power in the boundary of the obstacles, B. We consider a two-dimensional problem involving a linear array of N isotropic sources with $\lambda/2$ spacing, as shown in Fig. 1.

The boundary of the obstacle is sampled at a set of M matching points (ten matching points per wavelength have been used) and a matrix, C, that relates the free space electric near field in these points with the array coefficients is calculated. Thus, the field in these matching points is obtained as a column vector of M coefficients:

$$\mathbf{e} = \mathbf{C}\mathbf{x} \tag{1}$$

where x is a column vector of N elements that contains the excitation coefficients x_i for the array, and C is a matrix of $M \times N$ elements of the form

$$c_{ij} = \frac{e^{-jkr_{ij}}}{\sqrt{r_{ij}}} \tag{2}$$

where r_{ij} notes the distance between the ith matching point and the jth element of the array. The power magnitude in the boundary of the obstacles is defined as

$$P_b = \|\mathbf{C}\mathbf{x}\|_2^2 \tag{3}$$

which will be minimised in order to isolate the obstacles. The synthesis problem can therefore be formulated as

$$\min_{\mathbf{x}}\left\{\int_{-1}^{1} |f_d(u) - f(u)|^2 du\right\} \text{ constrained to } \|\mathbf{C}\mathbf{x}\|_2^2 \leq \alpha \tag{4}$$

where $u = \sin\theta$ and f is the free-space far field pattern of the array whose coefficients are given by x.

Considering the Fourier relation between the aperture distribution and the far field [1, 4], and using Lagrange multipliers, the last equation can be written as

$$\min_{\mathbf{x}} \{\|\mathbf{x}_d - \mathbf{x}\|_2^2 + \lambda^2 \|\mathbf{C}\mathbf{x}\|_2^2\} \tag{5}$$

where the parameter λ is related to α in a nonlinear sense, and the column vector $\mathbf{x}_d$ represents the free-space array coefficients for the prescribed pattern f_d This equation can be reformulated in an overdetermined system as

$$\begin{pmatrix} \mathbf{I} \\ \lambda\mathbf{C} \end{pmatrix} \mathbf{x} \simeq \begin{pmatrix} \mathbf{x}_d \\ 0 \end{pmatrix} \tag{6}$$

which can be solved, in a mean least square sense, by using the normal equation or the QR decomposition.

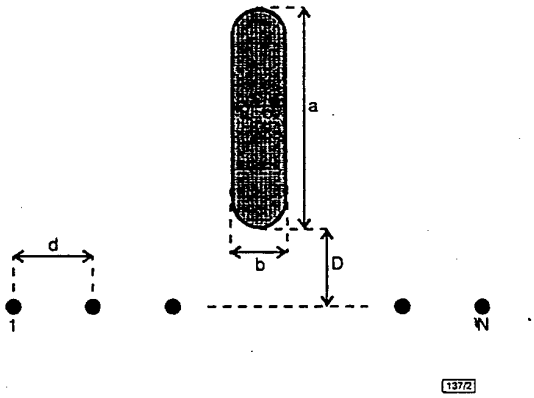

Fig. 2 *Geometry of array antenna in presence of PEC cylinder*
$a = 9\lambda$, $b = 0.8\lambda$, $N = 41$, $d = 0.5\lambda$, $D = 8\lambda$

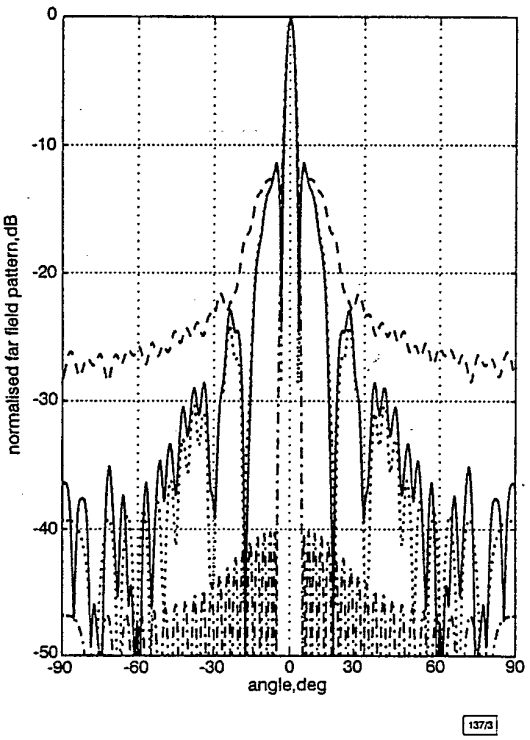

Fig. 3 *far field patterns*

- - - - original Taylor pattern
– – – – blocked Taylor pattern
····· radiation pattern synthesised with proposed method (free space)
——— radiation pattern obtained with proposed method (blocked)

In the solution of eqn. 6, the parameter λ (which must be real and positive) weighs up the importance of the boundary power (P_b) restriction in the synthesis procedure. Small values of λ correspond with a poor isolation of the obstacles; in this case, although the pattern prediction may be good (compared with the prescribed pattern), the scattered field radiated by the obstacle highly degrades this prediction, so the total far field pattern becomes poor. Otherwise, for large values of λ, the problem is dominated by the boundary power restriction; hence, although the obstacle's radiation does not disturb the far field pattern, this pattern prediction may be far from the prescribed pattern. It is clear, therefore,

that a good selection for λ is required; namely, λ must be adequately selected for balancing a good isolation of the obstacle and a pattern prediction close to the prescribed one.

Results: Eqn. 6 is used in this Section in order to approximate, in a mean least square sense, a Taylor pattern of SLL = 40dB and $\bar{n}$ = 3, with a linear array antenna blocked by a perfect electric conducting (PEC) cylinder whose geometry and dimensions are shown in Fig. 2. Fig. 3 shows the radiation patterns obtained in the following cases: (i) prescribed Taylor pattern without obstacle, (ii) prescribed Taylor pattern blocked by the obstacle, (iii) free-space radiation pattern synthesised with the proposed method (λ = 0.7) and (iv) radiation pattern obtained with the proposed method including the scattering of the obstacle. It is important to note the good agreement between (iii) and (iv) which demonstrates that the synthesised array does isolate the obstacle; otherwise, (iv) provides an important improvement with respect to the blocked array (ii). In (ii) and (iv), the scattering from the obstacle is obtained by determining the induced currents over the surface B via a method of moments formulation [5].

Conclusions: A new method for synthesising array antennas in the presence of arbitrary obstacles has been presented, which allows the synthesis of a prescribed far field pattern while trying to isolate near field obstacles through a minimisation performed over a power magnitude in their boundary. This technique is straightforward to apply and does not require the use of numerical electromagnetic methods for characterising the coupling of the obstacle. It has been shown to be very efficient, providing results that can be as good as those obtained with previous more rigorous techniques [2]. Although numerical results have been presented for PEC obstacles, the method is general for any kind of material obstacles.

Acknowledgments: This work has been supported by Spanish CICYT, Project Ref. TIC97-0821-C02-01 and by the U.S. European Office of Aerospace Research and Development (EOARD) and the U.S. Air Force Office of Scientific Research (AFOSR).

18 June 1998

Electronics Letters Online No: 19981081

L. Landesa, F. Obelleiro, J.L. Rodríguez and A.G. Pino (*Departamento de Tecnoloxías das Comunicacións, E.T.S.E Telecomunicación, Universidade de Vigo, Campus Universitario S/N, 36200 Vigo, Spain*)

E-mail: landesa@tsc.uvigo.es

J.A. Rodríguez and F. Ares (*Departamento de Física Aplicada, Grupo de Sistemas Radiantes, Facultade de Física, Universidade de Santiago de Compostela, 15706 Santiago de Compostela, Spain*)

References

1 STEYSKAL, H.: 'Synthesis of antenna patterns with imposed near field nulls', *Electron. Lett.*, 1994, **30**, (24), pp. 2000–2001

2 LANDESA, L., OBELLEIRO, F., RODRÍGUEZ, J.L., and PINO, A.G.: 'Pattern synthesis of array antennas in presence of conducting bodies of arbitrary shape', *Electron. Lett.*, 1997, **33**, (18), pp. 1512–1513

3 OBELLEIRO, F., LANDESA, L., RODRÍGUEZ, J.L., PINO, A.G., and PINO, M.R.: 'Directivity optimisation of an array antenna with obstacles within its near field region', *Electron. Lett.*, 1997, **33**, (25), pp. 2087–2088

4 STEYSKAL, H.: 'Synthesis of antenna patterns with prescribed nulls', *IEEE Trans. Antennas Propag.*, 1982, **30**, (2), pp. 273–279

5 HARRINGTON, R.F.: 'Field computation by moment method' (IEEE Press, 1993)

Small slot-coupled circularly-polarised microstrip antenna with modified cross-slot and bent tuning-stub

Kin-Lu Wong and Ming-Huang Chen

A novel design of small slot-coupled circularly-polarised circular microstrip antenna with a modified cross-slot cut in the patch and a bent tuning-stub aligned along the patch boundary is proposed and experimentally studied. Results show that, for fixed circular polarisation (CP) operation, the antenna proposed can have an antenna size reduction of ~80%, as compared to a regular-size CP design. The significant size reduction of the proposed antenna is due to the novel modified cross-slot cut in the patch, and CP operation is obtained using a bent tuning-stub incorporating a properly oriented coupling-slot in the ground plane of the microstrip feed line.

Introduction: Owing to recent requirements in the miniaturisation of personal communications systems, the design of small or reduced-size microstrip antennas has become an important subject. Several reduced-size CP designs have also been reported [1, 2] in which CP operation is achieved by adjusting the embedded slot in the patch centre or the inserted slits at the patch edges to be slightly asymmetric. Such reduced-size CP designs usually exhibit stringent fabrication tolerances when the antenna size reduction is > 50%. This is because, in such cases, very small asymmetry in the embedded slot or inserted slits is required to achieve CP operation. To ease the problem, the reduced-size CP design with a symmetric cross-slot embedded in the patch centre has been shown [3] in which CP operation is achieved by using a straight tuning-stub loaded at the patch boundary, and the required tuning-stub length for CP operation at a large antenna size reduction can be as large as ~26% of the patch's linear dimension, which significantly eases the stringent fabrication tolerances as required in [1, 2]. In this Letter, we demonstrate another promising reduced-size CP design using a novel symmetric slot embedded in the patch, and the CP operation is adjusted by using a bent tuning-stub aligned along the patch boundary to make the proposed antenna more compact in total size. Excitation of the proposed antenna is through a properly oriented coupling-slot in the ground plane of the microstrip feed line. Details of the proposed antenna are described, and experimental results of the CP performance are shown.

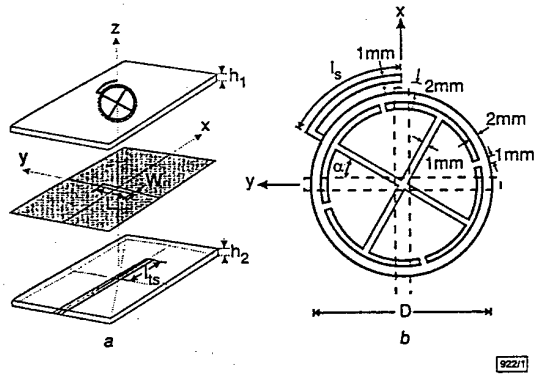

Fig. 1 *Exploded view and top view of circularly-polarised circular microstrip antenna with modified cross-slot and bent tuning-stub*

a Exploded view
b Top view

Antenna design and experimental results: Fig. 1 shows the geometry of the proposed design. The circular patch has a diameter of 25mm (D) and is printed on a substrate of thickness 1.6mm (h_1) and relative permittivity 4.4 (ε_1). A modified cross-slot of equal slot lengths is cut in the patch. The slot length is chosen to be greater than 0.8 times the diameter of the circular patch in order to result in a large meandering of the excited fundamental patch surface current path to lower the resonant frequency of the micro-

Date: Thu, 21 Jan 1999 19:50:20 -0600
From: Kai Chang <chang@ee.tamu.edu>
To: faares@usc.es
Subject: paper acceptance

No: 98445
Authors: J.A. Rodriguez, et al.
Title: Antenna Array Pattern Synthesis in ...

Dear Dr. Ares:

I am pleased to inform you that your paper has been accepted for publication in the Microwave and Optical Technology Letters and will appear in the May 20, 1999 issue.

I would like to emphasize that the editing of your manuscript is very light,
and for this reason as well as time constraints, we will not show you any proof.
If there are problems with your manuscript we will return it to you before typesetting.

There is no page charge, and the corresponding author will receive six copies of the issue in which this article appears without charge in 4-6 weeks after publication. Additional prints can be ordered on the form provided by Wiley later. If there is a problem in receiving the free copies, please contact: Mr. George Telecki, John Wiley & Sons, Inc., 605 Third Avenue, New York, NY 10158-0012, USA. Tel: 212-850-6317, Fax:212-850-6264. To keep current with new technologies and developments, please ask your library to subscribe this journal. For subscription information, please contact: Journal Subscription Department, John Wiley & Sons, Inc., 605 Third Avenue, New York, NY 10158-0012,
USA. Email:subinfo@jwiley.com

Sincerely,

Kai Chang
Editor
Tel:409-845-5285
Fax:409-845-6259
Email:chang@ee.tamu.edu

20-10-98
(MOTL)

ANTENNA ARRAY PATTERN SYNTHESIS IN THE PRESENCE OF NEAR-ZONE SCATTERERS: TWO-DIMENSIONAL SCALAR CASE

J.A. Rodríguez, M.V. Lozano, F. Ares.

Grupo de Sistemas Radiantes,
Departamento de Física Aplicada. Facultad de Física,
Universidad de Santiago de Compostela,
15706 Santiago de Compostela.
SPAIN
E-mail: faares@usc.es
Fax: +34-981-520676

ABSTRACT

A new method for the array pattern synthesis in presence of near-zone scatterers in the two-dimensional scalar case is presented. The synthesis is based on the minimization of an objective function using the simulated annealing technique. To take into account the effects of the scatterers the physical optics approximation is used. Examples for a 41-element linear array in presence of perfectly electric conducting cylinders are performed.

INTRODUCTION

The pattern perturbations caused by a scatterer in the proximity of an array antenna is a problem of practical interest, since, for example, masts or wing tips often are within the radiative near-zone of a ship or airborne antenna. In the literature exist some methods to solve this problem in the two-dimensional scalar case. For instance, in [1] an adapted pattern that avoids illuminating

such near-field scatterers on transmit, or rejects the corresponding scattered waves on receive, can result in a significantly improved antenna far-field response. However, this method imposes a more severe field constraint than necessary and it does not allow direct sidelobe control. Recently, a generalization of this method for large objects has been presented [2], nevertheless it shows the same limitations as [1]. Another solution in the two-dimensional case, presented in [3], tries to take into account the obstacles as parasitic elements, including them in a pattern synthesis algorithm, which allows to take advantage of their scattering even for large obstacles. This method only considers scatterers with cross sections oblong in the direction of the propagation of the wave, which has been demonstrated that reduce the blockage width (width of an equivalent ideal shadow which produce the same forward scattered field as the actual cylinder) with respect to cylinders with circular sections [4]. Furthermore, the improvement on the sidelobe level obtained in comparison to the blocked pattern is limited to about 8 dB.

In this letter we present a new method based on the use of the simulated annealing technique [5, 6] along with the physical optics approximation [7] to minimise iteratively, an objective function, which is the difference between the desired specifications of the problem and the obtained ones in each iteration. This optimization is accomplished changing the amplitude and/or the phase of each element excitation. The physical optics approximation is used to compute the influence of the scatterer because, with this approximation, we get acceptable first-order results, only taking minutes for each iteration of run time on a computer instead of hours that would be necessary using other more accurately techniques such as moment methods.

METHOD

Let us consider a linear array of N equispaced isotropic sources, laid out along the x axis (that leads to a scalar problem and is representative of a large aperture antenna with weight control in one plane) and a cylinder with radius r located in front of it in the $(pos_x pos_y)$ position, as indicated in Figure 1. The resulting radiation pattern taking into account this scatterer is given by:

$$F(\phi) = \sum_{i=1}^{N} I_i e^{j\alpha_i} e^{jkx_i \cos\phi} + \sum_{m=1}^{M} I_{ind_m} e^{jk(x_{cm}\cos\phi + y_{cm}\sin\phi)} \qquad (1)$$

where x_i is the position of the *i-th* element of the array, I_i and α_i the amplitude and phase respectively of the *i-th* element excitation and I_{ind_m} is the complex excitation induced in the point m in the cylinder surface. In order to simulate the scattering it was taken M points from the cylinder surface and the induced excitations in these points were calculated using the physical optics approximation by means of:

$$I_{ind_m} = \Delta a_m \sum_{\forall i \in U}^{N} I_i e^{j\alpha_i} e^{\frac{-jk|\vec{r}_{im}|}{\sqrt{|\vec{r}_{im}|}}} 2\sin(\hat{n}_m, \vec{H}_{im}) \qquad (2)$$

where U is the set of array elements that "can see" the m point in the cylinder surface. The term $\vec{r}_{im}$ is the relative vector between the *i-th* element in the array and the m point in the cylinder surface.

Once known the power pattern, the objective function was constructed through the square of the difference between the desired sidelobe level and the obtained sidelobe level. In the case of

amplitude and phase control, it was also included the square of dynamic range ratio (I_{max}/I_{min}) and the square of the difference between the initial amplitude and the current amplitude in every iteration. Besides, all the terms are multiplied by weight constants adjusted to obtain the best results. The minimization of this cost function is accomplished varying I_i and α_i in the case of using amplitude and phase changes or α_i in the case of phase-only control.

RESULTS

We started from a linear array of 41 isotropic sources with $d = \lambda/2$ interelement spacing. Using initial excitations for this array to produce a -40 dB Taylor pattern ($\bar{n}$=10), two examples were performed using a cylinder with r = 1.0 λ and taking $M = 200$ points in the cylinder surface. In the first example the cylinder location was (0λ, 10λ). Since the cylinder is located in the centre of the linear array, symmetric amplitudes and phases for the excitations in the array were used. In Figure 2 they are shown the blocked pattern that has a sidelobe level of about -12 dB, the optimized pattern with phase-only control with a sidelobe level of -23.4 dB and the optimized pattern with amplitude and the phase control, which has a sidelobe level of -29.7 dB. In this last case the calculated dynamic range ratio was 6.94 and, obviously, for the phase-only control case the dynamic range ratio was the same as the original Taylor pattern (9.31). Therefore depending on the method performed, an improvement of 11.4 dB (phase-only control) or 17.7 dB (amplitude and phase control) is obtained.

In the second example the cylinder is located in (5λ, 10λ), therefore we do not used symmetric amplitudes and phases. In Figure 3, there are shown again the blocked pattern, the optimized

pattern with phase-only control and the one with amplitude and phase changes. The sidelobe levels in both sides left and right for each pattern are, respectively: -15.3 dB and -15.1 dB for the blocked pattern, -29.7 dB and -24.2 dB for the pattern obtained with phase-only control optimization and -34 dB and -29 dB for the optimized pattern using amplitude and phase control. The dynamic range ratio in this last case is 9.3.

CONCLUSIONS

We have presented an array pattern synthesis method to take into account the presence of near-field scatterers using the simulated annealing technique and the physical optics approximation in order to minimize an objective function. This minimization was performed in two ways: changing both amplitude and phase of the excitations of the array or only changing the excitation phase. This method can be applicable to the more complicated three-dimensional problem directly, in which is necessary to consider finite cylinders and to take into account the polarization. In fact, dipole planar arrays for a ground-mapping radar (with a $\csc^2(\theta)\cos(\theta)$ vertical pattern over a specific range and a pencil beam horizontal pattern) in presence of finite cylinders is being studied.

Finally, it is possible to apply the method to scatterers with arbitrarily sections (not only circular).

ACKNOWLEDGEMENTS

This work has been supported by the U.S. European Office of Aerospace Research and Development Board (EOARD) and the U.S. Air Force Office of Scientific Research (AFOSR).

The authors are also grateful to Dr. Hans Steyskal of Air Force Research Laboratory / SNHA Hanscom AFB, Massachusetts for many discussions on this topic.

REFERENCES

[1] H. Steyskal, "Synthesis of antenna patterns with imposed near-field nulls", Electron. Lett., 1994, 30, (24), pp. 2000-2001.

[2] L. Landesa, F. Obelleiro, J.L. Rodríguez, J.A. Rodríguez, F. Ares, and A.G. Pino, "Pattern synthesis of array antennas with additional isolation of near-field arbitrary objects", To be published in Electron. Lett.

[3] L. Landesa, F. Obelleiro, J.L. Rodríguez, and A.G. Pino, "Pattern synthesis of array antennas in presence of conducting bodies of arbitrary shape", Electron. Lett., 1997, 33 (18), pp. 1512-1513.

[4] P-S. Kildal, A. Kishk, and A. Tengs, "Reduction of forward scattering from cylindrical objects using hard surfaces", IEEE Trans. Antennas and Propag., 1996, 44 (11), pp. 1509-1520.

[5] F. Ares, J.A. Rodríguez, E. Villanueva, and S.R. Rengarajan, "Application of genetic algorithms in the design an optimization of array patterns", To be published in IEEE Trans. Antennas and Propag. Special Issue on Phased-array Antennas.

[6] F. Ares, "Application of genetic algorithms and simulated annealing to some antenna problems", chapter of the book: "Electromagnetic system design using evolutionary optimization genetic algorithms", Rahmat Samii, Y., Michielsen, E. Eds. John Wiley and Sons, to be published in 1998.

[7] L. Díaz. and T. Milligan, "Antenna engineering using physical optics, practical CAD techniques and software", 1996, Artech House, Inc. Norwood, Massachusetts (USA).

Figure captions:

Figure 1: Geometry used for the two-dimensional problem of a linear array antenna in presence of a cylindrical scatter.

Figure 2: Power patterns optimized with phase-only control and using amplitude and phase changes in case of locating a cylinder in (0λ, 10λ). The initial blocked pattern, in dashed line, is also shown.

Figure 3: Power patterns optimized with phase-only control and using amplitude and phase changes in case of locating a cylinder off-centre ((5λ, 10λ) position) in relation to the centre of the array. The initial blocked pattern is shown in dashed line.

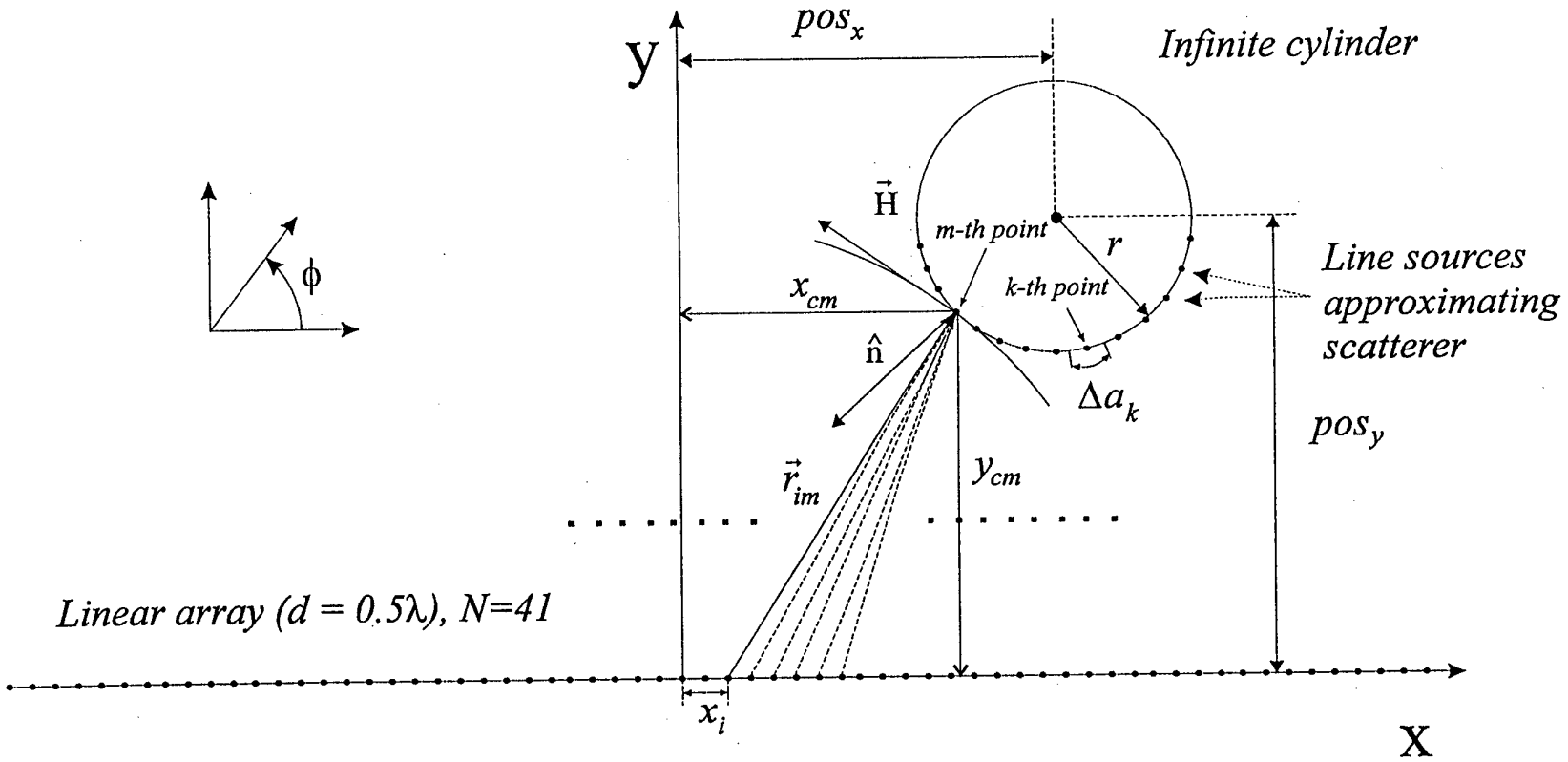
y
pos_x
Infinite cylinder
$\vec{H}$
m-th point
r
k-th point
x_{cm}
$\hat{n}$
Δa_k
Line sources approximating scatterer
pos_y
$\vec{r}_{im}$
y_{cm}
Linear array (d = 0.5λ), N=41
x_i
X
ϕ

Figure 1

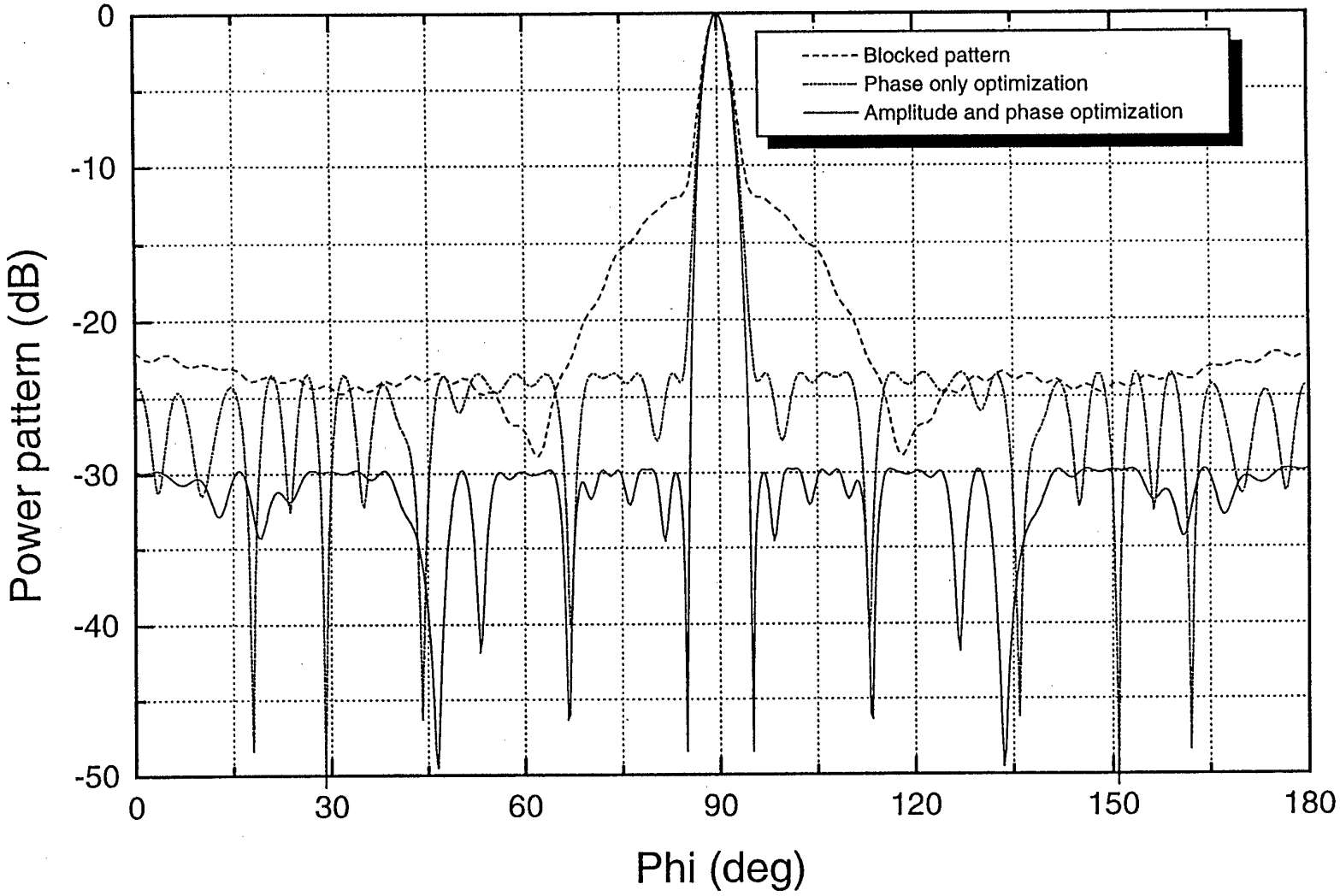
Blocked pattern
Phase only optimization
Amplitude and phase optimization
Power pattern (dB)
0
-10
-20
-30
-40
-50
0
30
60
90
120
150
180
Phi (deg)

Figure 2

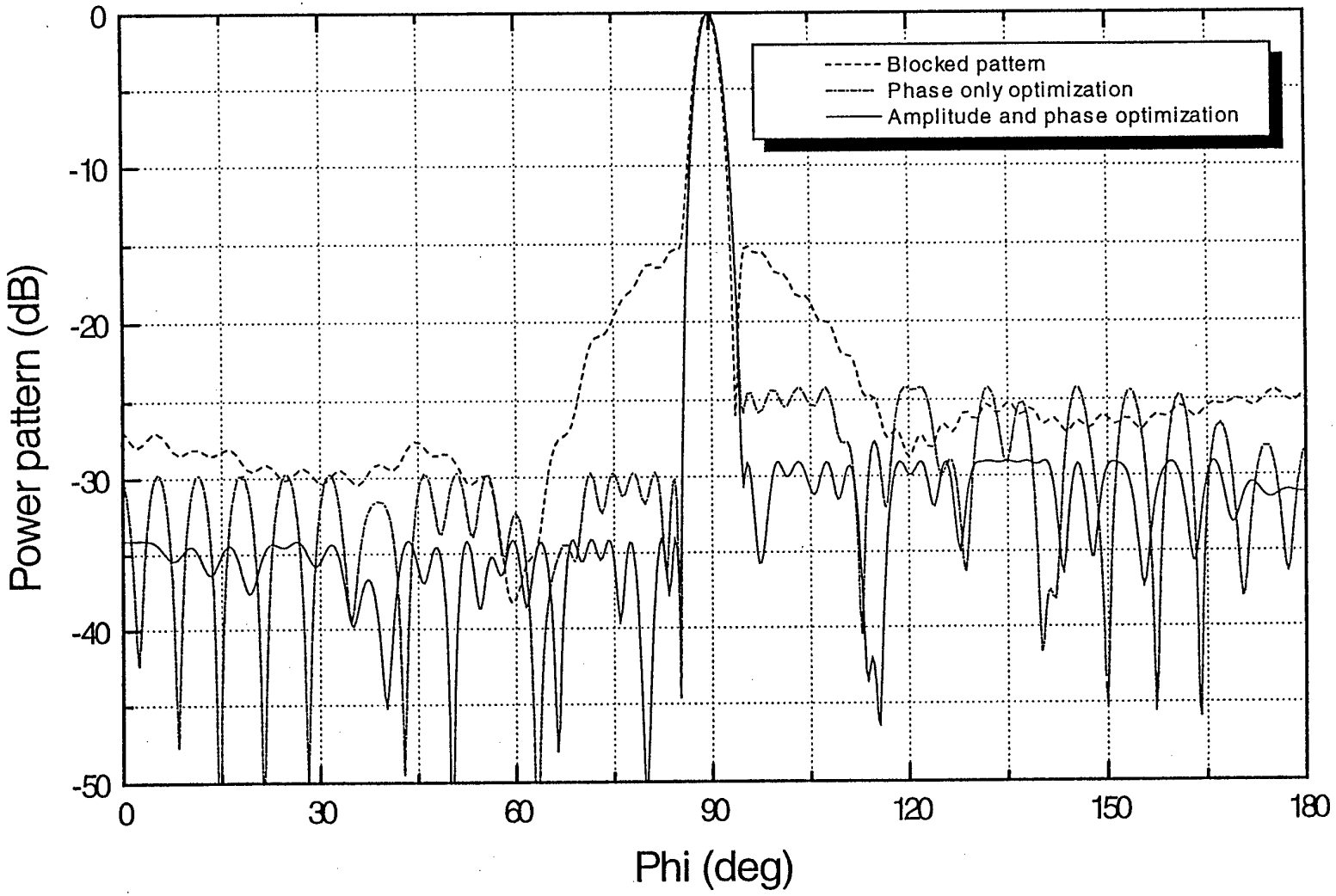
Blocked pattern
Phase only optimization
Amplitude and phase optimization
Power pattern (dB)
0
-10
-20
-30
-40
-50
0
30
60
90
120
150
180
Phi (deg)

Figure 3

JEWA: 5-III-99

ANTENNA ARRAY PATTERN SYNTHESIS IN THE PRESENCE OF NEAR-ZONE SCATTERERS: THREE-DIMENSIONAL VECTOR CASE

M. Vicente-Lozano and F. Ares-Pena.

Grupo de Sistemas Radiantes, Departamento de Física Aplicada

Facultad de Física, Universidad de Santiago de Compostela.

15706 Santiago de Compostela

SPAIN

Running Head: Pattern synthesis with near-zone scatterers: 3D analysis.

Author responsible for correspondence:

Francisco Ares-Pena.

Grupo de Sistemas Radiantes, Departamento de Física Aplicada.

Facultad de Física, Universidad de Santiago de Compostela.

Tel. +34 981 547084. Fax: +34 981 520676.

E-mail: faares@usc.es

Abstract:

A method for the array pattern synthesis in the presence of near-zone scatterers in the three-dimensional vector case is presented. The synthesis is based on the minimization of an objective function using the simulated annealing technique. In order to take into account the effects of the scatterers, the physical optics approximation is used. The polarization in both the incident and the scattered fields is also taken into account. Examples for a 10x10-element planar array of dipoles in the presence of a perfectly electric conducting cylinder are presented.

I. INTRODUCTION

The perturbations caused by a scatterer in the proximity of an array antenna are being a practical problem with applications in ship or airborne antennas. To solve this problem, some methods that deal with the two-dimensional problem have been developed in the literature. In [1] an adapted pattern which avoids illuminating near-field scatterers on transmit, or rejects the corresponding scattered waves on receive, is proposed by introducing nulls in the near-zone of the pattern. However the method may impose a more severe field constraint than necessary and does not allow direct sidelobe control. The method described in [2] has the same limitations as [1] but with a generalization for large objects. The solution presented in [3] uses a pattern synthesis algorithm including parasitic elements, trying to take into account their effects, which allows to take advantage of the scattering even for large obstacles. Nevertheless the method only considers scatterers with oblong cross sections, which has been demonstrated that reduce the blockage width with respect to scatterers with circular sections [4]. These scatterers with circular sections were also analyzed in [5] using the simulated annealing technique to avoid as much as possible the presence of the scatterer and taking a direct control to the sidelobe level of the scattered power pattern. The problem was also analyzed in two dimensions and the effects of the scatterer were simulated using physical optics [6].

In this paper, we present an extension of [5] to three dimensions, and taking into account the polarization to emulate a realistic situation, using again the simulated annealing along with the physical optics approximation. This method minimizes, iteratively, an objective function, which involves parameters of interest in the optimization: sidelobe levels and current dynamic range ratio. The optimization is performed by changing the amplitude and/or the phase of each element excitation. By using the physical optics approximation to compute the influence of the scatterer, acceptable first order results are obtained in only

minutes of computation time instead of hours if more accurately methods, such as moment methods, are used.

METHOD

Let us consider a planar array of $P \times Q = N$ dipoles with $2l = \lambda/2$ length located in the XZ plane, separated d_x in the x-direction and d_z in the z-direction. In front of the dipole array, a cylinder of radius r and height h is located, which acts as a scatterer, as it is shown in Figure 1.

The field pattern produced by the array of dipoles in the presence of the cylinder is calculated in two steps:

1. First of all we need to calculate the induced complex currents in the cylinder. We use physical optics approximation over the entire cylinder, which has been previously divided into a certain number of cells with area Δa_m, which depends on the cylinder size. The expression for every induced excitation over an m-th cell is given by:

$$I_{ind_m} = \Delta a_m \sum_{\forall i \in U} 2H_{\varphi_{im}} \sin(\hat{n}_m, \bar{H}_{\varphi_{im}}) \tag{1}$$

where $\hat{n}_m$ is the normal vector to the m-th cell surface, $\bar{H}_{\varphi_{im}}$ is the complex magnetic field produced by the *i-th* dipole in the *m-th* cell and U is the set of cells that are not in the "shadow" of the array radiation. The expression used for the magnetic field is given by [7]:

$$H_\varphi = \frac{jI_d}{4\pi\rho}\left[e^{-jkR_1} + e^{-jkR_1} - 2(\cos kl_1)e^{-jkr}\right] \tag{2}$$

where all the parameters are explained in Figure 2.

2. Once we have calculated every induced current in the cylinder, we can obtain the total field, which is the sum of the array contribution and the cylinder contribution. In order to calculate the scattered field we consider a local system in every cell of the cylinder. The contribution of every cell is added (in a global coordinate system) to calculate the contribution of the entire cylinder.

In Figure 3 it is shown that exist two currents in every cell, one in the z_m direction and other in the local ϕ_m direction. However, due to the physical optics approximation only a current in the z_m direction will exist. In any case, and trying to simulate the real situation, the existence of a current in the x_m direction and a current in the z_m-direction is considered. The presence of a current in the y_m direction is supposed to be negligible because the curvature of every local cell is small if we take M large enough. To calculate the value of each current (in the z_m and x_m directions) we suppose that the total current forms an angle β with the z_m axis, therefore:

$$\begin{aligned} I_{z_m} &= I_{ind_m} \cos\beta \\ I_{x_m} &= I_{ind_m} \sin\beta \end{aligned} \tag{3}$$

In other words we assume that there are two elementary electric dipoles in every cell, one along the z_m direction and another along the x_m direction.

With this assumption, the final vector field pattern is given by:

$$\vec{F}(\theta,\phi) = \overrightarrow{FE}(\theta)\sum_{i=1}^{N} I_i e^{jk(dpx_i \sin\theta\cos\phi + dpz_i\cos\theta)} + \sum_{m=1}^{M} \overrightarrow{FE}(\theta_m,\phi_m) I_{ind_m} e^{jk(clx_m \sin\theta_m\cos\phi_m + cly_m \sin\theta_m \sin\phi_m + clz_m\cos\theta_m)} \tag{4}$$

where the *i-th* dipole in the array is located in (dpx_i, 0, dpz_i) and the *m-th* cell in the (clx_m, cly_m, clz_m) position, the element vector factor $\overrightarrow{FE}(\theta) = FE(\theta)\hat{\theta}$ is the one associated to a dipole of $2l = \lambda/2$ length along the z direction:

$$\overrightarrow{FE}(\theta) = \frac{\cos\left(\frac{\pi}{2}\cos\theta\right)}{\sin\theta}\hat{\theta} \tag{5}$$

and $\overrightarrow{FE}(\theta,\phi) = FE_\theta(\theta_m,\phi_m)\hat{\theta} + FE_\phi(\theta_m,\phi_m)\hat{\phi}$, where:

$$FE_\theta(\theta_m,\phi_m) = \frac{1}{2} g_\theta(\theta_m,\phi_m)\left[1+\cos\alpha_m - \cos(2\phi_m+\alpha_m) + \cos(2\theta)\right] \tag{6}$$

$$FE_\phi(\theta_m,\phi_m) = g_\phi(\theta_m,\phi_m) \tag{7}$$

In the above equations, since the dipoles in the array produces a polarization field in the θ direction, the factors g_θ and g_ϕ are the copolar and crosspolar components of the element factors of each cell in the cylinder; the angles θ_m and ϕ_m are the angles related to the local system in the m-th cell. Finally, the global coordinate system and the local system of a m-th cell are related through a clockwise rotation about the z-axis of α_m. Therefore, we first calculate the element factor in each local system an then we move it to the global system for adding all cell contributions [8].

In order to manage a more suitable expression we separate the field pattern in its copolar (θ direction) and crosspolar (ϕ direction) components:

$$\vec{F}(\theta,\phi) = F_\theta\hat{\theta} + F_\phi\hat{\phi} \tag{8}$$

In the presence of the cylinder the initial power pattern is blocked and a rise in the sidelobe level is produced. Our goal is to obtain a suitable set of currents for the array of dipoles so that the cylinder contribution in the sidelobe level of the copolar component (F_θ) was minimized. The crosspolar component (F_ϕ) is also minimized as much as possible.

The initial currents of the dipoles were perturbed, through the simulated annealing technique, to accomplish the requirements about the sidelobe level and about the current dynamic range ratio ($|I_{max}/I_{min}|$), which should be maintained close (or reduced) to low values. The perturbation can be performed varying the amplitude and phase or varying only the phase of each dipole excitation. The choice of the better amplitudes and/or phases is made according to the minimization of a given cost function, which involves the parameters that need to be controlled (i.e. sidelobe levels and dynamic range ratio).

EXAMPLES

In this section we present some examples selected from all the examples performed. We chose a dipole array of 10×10 elements separated 0.7λ in both directions (z and x). The β

angle used was $\beta = 10$ deg. In all of them the initial power pattern used is a Chebyshev power pattern (without cylinder) with a sidelobe level of –40 dB and with a current dynamic range ratio of 31.1. Two different cylinders with 0.5λ radius were used; one was 6λ high and the other 4λ high. Each cylinder was located centered in front of the array of dipoles at distances of 5λ and 8λ. The cylinders were divided in the minimum number of cells as possible, maintaining the shape of the total power pattern, i.e., more cells in the cylinder did not alter the pattern in a significant way.

Example 1: Cylinder height $h = 6\lambda$, distance from the array $d = 8\lambda$. Number of cells in the cylinder: $25 \times 15 = 375$.

After locating the cylinder, the highest sidelobe level for the copolar component was –25.19 dB, and the crosspolar –39.23 dB, which occurs in the $\phi = 0$ cut.

1.a) Amplitude and phase control.

Performing the optimization with amplitude and phase control, the final sidelobe level was –30.31 dB, which implies an improvement of 5.12 dB. The crosspolar remained almost unaltered and its final value was –38.05 dB. In case of the current dynamic range ratio it was lowered to 16.97. In Figure 4 the blocked and the recovered power patterns (copolar and crosspolar components) in the $\phi = 0$ cut, which was always the most perturbed, are shown.

In order to have a more general view of the sidelobe level improvement, in Figures 5 and 6 a 3D representation of the blocked and the optimized copolar components of the power patterns are shown. The Figure's floor is set to –32 dB and in both of them $u = \sin\theta \cos\phi$ and $w = \cos\theta$, since the array of dipoles is located in the XZ plane. The Figure's floor and u and v will be the same in the rest of the paper.

1.b) Phase-only control.

In this case only a perturbation in the phases of the dipole excitations was introduced. The optimized pattern following this procedure had a sidelobe level in the copolar component

of –29.61 dB (4.37 dB less than the blocked pattern) and the crosspolar one has a level of –37.49 dB. The current dynamic range ratio, obviously, remained unaltered to 31.1.

The $\phi = 0$ cut of the blocked power pattern corresponding to the copolar component and the recovered power patterns (copolar and crosspolar components) are shown in Figure 7. Figure 8 shows a 3D plot of the copolar component of the recovered power pattern.

Example 2: Cylinder height $h = 4\lambda$, distance from the array $d = 5\lambda$. Number of cells in the cylinder: $20 \times 10 = 200$.

In this case, the initial copolar blocked component in the presence of the cylinder had a sidelobe level of –26.92 dB and the crosspolar of –40.60 dB.

2.a) Amplitude and phase control.

The optimization using amplitude and phase perturbations yielded a final power pattern with a sidelobe level of –30.90 dB for the copolar component (4.02 below the blocked pattern). The crosspolar component remained in –40.05 dB and the current dynamic range ratio for the final pattern was 22.34.

As in the previous example, Figure 9 shows the $\phi = 0$ cut of the copolar component of the blocked and recovered power patterns, and the crosspolar component of the recovered power pattern. A 3D representation of the copolar component of the blocked and recovered power patterns are shown, respectively, in Figures 10 and 11.

2.b) Phase-only control.

The searching for the best solution using phase-only control gave an optimized pattern with a sidelobe level of –28.07 dB (1.15 dB less than the blocked patter) for the copolar component and –40.03 for the crosspolar component. The initial copolar component of the blocked pattern and the copolar and crosspolar components of the optimized power patterns

are shown, for the $\phi = 0$ cut, in Figure 12. Finally, Figure 13 shows a 3D representation of the copolar component of the recovered pattern.

Example 3: Cylinder height $h = 6\lambda$, distance from the array $d = 5\lambda$. Number of cells in the cylinder: $25 \times 15 = 375$.

In this example we tried to test the importance of the cylinder height locating the same cylinder as in the first example at a distance $d = 5\lambda$ (the distance used in the second example). The results are shown in Table 1.

Finally, examples 1 and 2 were performed again but using $\beta = 0$ deg., i.e., the current in every cylinder cell had z direction, thus the power pattern has only a copolar component. The results are summarized in Table 2.

CONCLUSIONS

A very important factor in the optimization is the scatterer's height (with reasonable diameters). The distance is also important (large distances imply better results) but with two scatterers with different heights located at the same distance from the array, we obtained better results for the higher scatterer. Examples with greater diameters were performed obtaining similar results as the presented ones, confirming the theory of the height importance.

With regard to the optimization methods, with amplitude and phase control we got results, in most cases, only a few dB's better than using phase-only control. This implies that only changing the phase of the currents in the dipole array, which is physically easier than change the amplitude and the phase, we can obtain good results that improve the scattered power pattern.

In relation to the β angle, with small values the optimization is satisfactory and similar to the case with β = 0 deg. (only a copolar component). As the value of β increases the results are worse, since there are more difference between the copolar and crosspolar components of the scattered field.

ACKNOWLEDGEMENTS

This work has been supported by the U.S. European Office of Aerospace Research and Development Board (EOARD) and the U.S. Air Force Office of Scientific Research (AFOSR).

The authors want also to express their acknowledgement to Dr. Hans Steyskal at Air Force Research Laboratory/SNHA for suggesting this problem, his guidance and helpful discussions about this work.

REFERENCES

[1] Steyskal, H., "Synthesis of antenna patterns with imposed near-field nulls", Electronics Letters, Vol. 20, 2000-2001, 1994.

[2] Landesa, L., Obelleiro, F., Rodríguez, J. L., Rodríguez, J. A., Ares F., and Pino. A. G., "Pattern synthesis of array antennas with additional isolation of near-field arbitrary objects", Electronics Letters, Vol. 34, 1540-1542, 1998.

[3] Landesa, L., Obelleiro, F., Rodríguez, J. L., and Pino. A. G., "Pattern synthesis of array antennas in presence of conducting bodies of arbitrary shape", Electronics Letters, Vol. 33, 1512-1513, 1997.

[4] Kildal, P-S., Kishk, A., and Tengs, A., "Reduction of forward scattering from cylindrical objects using hard surfaces", IEEE Trans. Antennas and Propag., Vol 44, 1509-1520, 1996.

[5] Rodríguez, J. A., Lozano, M. V. and Ares, F., "Antenna array pattern synthesis in presence of near-zone scatterers: two-dimensional scalar case", to be published in Microwave Optical Technology Letters.

[6] Díaz, L., and Milligan, T., *Antenna engineering using physical optics, practical CAD techniques and software"*, Artech House, Inc. Norwood, Massachusetts (USA), 1996.

[7] Elliott, R. S., *Antenna Theory and Design,* Ed. Prentice-Hall Inc., New Jersey, 329-332, 1981.

[8] Duan, D-W., and Rahmat-Samii, Y., "Novel coordinate system an rotation transformations for antenna applications", Electromagnetics, Vol. 15, 17-40, 1995.

Figure Captions:

Figure 1. Array of dipoles in presence of a scatterer cylinder.

Figure 2. Situation of every dipole in the array and parameters used in equation (2).

Figure 3. Current distribution in an *m-th* cell of the cylinder.

Figure 4. $\phi = 0$ cut of the optimized (crosspolar and copolar components) and initial (copolar component) power patterns using amplitude and phase control, $h = 6\lambda$, $d = 8\lambda$.

Figure 5. Surface plot of the initial copolar component of the power pattern, $h = 6\lambda$, $d = 8\lambda$.

Figure 6. Copolar component of the power pattern after performing the optimization using amplitude and phase control $h = 6\lambda$, $d = 8\lambda$.

Figure 7. $\phi = 0$ cut of the optimized (crosspolar and copolar components) and initial (copolar component) power patterns using phase-only control $h = 6\lambda$, $d = 8\lambda$.

Figure 8. Surface plot of the recovered copolar component of power pattern using phase-only control, $h = 6\lambda$, $d = 8\lambda$.

Figure 9. $\phi = 0$ cut of the optimized (crosspolar and copolar components) and initial (copolar component) power patterns using amplitude and phase control $h = 4\lambda$, $d = 5\lambda$.

Figure 10. Surface plot of the initial copolar component of the power pattern, $h = 4\lambda$, $d = 5\lambda$.

Figure 11. Copolar component of the power pattern after performing the optimization using amplitude and phase control, $h = 4\lambda$, $d = 5\lambda$.

Figure 12. $\phi = 0$ cut of the optimized (crosspolar and copolar components) and initial (copolar component) power patterns using phase-only control, $h = 4\lambda$, $d = 5\lambda$.

Figure 13. Surface plot of the recovered copolar component of power pattern using phase-only control, $h = 4\lambda$, $d = 5\lambda$.

Table captions:

Table 1. Results obtained for a cylinder with $h = 6\lambda$, $d = 5\lambda$ and $\beta = 10$ deg.

Table 2. Summary of results using $\beta = 0$ deg.

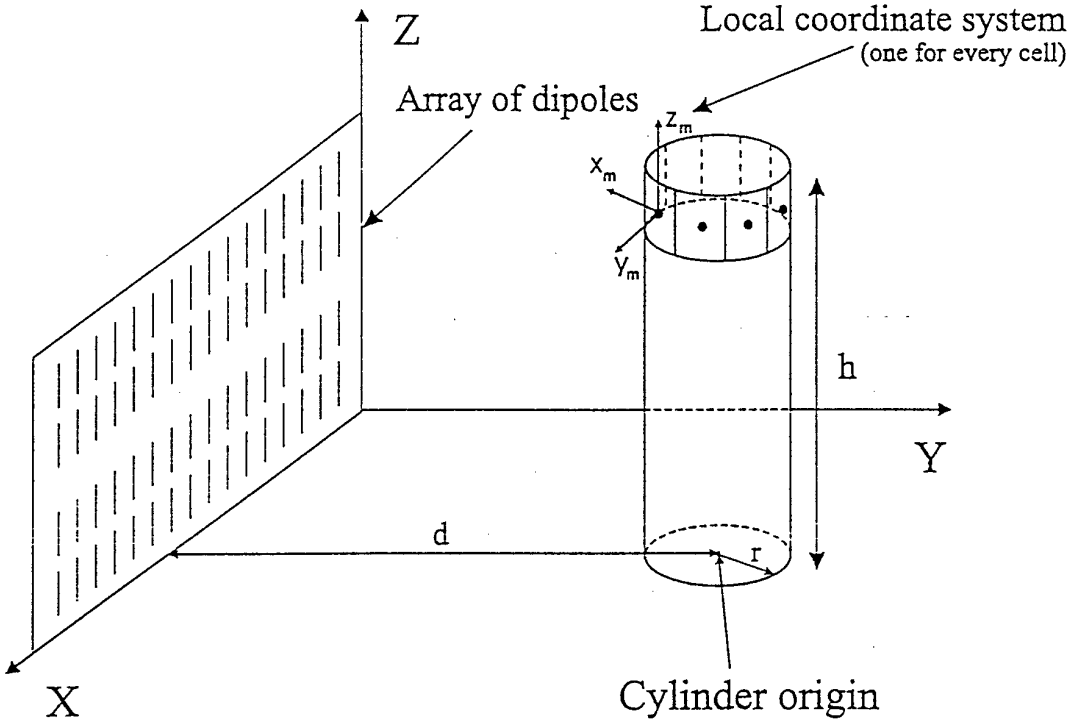
Z
Local coordinate system
(one for every cell)
Array of dipoles
Z_m
X_m
Y_m
h
Y
d
r
X
Cylinder origin

Figure 1.

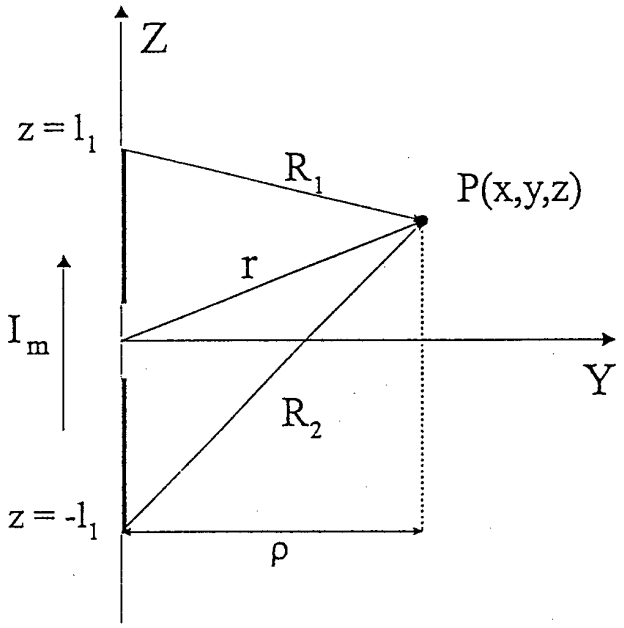

Figure 2.

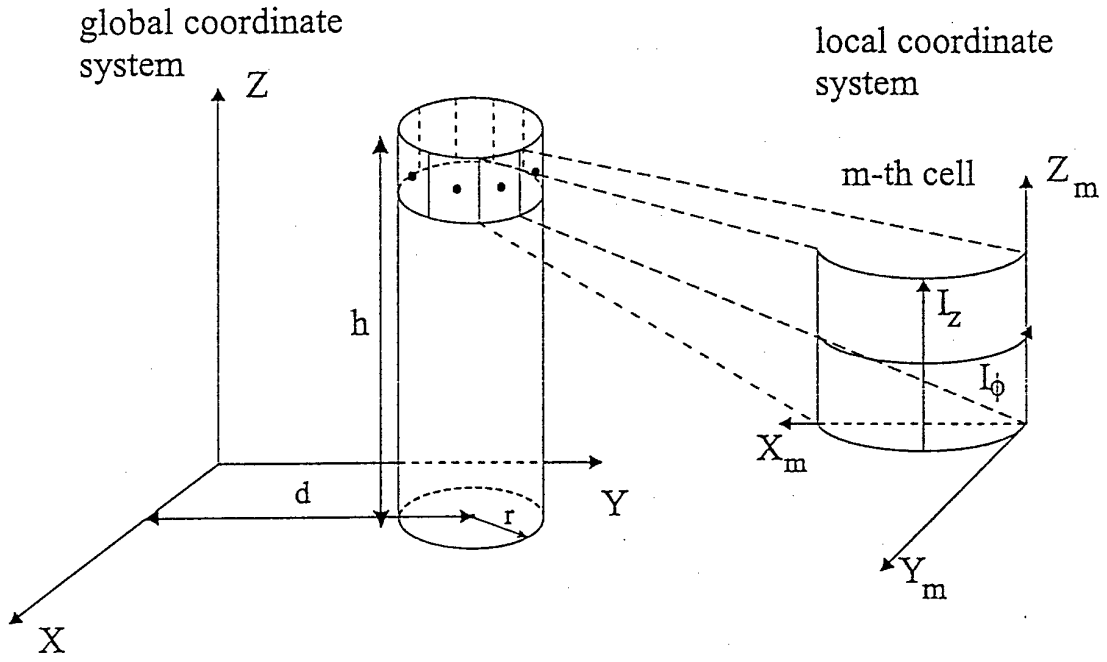
global coordinate system
Z
local coordinate system
m-th cell
Z_m
h
l_z
l_ϕ
X_m
d
r
Y
Y_m
X

Figure 3.

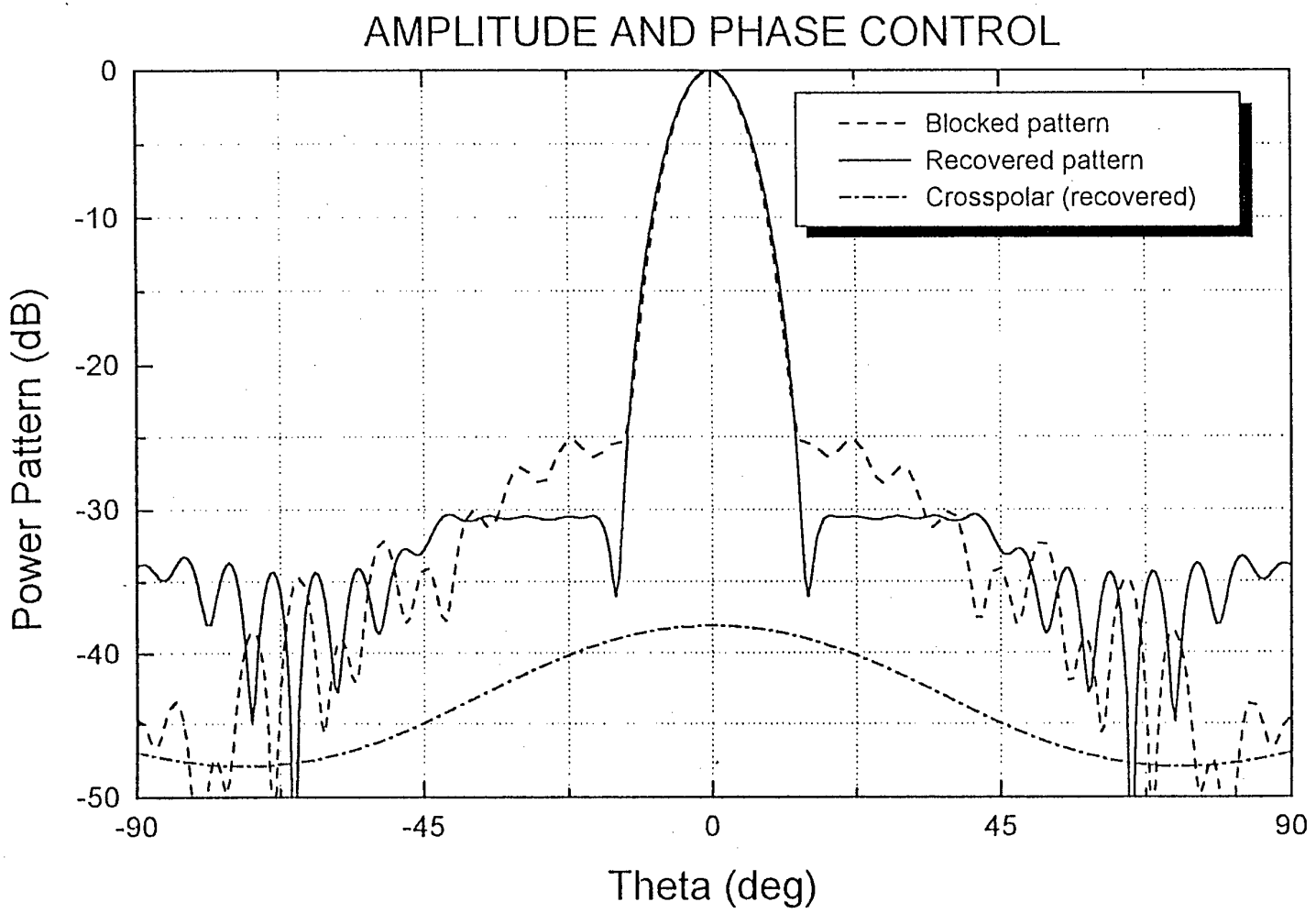
AMPLITUDE AND PHASE CONTROL
Blocked pattern
Recovered pattern
Crosspolar (recovered)
Power Pattern (dB)
0
-10
-20
-30
-40
-50
-90
-45
0
45
90
Theta (deg)

Figure 4

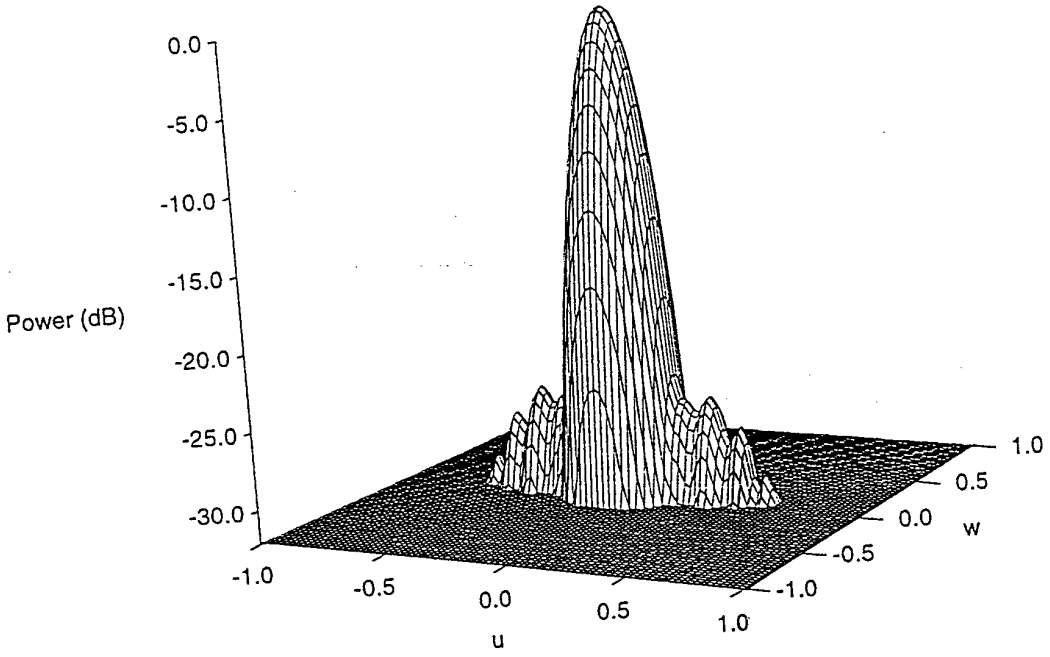

Figure 5.

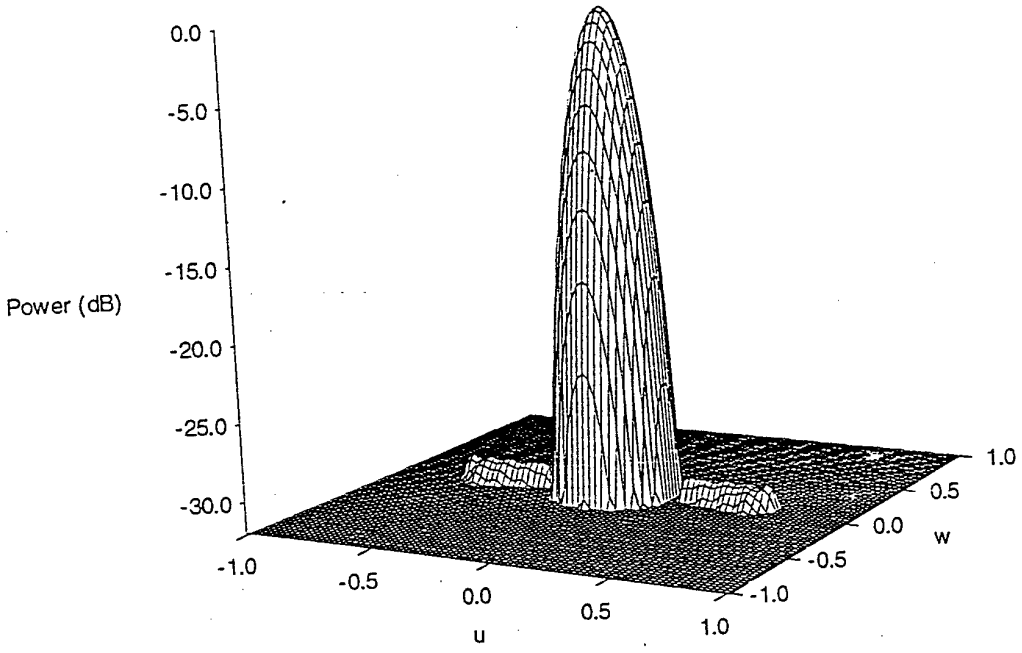

Figure 6.

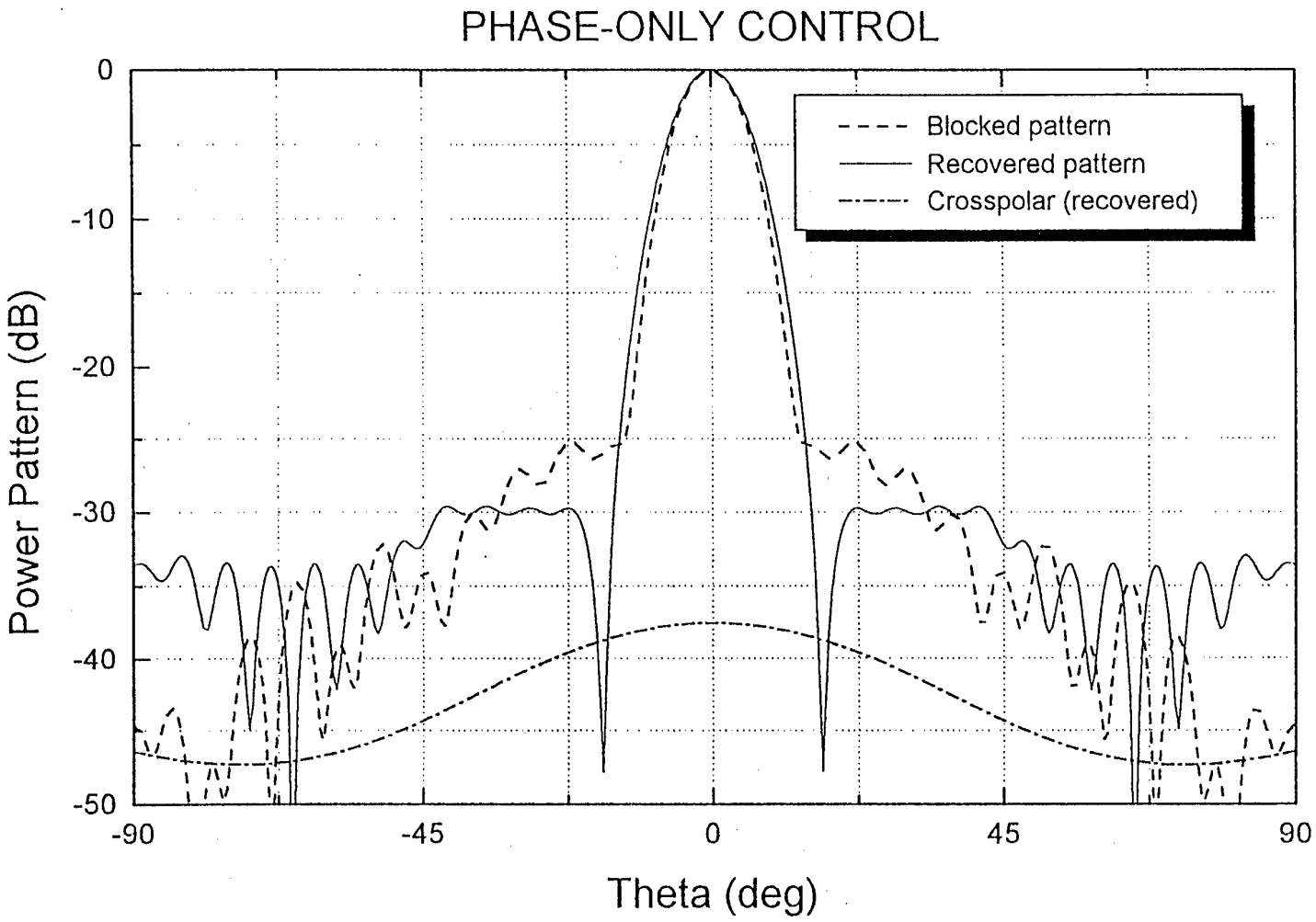
PHASE-ONLY CONTROL
Blocked pattern
Recovered pattern
Crosspolar (recovered)
Power Pattern (dB)
0
-10
-20
-30
-40
-50
-90
-45
0
45
90
Theta (deg)

Figure 7

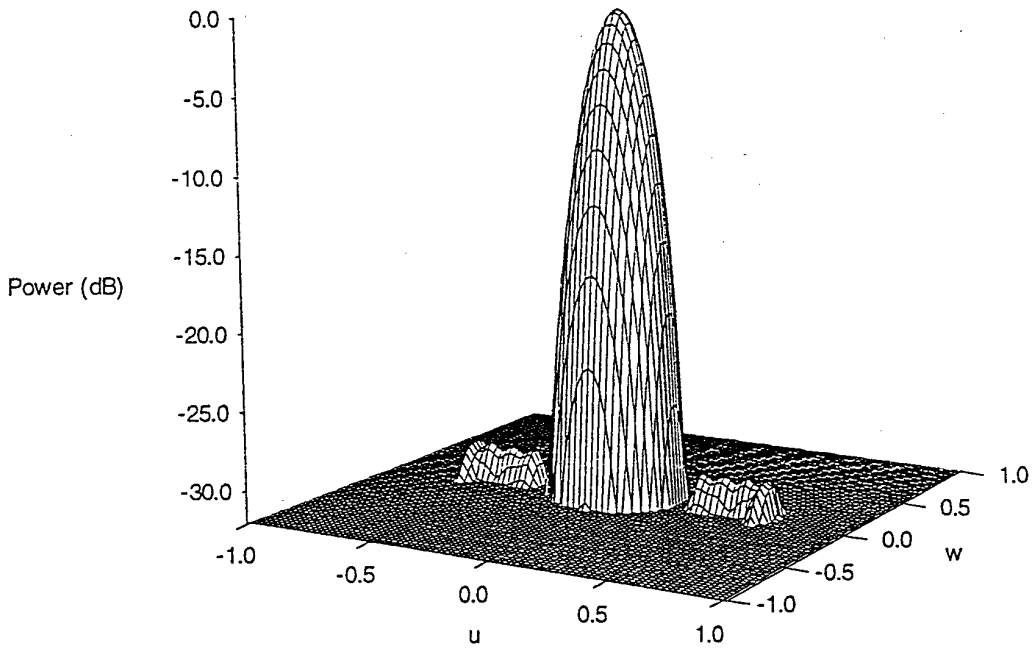

Figure 8.

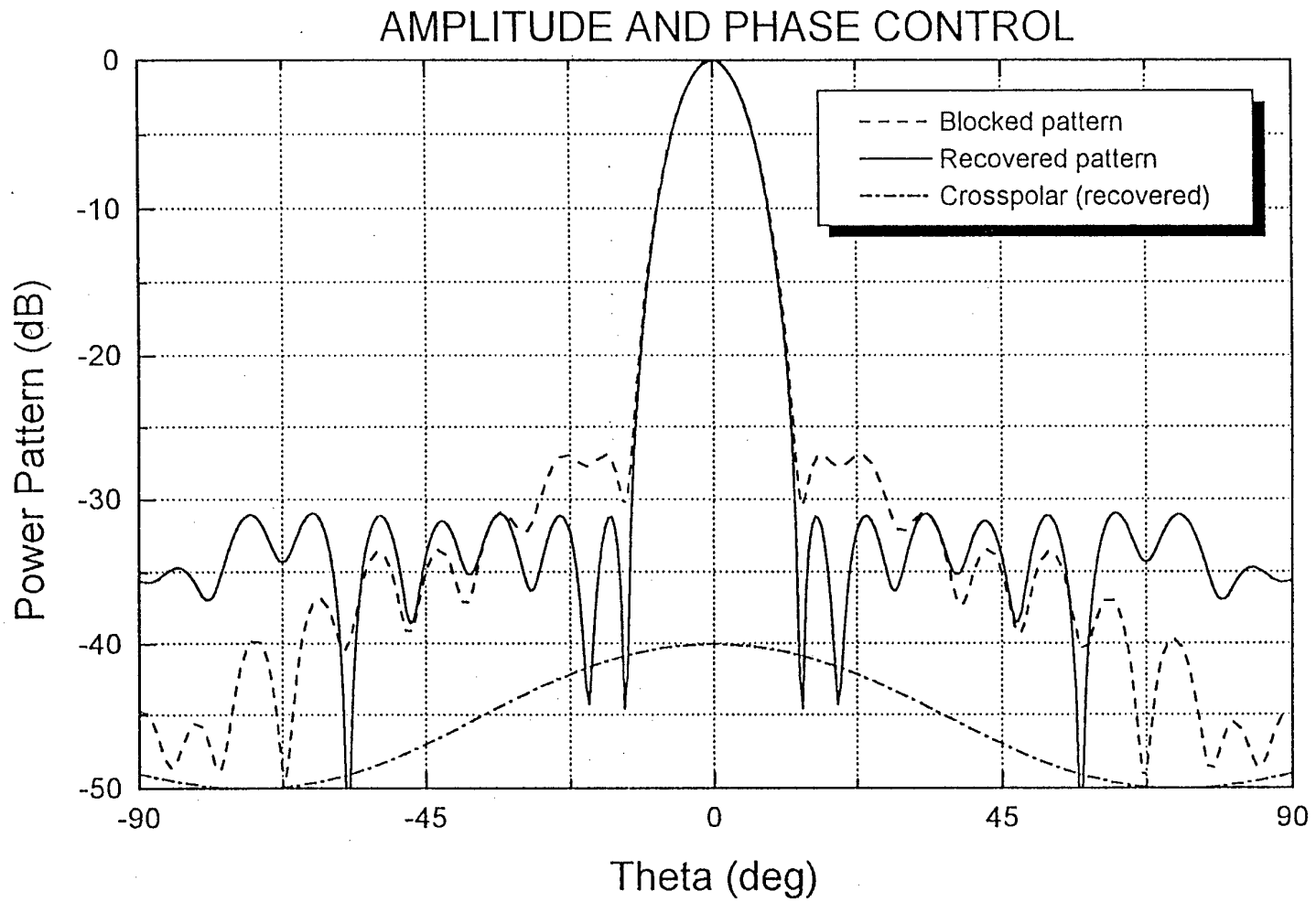
AMPLITUDE AND PHASE CONTROL
Blocked pattern
Recovered pattern
Crosspolar (recovered)
Power Pattern (dB)
0
-10
-20
-30
-40
-50
-90
-45
0
45
90
Theta (deg)

Figure 9

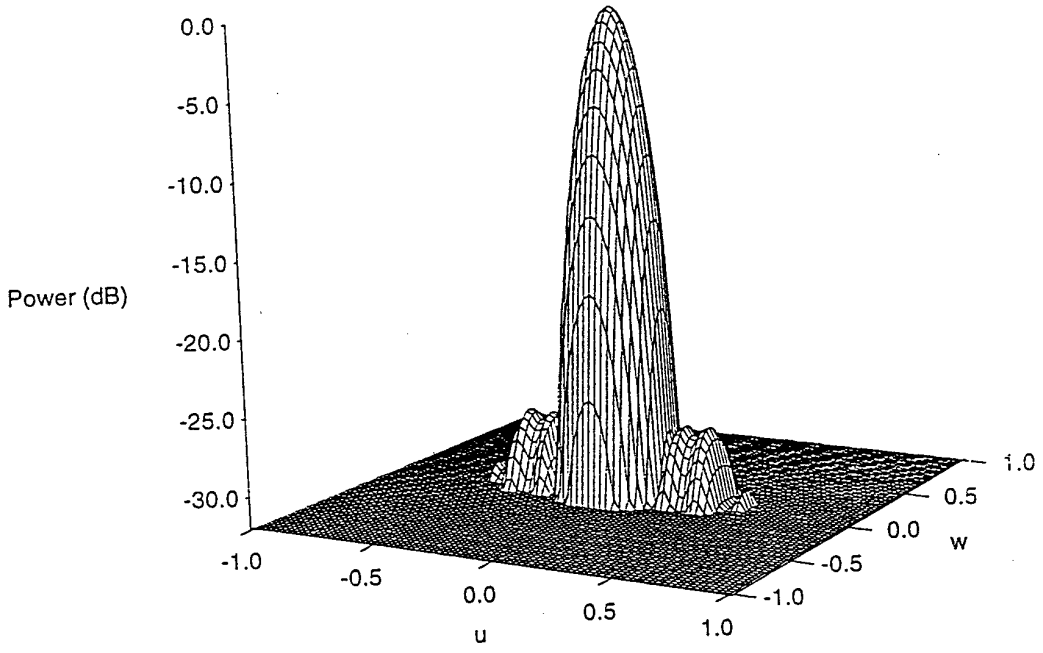

Figure 10.

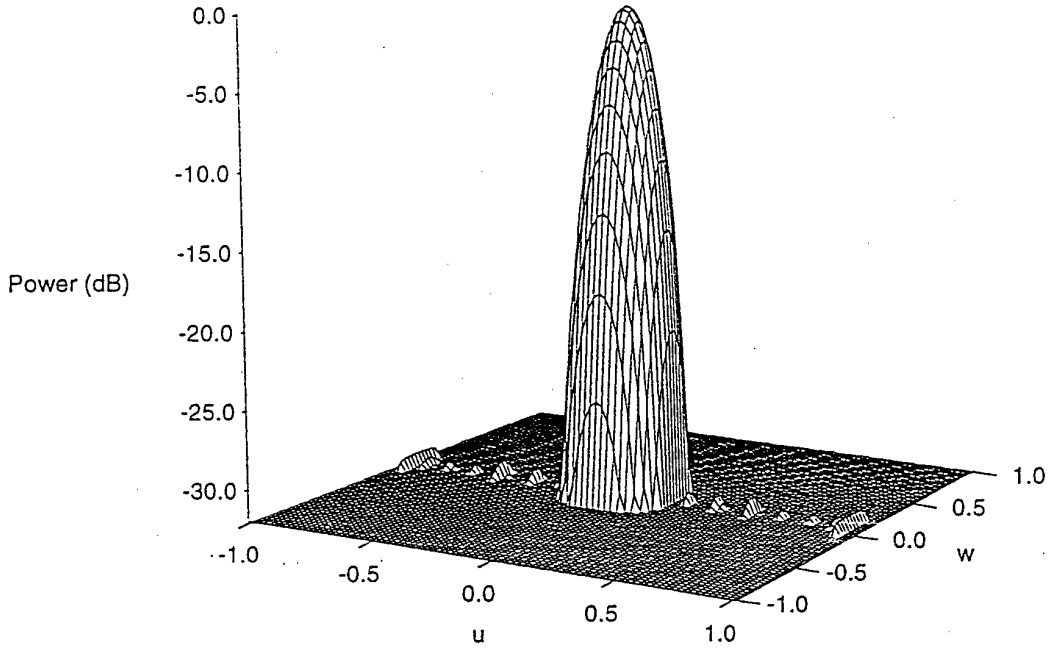

Figure 11.

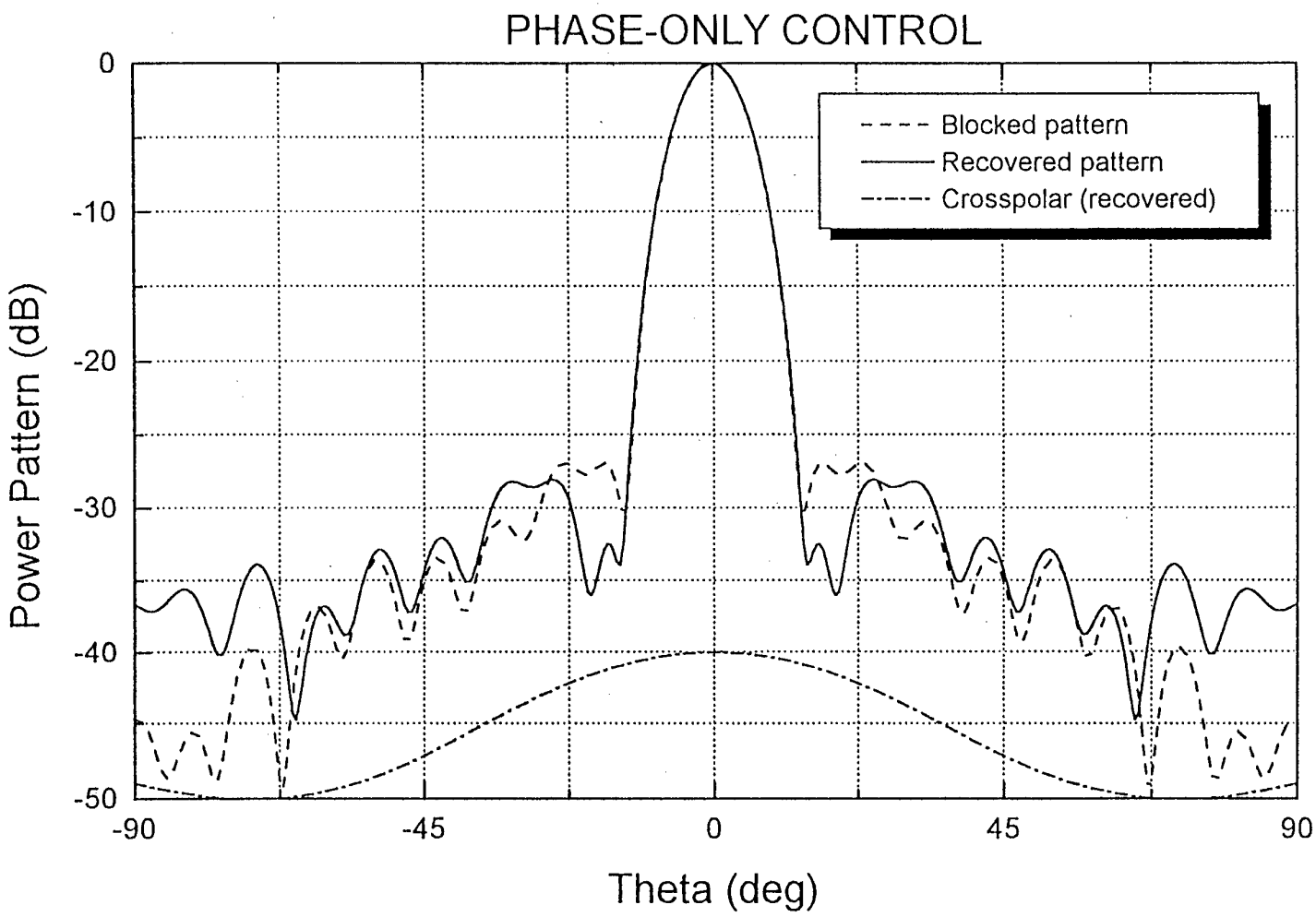
PHASE-ONLY CONTROL
Blocked pattern
Recovered pattern
Crosspolar (recovered)
Power Pattern (dB)
0
-10
-20
-30
-40
-50
-90
-45
0
45
90
Theta (deg)

Figure 12.

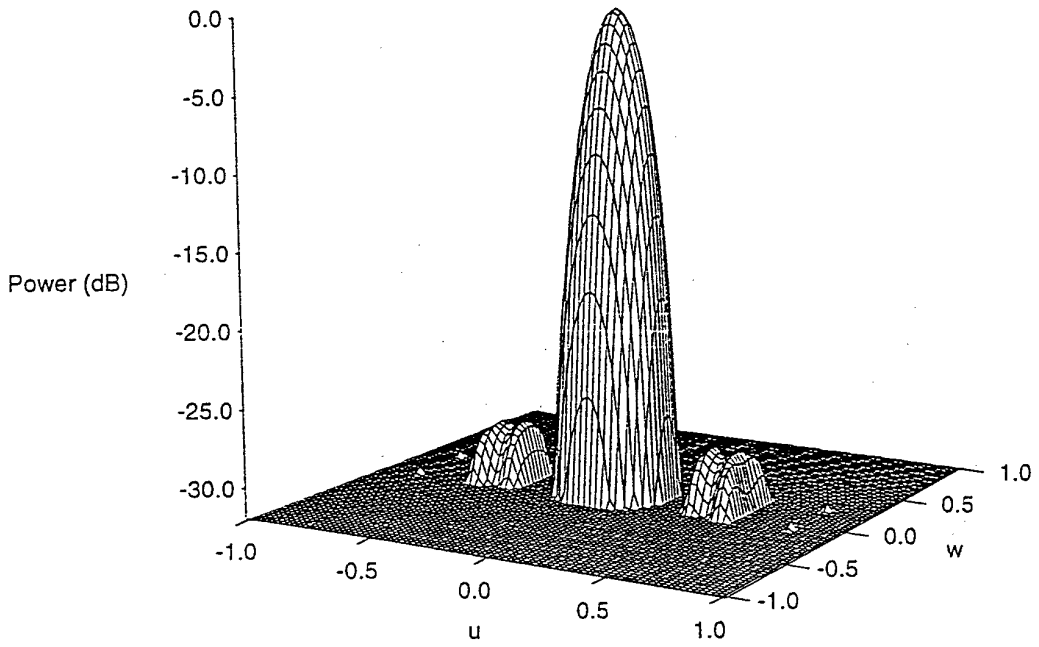

Figure 13.

	Copolar component			Crosspolar component		
Optimization method	Initial SLL (dB)	Final SLL (dB)	Improv. (dB)	Initial SLL (dB)	Final SLL (dB)	$\lvert I_{max}/I_{min} \rvert$
Amplitude and phase control	-25.35	-30.45	5.10	-38.97	-38.30	15.90
Phase-only control	-25.35	-28.97	3.42	-38.97	-38.38	31.10

Table 1.

Optimization Method	h (λ)	d (λ)	Initial sidelobe level	Opmitized sidelobe level	Improvement (dB)	$\lvert I_{max}/I_{min} \rvert$
Amplitude and Phase Control	6	8	-25.08	-30.19	5.11	18.15
Phase-Only Control	6	8	-25.08	-29.53	4.45	31.10
Amplitude and Phase Control	4	5	-26.96	-30.96	4.00	31.67
Phase-Only Control	4	5	-26.96	-28.39	1.43	31.10

Table 2.

Manuel Vicente-Lozano was born in Madrid, Spain, in 1972. He received his B.S. and M.S. degrees in Physics from the University of Santiago de Compostela, Spain. Nowadays he is a Ph. D. student in Physics. His main research activities are focused in microwave circuits and antenna array pattern synthesis. Other activities or interests are programming languages and computer simulation.

Francisco J. Ares-Pena received the B. S. and M. S. degrees from the University of Santiago de Compostela, Spain, in 1986 and 1987 respectively, and the Ph.D. from the same institution in 1993, all in Physics. He is currently an Associate Professor in the Department of Applied Physics at the University of Santiago de Compostela, Spain. He has published more than 80 journal and conference papers. Dr. Ares is a Senior Member of IEEE and a member of the New York Academy of Sciences. His main research interests are antenna array pattern synthesis and design of slot arrays.

EuMC: 2 Marzo 99

ANTENNA ARRAY PATTERN SYNTHESIS IN THE PRESENCE OF NEAR-ZONE SCATTERERS: THREE DIMENSIONAL VECTOR CASE.

M. Vicente-Lozano and F. Ares-Pena

Grupo de Sistemas Radiantes,Departamento de Física Aplicada.
Facultad de Física, Universidad de Santiago de Compostela.
15706 Santiago de Compostela, SPAIN
Tel: +34-981-547084, Fax:+34-981-520676, E-mail: faares@usc.es

Abstract:

A method for the array pattern synthesis in the presence of near-zone scatterers in the three dimensional vector case is presented. The synthesis is based on the minimisation of an objective function using the simulated annealing technique. To take into account the effects of the scatterers, the physical optics approximation is used. The polarisation in both the incident and the scattered fields is also taken into account. An example for a 10x10-element planar array of dipoles in presence of perfectly electric conducting cylinder is presented.

INTRODUCTION

The pattern perturbations caused by a scatterer in the near-zone of an array antenna are a problem of practical interest since, for example, masts or wing tips often are within the radiative proximity of a ship or airborne antenna. In the literature, there exist some methods that deal with the two-dimensional problem [1-3], even using the simulated annealing technique [4]. In this paper, we present an extension to 3D of [4] using again the simulated annealing technique along with the physical optics approximation. This method minimises, iteratively, an objective function, which involves parameters of interest in the optimisation: sidelobe levels, current dynamic range ratio, etc. This optimisation is performed by changing the amplitude and/or the phase of each element excitation. By using the physical optics approximation to compute the influence of the scatterer, acceptable first order results are obtained in only minutes of computation time instead of hours if more accurately methods, such as moment methods, are used.

METHOD

Let us consider a planar array of $P \times Q = N$ dipoles with $2l = \lambda/2$ length located in the XZ plane, separated d_x in the x-direction and d_z in the z-direction. In front of the dipole array, a cylinder of radius r and height h is located, which acts as a scatterer, as it is shown in Figure 1.

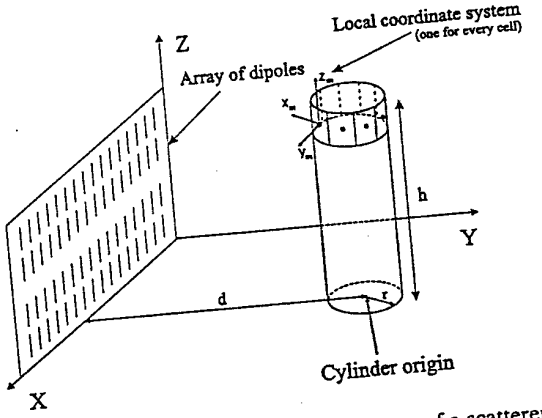

Figure 1: Array of dipoles in the presence of a scatterer cylinder.

The field pattern produced by the array of dipoles in the presence of the cylinder is calculated in two steps:
1.- First of all we need to calculate the induced complex currents in the cylinder. We use physical optics approximation over the entire cylinder, which has been previously divided in a certain number of cells with area Δa_m (depends on the cylinder size). The expression for every induced excitation over a m-th cell is given by:

$$I_{ind_m} = \Delta a_m \sum_{\forall i \in U} 2H_{\phi_{im}} \sin(\hat{n}_m, \vec{H}_{\phi_{im}}) \quad (1)$$

where $\hat{n}_m$ is the normal vector to the *m-th* surface, $\vec{H}_{\phi_{im}}$ is the complex magnetic field produced by the *i-th* dipole in the *m-th* cell and U is the set of cells that are not in the "shadow" of the array radiation.

2.- Once we have calculated every induced current in the cylinder, we can obtain the final field pattern, which is the sum of the array contribution and the cylinder contribution:

$$\vec{F}(\theta,\phi) = \vec{FE}(\theta) \sum_{i=1}^{N} I_i e^{jk(dpx_i \sin\theta\cos\phi + dpz_i \cos\theta)} + \sum_{m=1}^{M} \vec{FE}(\theta_m,\phi_m) I_{ind_m} e^{jk(clx_m \sin\theta\cos\phi + cly_m \sin\theta\sin\phi + clz_m \cos\theta)} \quad (2)$$

where the element vector factor $FE(\theta)\hat{\theta}$ is the one associated to a dipole of $2l = \lambda/2$ length along the z direction and $\vec{FE}(\theta_m,\phi_m) = FE_\theta(\theta_m,\phi_m)\hat{\theta} + FE_\phi(\theta_m,\phi_m)\hat{\phi}$, where FE_θ and FE_ϕ are, respectively, the copolar and crosspolar components of the vector element factor for each cell in the cylinder. The *i-th* dipole in the array is located in (dpx_i, dpy_i, dpz_i) position and the *m-th* cell in the (clx_m, cly_m, clz_m) position.

Using the physical optics, the induced current in every cell has only a z component. Therefore, to simulate the actual presence of the copolar and crosspolar components of the scatterer field we make the assumption that in every cell the current forms an angle (β) with the z_m axis which is the z axis of the local coordinate system of the m-th cell. Therefore, there exist two components of the current, one in the z_m direction and the other in the x_m direction, i.e, the field associated to every cell is supposed to be the field produced by two elementary electric dipoles, one along the local x_m axis and another along the local z_m axis. We do not include a dipole in the local y_m direction because the curvature of each cell is small enough to consider a plannar cell.

To manage a more suitable expression of the total field, we divide it in its copolar and crosspolar components, so that the total field is: $\vec{F}(\theta,\phi) = F_\theta\hat{\theta} + F_\phi\hat{\phi}$. In the presence of the cylinder, the initial power pattern is blocked and a rise in the sidelobe level is produced. Our goal is to obtain a suitable set of currents for the array of dipoles so that the cylinder contribution in the sidelobe level of the final pattern copolar component (F_θ) is minimised. The crosspolar component (F_ϕ) is also minimised as much as possible.

The initial excitation currents of the dipoles are perturbed, through the simulated annealing technique, to accomplish the requirements about the sidelobe level and even about the current dynamic range ratio ($|I_{max}/I_{min}|$), which should be maintained (or reduced to) low values. This perturbation can be performed by varying the amplitude and phase or varying only the phase of each dipole excitation. The choice of better amplitudes and/or phases is made according to the minimisation of a given cost function, which involves the parameters that need to be controlled (i.e. sidelobe levels and current dynamic range ratio).

EXAMPLE:

An example selected between all examples performed is presented in this section. We chose a dipole array of 10 × 10 elements separated 0.7 λ in both directions (z and x). The angle β was set to 10°. The initial power pattern used is a Chebyshev power pattern (without cylinder) with a sidelobe level of -40dB and a current dynamic range ratio of 31.1. As scatterer, we use a cylinder with height h = 6λ, lotaced at a distance from the array d = 8λ, and the number of cells used in the cylinder was 25 x 15 = 375. After locating the cylinder, the highest sidelobe level for the copolar component is -25.19 dB, and the crosspolar -39.23 dB, which occurs in the ϕ = 0 cut.

Performing the optimisation with amplitude and phase control, the final sidelobe level is -30.31dB, which implies an improvement of 5.12 dB. The crosspolar component remained almost unaltered and its final value was -38.05 dB. The dynamic range ratio was lowered to 16.97.

In Figure 2 the blocked and the recovered power patterns (copolar and crosspolar) in the ϕ = 0 cut (the most perturbed) are shown. In Figures 3 and 4 we show a 3D representation of the initial and recovered copolar components of the power patterns. Using phase-only control the final sidelobe level was -29.61dB (4.37 dB less than the blocked pattern) for the copolar component and the crosspolar component had a level of -37.39 dB.

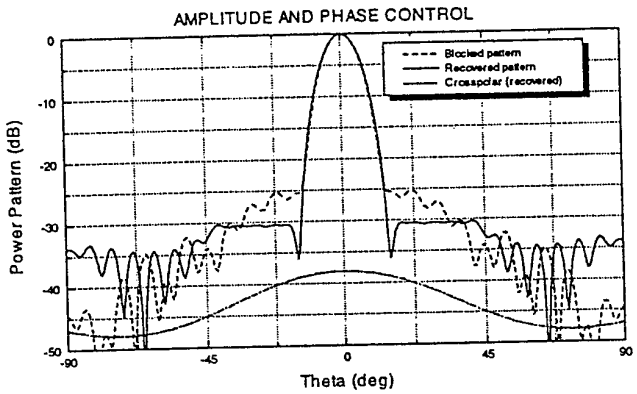

Figure 2. $\phi = 0$ cut.

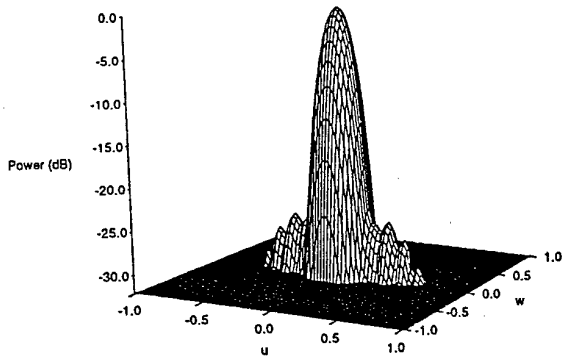

Figure 3. Initial Power Pattern

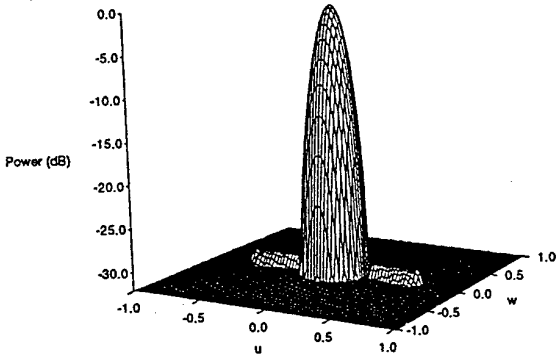

Figure 4. Optimised Power Pattern

CONCLUSIONS

First of all, an important factor in the optimisation is, with reasonable diameters, the scatterer's height. The distance is also important (larger distances imply better results) but with two scatterers with different heights located at the same distance from the array, we obtain better results for the higher scatterer. In addition several examples using scatterers with the same height and different diameters gave similar results. Besides, with amplitude and phase control we get results only about 1dB better than using phase-only control.
Regarding the β angle, with small values the optimisation is satisfactory and similar to the case with $\beta = 0$, which implies the existence of only a copolar component. As the value of β increases the results are worse, since there are more difference between the copolar and crosspolar components of the scattered field. Finally, in the symposium we will also shown results using this technique but minimising the field in every cell, i.e., minimising the induced currents.

ACKNOWLEDGEMENTS

The authors want to express their acknowlegment to Dr. Hans Steyskal at Air Force Research Laboratory /SNHA for suggesting this problem, his guidance and helpful discussions about this work and also to the U.S. Air Force for their economical aid.

REFERENCES

[1] H. Steyskal, "Synthesis of antenna patterns with imposed near-field nulls", Electron. Lett., 1994, 20,(24), pp. 2000-2001.

[2] L. Landesa, F. Obelleiro, J.L. Rodríguez, J.A. Rodríguez, F. Ares, and A.G. Pino, "Pattern synthesis of array antenas in presence of conducting bodies of arbitrary shape", Electron. Lett., 1997,33,(18), pp. 1512-1513.

[3] L. Landesa, F. Obelleiro, J.L. Rodríguez, J.A. Rodríguez, F. Ares, and A.G. Pino, "Pattern synthesis of array antennas with additional isolation of near-field arbitrary objects", Electron. Lett., 1998, 34,(16), pp. 1540-1542.

[4] J.A. Rodríguez, M.V. Lozano and F. Ares.,"Antenna array pattern synthesis in presence of near-zone scatterers:two-dimensional scalar case", to be published in Microwave Optical Technology Lett.

ELECTRONICS LETTERS

AN INTERNATIONAL PUBLICATION

CONTENTS

pages 1897 - 1988

1st October 1998 Vol. 34 No. 20

(continued on back cover)

Phase-only synthesis of continuous linear aperture distribution patterns with asymmetric side lobes

A. Trastoy and F. Ares

A method for synthesising linear aperture distribution patterns with different side lobe levels (SLLs) on both sides of the main beam is proposed. This phase-only control method was applied to a Taylor distribution as well as to a uniform amplitude distribution and achieved differences in the SLL on both sides of the main beam as great as 23dB, improving on a previous procedure that had achieved a gap of little more than 10dB.

Introduction: Radar and communication applications exist in which asymmetric side lobes provide a system advantage. Besides, phase control is less complicated and far cheaper to provide than amplitude control. Focusing on these ideas, Frey and Elliott [1] froze the amplitude distribution and the shape of the phase distribution of a modified Taylor pattern. They calculated an analytic function that fitted the shape of that phase distribution and, by controlling the magnitude of the swing, they obtained differentials as great as 10 dB between the two side lobe levels (SLLs) on each side of the main beam. In this Letter, a method based on the numerical calculation of the odd phase distribution necessary to achieve an asymmetric pattern with a greater difference between the levels on the two sides of the main beam, through variation of the roots in the modified Taylor distribution, is described and applied to a Taylor distribution as well as to the important case of uniform amplitude distribution.

Description of method: Given a linear Taylor or uniform amplitude distribution, we freeze the amplitude of the aperture distribution. We then slightly modify the associated roots u_n of a modified Taylor pattern developed by Elliott [2]:

$$S_0(u) = \frac{\sin \pi u}{\pi u} \frac{\prod_{n=-(\bar{n}_L-1)}^{\bar{n}_R-1} (1 - u/u_n)}{\prod_{n=-(\bar{n}_L-1)}^{\bar{n}_R-1} (1 - u/n)} \quad (1)$$

and use the following formula to calculate their associated aperture distribution:

$$h(\zeta) = \frac{1}{2a} \sum_{m=-(\bar{n}_L-1)}^{\bar{n}_R-1} S_0(m) e^{-jm\pi\zeta/a} \quad (2)$$

where m is an integer, $2a$ is the length of the aperture, and $\bar{n}_R$ and $\bar{n}_L$ are positive integers that denote the transition roots on the right and left sides of the main beam, respectively.

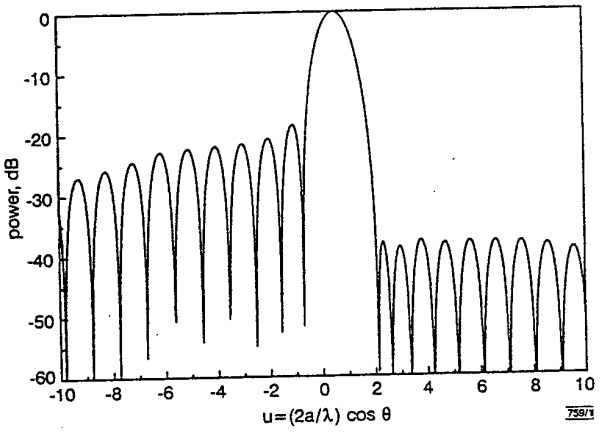

Fig. 1 *Obtained pattern corresponding to –25dB, $\bar{n}$ = 7 Taylor amplitude distribution*

The frozen amplitude distribution and the phase distribution (odd about the centre) obtained from eqn. 2 produce an asymmetric pattern. The simulated annealing technique [3] is used to find the location of the roots whose phase distribution provides the highest difference between SLLs on both sides of the main beam through the minimisation of an objective function that takes into account the SLLs on both sides of the main beam.

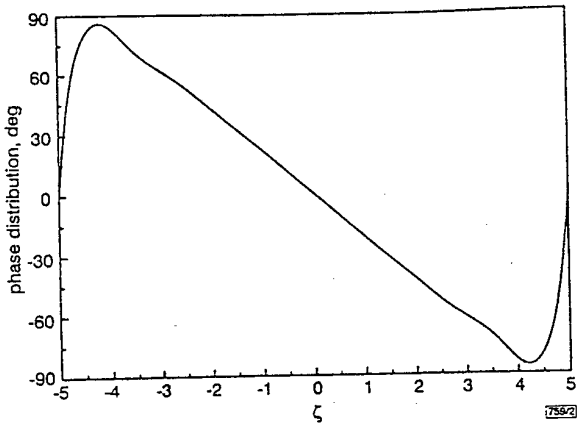

Fig. 2 *Phase distribution of pattern shown in Fig. 1*

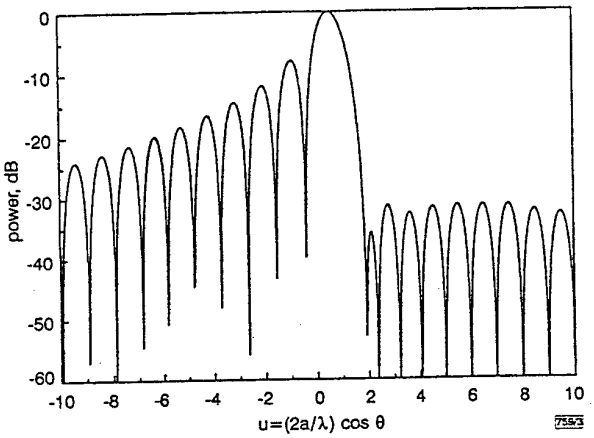

Fig. 3 *Obtained pattern corresponding to uniform amplitude distribution*

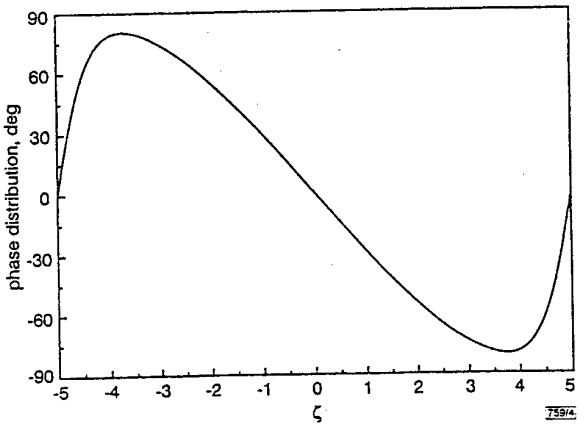

Fig. 4 *Phase distribution of pattern shown in Fig. 3*

Results: To illustrate the method described above, two examples are presented. In both cases, the pattern is produced by an aperture of length $2a = 10\,\lambda$ and only the SLL of the lower side of the main beam was included in the objective function, with the other side being uncontrolled. The first example starts from a linear Taylor distribution calculated for an SLL of –25dB and $\bar{n} = 7$. We set $\bar{n}_R = \bar{n}_L = 7$ in eqns. 1 and 2 and we obtain the phase distribution shown in Fig. 2 that corresponds to the pattern shown in Fig. 1 and presents a difference between SLLs of 19dB. It can be seen that, by using the actual phase distribution instead of that obtained by the fitness function described in [1], an improvement in the gap of ~9dB is obtained. In the second example (Fig. 3), starting from a uniform amplitude distribution, we obtain a gap of 23dB between both sides of the main beam (this time an improvement of 13dB over the results reported in [1] has been achieved). Its phase distribution is shown in Fig. 4. Note that in both examples the main beam peak is shifted from $u = 0$. This effect can be

gressive phase to the aperture distribution.

Conclusions: A method for synthesising asymmetric patterns with phase-only control has been presented. Previous results obtained by Frey and Elliott [1] have been improved and patterns with gaps of ~20dB achieved. The computational time for the two examples shown above was ~10min using a Pentium 200MHz processor. It is possible to extend this method in order to fix nulls with phase-only control and also to lower the whole side lobe level of both linear and circular apertures using, in this case, an even phase shift about the centre for linear apertures and a ϕ-symmetric phase distribution for circular apertures, reported in [4] for patterns with null filling.

Acknowledgments: This work was supported by the European Office of the US Aerospace Research and Development Board (EOARD) and the US Air Force Office of Scientific Research (AFOSR).

21 July 1998
Electronics Letters Online No: 19981340

A. Trastoy and F. Ares (*Grupo de Sistemas Radiantes, Departamento de Física Aplicada, Facultad de Física, Universidad de Santiago de Compostela, 15706 Santiago de Compostela, Spain*)

E-mail: faares@usc.es

References

1 FREY, J.R., and ELLIOTT, R.S.: 'Phase-only changes in aperture excitation to achieve sum patterns with asymmetric side lobes', *Alta Freq.*, 1982, **51**, pp. 31–35
2 ELLIOTT, R.S.: 'Design of line source antennas for sum patterns with sidelobes of individually arbitrary heights', *IEEE Trans.*, 1976, **AP-24**, pp. 76–83
3 PRESS, W.H., TEUKOLSKY, S.A., VETTERLING, W.T., and FLANNERY, B.P.: 'Numerical recipes in C' (Cambridge University Press, 1992)
4 ARES, F., RENGARAJAN, S.R., and MORENO, E.: 'Optimization of aperture distributions for sum patterns', *Electromagnetics*, 1996, **16**, (2), pp. 129–143

Property of vanishing moments of orthogonal *M*-band compactly supported interpolating scaling function

Zhang Jiangkang and Bao Zheng

It is shown that the number of vanishing moments of the even number-order orthogonal M-band compactly supported interpolating scaling function increases by one. Consequently, the asymptotic performance of the Mallat projection is the same as the orthogonal projection for the L_2-approximation of smooth functions.

Introduction: The main advantages of interpolating wavelet transforms are:
(i) The wavelet series transform of a signal in the multiresolution subspace is exactly consistent with its discrete wavelet transform [1] when the synthesis scaling function has the interpolating property, i.e. $\varphi(n) = \delta(n)$, where $\delta(n)$ is the Kronecker sequence.
(ii) The first N moments of the N-order interpolationg scaling function are vanishing except for the first moment. However, in the two-band case, orthogonal wavelets do not exist which have both the interpolating property and compact support except for the Haar wavelet.
Therefore, in [2, 3], we constructed high-order, orthogonal, M-band and compactly supported interpolating scaling functions. In this Letter we reveal furthermore that the orthogonality brings the interpolating scaling function an extra vanishing moment property.

Definition of moments: The p-order moments of a scaling filter and the scaling function are defined as, respectively,

$$M_k(h) = \sum_n n^k h_k \qquad k = 0, 1, ..., p-1 \tag{1}$$

$$M_k(\varphi) = \int_{-\infty}^{\infty} t^k \varphi(t)\, dt \qquad k = 0, 1, ..., p-1 \tag{2}$$

It is well-known that if $\varphi(t)$ is an N-order interpolating scaling function, then it has the Coiflet property [4] or vanishing moment property, i.e.

$$M_k(h) = M_k(\varphi) = \delta(k) \qquad k = 0, 1, ..., N-1 \tag{3}$$

In general cases, $M_N(h) \neq 0$ and $M_N(\varphi) \neq 0$. However, in the case of an even number-order, orthogonal and M-band interpolating scaling function, the orthogonality forces the number of vanishing moments to increase by one.

Property: Throughout this Letter, we assume that the interpolating scaling function $\varphi(t)$ satisfies

$$\varphi(t) = \sqrt{M} \sum_{k=0}^{L} h_k \varphi(Mt - k) \tag{4}$$

and that the scaling filter **h** satisfies

$$H(z) = \left(\frac{1 + z + \cdots + z^{M-1}}{M}\right)^N Q(z) \tag{5}$$

and

$$H(1) = \sqrt{M} \tag{6}$$

Furthermore, $\varphi(t)$ is assumed to satisfy the orthogonal condition

$$\sum_k |\hat{\varphi}(2k\pi + \omega)|^2 = 1 \tag{7}$$

An immediate consequence of eqn. 7 is

$$\sum_{r=0}^{M-1} \left|H\left(\frac{2\pi r}{M} + \omega\right)\right|^2 = M \tag{8}$$

Now we claim that the moments of $\varphi(t)$ have the following property:

Theorem: If the interpolating scaling filter **h** and the corresponding interpolating scaling function $\varphi(t)$ satisfy eqns. 4 – 8, then,

$$M_k(h) = \delta(k) \qquad k = 0, 1, ..., N-1 \tag{9a}$$
$$M_k(\varphi) = \delta(k) \qquad k = 0, 1, ..., N-1 \tag{9b}$$

In particular, if N is an even number, then

$$M_k(h) = 0 \qquad k = N, N+2, N+4, ..., 2N-2 \tag{10a}$$
$$M_k(\varphi) = 0 \qquad k = N, N+2, N+4, ..., 2N-2 \tag{10b}$$

Remarks: By using the theorem and Unser's methods [5], it can be shown that the Mallat projection of $f(t)$ onto the multiresolution subspace $V_J(\varphi)$

$$M_J(f) = \sum_k f\left(\frac{k}{M^J}\right) \varphi(M^J t - k)$$

has the same asymptotic performance as the corresponding orthogonal projection

$$P_J f = \sum_k \langle f(t), \varphi_{J,k} \rangle \varphi_{J,k}(t)$$

i.e. both $M_J(f)$ and $P_J f$ are L_2-approximations of the smooth function $f(t)$ as the scale approaches zero. In this sense, the orthogonal M-band compactly supported interpolating wavelet compares favourably with the two-band compactly supported interpolating wavelet.

Proof of theorem: We know that the scaling filter and its polyphases satisfy the relationship

$$H(z) = \sum_{r=0}^{M-1} z^{-r} H_r(z^M) \tag{11}$$

JOURNAL OF ELECTROMAGNETIC WAVES AND APPLICATIONS

PROGRESS IN ELECTROMAGNETICS RESEARCH

Professor J. A. Kong
Room 26-305
77 Massachusetts Avenue
Cambridge, MA 02139, USA

January 31, 1999

Professor Francisco J. Ares
Departamento de fisica Aplicada
Grupo de Sistemas Radiantes
Facultad de Fisica
Universidad de Santiago de Compostela
15706 Santiago de Compostela
Spain

Dear Professor Ares:

9812091.CR.Ares: SHAPED POWER PATTERNS PRODUCED BY EQUISPACED LINEAR ARRAYS: OPTIMIZED SYNTHESIS USING ORTHOGONAL sin(Nx)/sin(x) BEAMS by J. M. Cid, J. A. Rodriguez, and F. Ares

Enclosed please find a preprint of the above article, which has been scheduled for publication in the Journal of Electromagnetic Waves and Applications. It contains the information of the year of publication, and issue and page numbers.

Thank you very much for your contribution and with my best regards.

Sincerely yours,

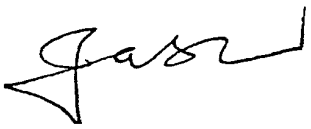

J. A. Kong
Chief Editor

Journal of Electromagnetic Waves and Applications, Vol. 13, 985–992, 1999

SHAPED POWER PATTERNS PRODUCED BY EQUISPACED LINEAR ARRAYS: OPTIMIZED SYNTHESIS USING ORTHOGONAL $\sin(Nx)/\sin(x)$ BEAMS

J. M. Cid, J. A. Rodriguez, and F. Ares

Departamento de Física Aplicada
Grupo de Sistemas Radiantes
Facultad de Física
Universidad de Santiago de Compostela
15706 Santiago de Compostela
SPAIN

Abstract–The major defects of the Woodward-Lawson method of shaped pattern synthesis (lack of control over side lobes and ripple, and high dynamic range ratios) can be overcome by perturbing the field samples weighting the component $\sin(Nx)/\sin(x)$ beams. If a real field is not necessary, further improvement (especially as regards dynamic range ratio) can be achieved by optimizing the phases of the coefficients of the component beams. These procedures are illustrated by linear arrays producing a symmetric flat-topped beam and a cosecant squared pattern.

1. INTRODUCTION

Multi-beam antenna arrays have applications in the field of electronic countermeasures, in satellite communications, and in adaptive nulling [1]. For these systems, the most natural method for synthesizing multiple beams is the Woodward-Lawson method, which can be imple-

mented using lossless orthogonal beam-forming networks such as the Butler matrix [2]. The major objections to the Woodward-Lawson method have been its inability to control either the amplitude of the ripple in the shaped region of the pattern, or the heights of side lobes in the unshaped region [2, 3]. Another telling objection is that the excitations it prescribes often have very high dynamic range ratios, and may not be physically realizable in the presence of mutual coupling [4–6]. These weaknesses are ultimately due partly to the fact that the Woodward-Lawson method constrains all the beams with which it synthesizes the desired pattern to have the same phase, so that the far field pattern is real, and partly to its zero tolerance of deviation from the desired field at the points at which it samples this field. When the component beams can differ in phase (because a real far field is not necessary) and/or perturbation of sample amplitudes is allowed, the extra degrees of freedom that thereby become available should in principle allow calculation of excitation distributions that are more easily realized and/or afford better side lobe levels and ripple characteristics. In this paper we describe how this may be achieved using simulated annealing optimization methods [7]. We know of no previous attempt to improve the Woodward-Lawson method in this way.

2. DESCRIPTION OF THE METHOD

Briefly, the Woodward-Lawson method for a linear array of N antenna elements spaced a distance d apart consists in first sampling a desired field pattern $F(\theta)$ in $2M+1$ directions θ_i spaced $\cos^{-1}(\lambda/Nd)$ apart (where θ is measured from endfire and M is such that the visible region is just covered), and then approximating $F(\theta)$ by

$$WL(\theta) = \frac{1}{N} \sum_{i=-M}^{M} F(\theta_i) \frac{\sin(Nu_i)}{\sin(u_i)} \tag{1}$$

where $u_i = (\pi d/\lambda(\cos(\theta) - \cos(\theta_i))$. Each of the component quasi-sinc beams $\sin(Nu_i)/\sin(u_i)$ is realized by an excitation distribution with uniform amplitude and uniform phase differences between the elements, and $WL(\theta)$ is produced by the weighted sum of these distributions, with weights $F(\theta_i)/N$. $WL(\theta)$ reproduces $F(\theta)$ exactly at each sample point because all the component quasi-sinc beams except the i-th are zero at θ_i.

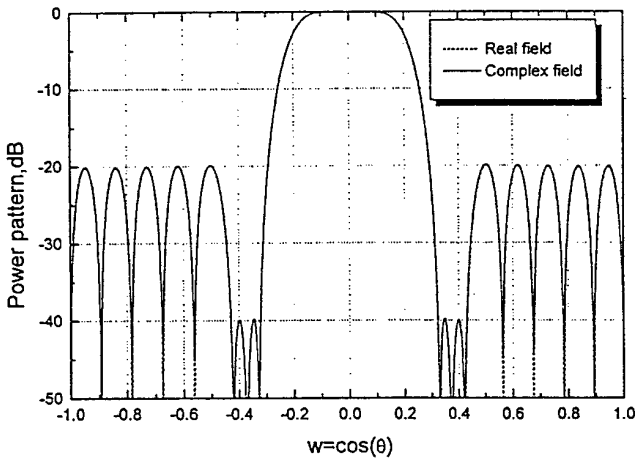

Figure 1. Flat-topped power patterns obtained by optimizing the amplitudes of a linear combination of $\sin(Nx)/\sin(x)$ beams (real field) and then optimizing their phases (complex field).

As noted above, the original Woodward-Lawson method assumes that all the $F(\theta_i)$ are in phase, and the coefficient of the i-th quasi-sinc beam is exactly $F(\theta_i)$. In this work we perturbed the amplitude of each $F(\theta_i)$ by δ_i and/or multiplied all but one by a phase factor $e^{j\phi_i}$:

$$\hat{F}(\theta) = \frac{1}{N}\sum_i e^{j\phi_i}(F(\theta_i) + \delta_i)\frac{\sin(N\pi u_i)}{\sin(\pi u_i)} \qquad (2)$$

We used simulated annealing to determine the set of ϕ_i and/or δ_i minimizing a cost function that penalized both the deviation of $\hat{F}(\theta)$ from desired pattern characteristics (side lobe levels, ripple levels and beamwidth) and the dynamic range ratio of the excitation distribution.

3. EXAMPLES

A) Suppose that we require a 20-element $(\lambda/2)$-spaced linear array to produce a flat-topped power pattern with a -3 dB beamwidth of $\cos^{-1}(0.4)$ and side lobe levels of -40 dB for the two inner lobes and -20 dB for the others. Fig. 1 ("real field" pattern) shows that the specified side lobe levels and ripple levels of about ± 0.01 dB can be achieved by optimizing just the amplitudes of the beam coefficients; the optimal amplitudes are listed in Table

1. If the amplitudes are now fixed at these values and the phases of the beam coefficients are optimized (the optimal phases are also listed in Table 1), there is virtually no change in the power pattern (Fig. 1) but the dynamic range ratio of the excitation distribution falls from 17.09 to 6.83, an improvement of 60%. Fig. 2 shows the phase pattern of the resulting complex field.

Table 1. Beam coefficients corresponding to the flat-topped power patterns shown in Fig. 1 (the coefficients for $i = \pm 10$ are not shown because for a symmetric pattern these beams cancel each other).

i	Amplitudes	Phases (deg)	
		Real field	Complex field
0	1.134	0	−70.124
±1	1.130	0	−43.706
±2	0.822	0	−5.389
±3	0.078	0	19.760
±4	0.011	0	20.807
±5	0.115	180	201.042
±6	0.099	0	29.516
±7	0.076	180	215.331
±8	0.051	0	40.600
±9	0.026	180	215.337

B) Using the same 20-element $(\lambda/2)$-spaced linear array as above, we desire to synthesize a pattern with a cosecant squared beam in the sector $\cos\theta \in [0.1 - 0.5]$, four -30 dB side lobes to the left of the cosecant beam and no other side lobe higher than -20 dB. Fig. 3 ("real field pattern") shows the result of optimizing just the amplitudes of the quasi-sinc beam coefficients: maximum ripple in the cosecant region is ± 0.6 dB. The optimal amplitudes are listed in Table 2. As before, if these amplitudes are fixed and the phases of the beam coefficients are optimized (the optimal phases are also listed in Table 2), there is no significant change in the power pattern (Fig. 3) but the dynamic range ratio of the excitation distribution falls from 12.05 to 8.22, an improvement of 32%. Fig. 4 shows the phase pattern of the resulting complex field.

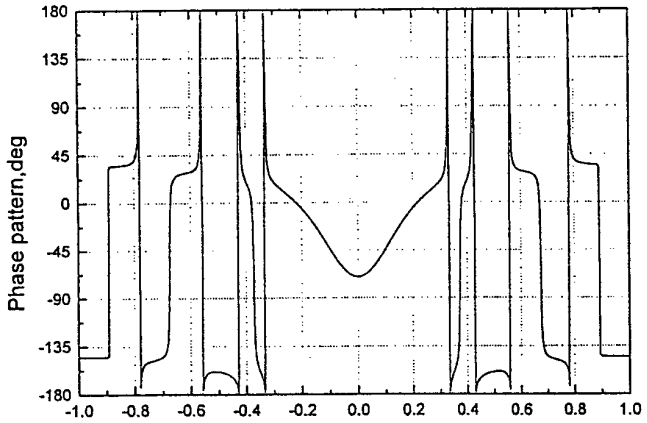

Figure 2. Phase pattern of the complex field of Fig. 1.

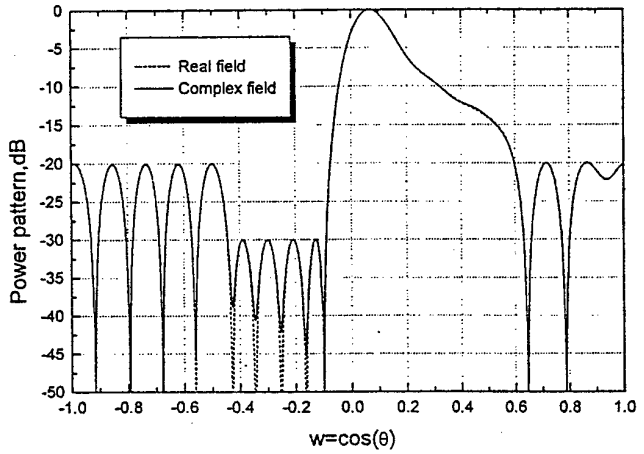

Figure 3. Cosecant squared patterns obtained by optimizing the amplitudes of a linear combination of $\sin(Nx)/\sin(x)$ beams (real field) and then optimizing their phases (complex field).

Table 2. Beam coefficients corresponding to the cosecant squared patterns shown in Fig. 3.

i	Amplitudes	Phases (deg)	
		Real field	Complex field
−10	0.074	180	195.126
−9	0.051	0	19.304
−8	0.022	0	20.278
−7	0.078	180	192.667
−6	0.114	0	14.165
−5	0.131	180	194.168
−4	0.038	0	0.411
−3	0.042	180	179.153
−2	0.040	0	−3.660
−1	0.002	0	28.173
0	0.927	0	−3.324
1	1.224	0	1.562
2	0.651	0	8.696
3	0.443	0	−1.586
4	0.326	0	12.995
5	0.261	0	11.997
6	0.127	0	−13.026
7	0.123	180	166.678
8	0.036	0	−14.167
9	0.118	0	−8.275
10	0.057	0	13.531

4. CONCLUSIONS

By means of simulated annealing, the amplitudes and/or phases of a linear combination of orthogonal quasi-sinc $(\sin(Nx)/\sin(x))$ beams can be optimized so as to achieve a shaped power pattern with specified beamwidth and side lobe topography and low ripple while minimizing the dynamic range ratio of the excitation distribution. This procedure overcomes the major weaknesses of Woodward-Lawson pattern synthesis when field phase is irrelevant. Side lobe level and ripple depend mainly on beam coefficient amplitudes, dynamic range ratio on phases. If the beam amplitudes of standard Woodward-Lawson patterns are fixed and only their phases optimized, the dynamic range

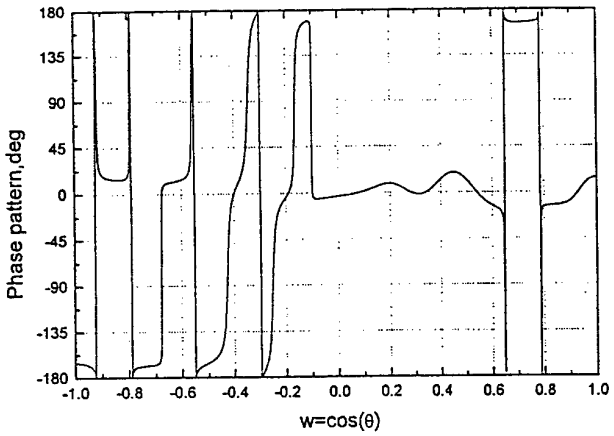

Figure 4. Phase pattern of the complex field of Fig. 3.

ratio can improve by 70% or more (results not shown). The new synthesis method may be extended to direct broadcast satellite phased arrays by combining it with the sampling function method developed by Richie and Kritikos [8].

ACKNOWLEDGMENT

This work was supported by the Xunta de Galicia under Project XUGA 20601B98, by the U.S. European Office of Aerospace Research and Development (EOARD), and by the U.S. Air Force Office of Scientific Research (AFOSR).

REFERENCES

1. Hansen, R. C., *Phased Array Antennas,* 330–335, John Wiley & Sons, Inc., New York, 1998.
2. Mailloux, R. J., *Phased Array Antenna Handbook,* 116–119, Artech House Inc., Norwood, MA, 1994.
3. Elliott, R. S. and G. J. Stern, "A new technique for shaped beam synthesis of equispaced arrays," *IEEE Trans.,* Vol. AP-32, No. 10, 1129–1133, 1984.
4. Orchard, H. J., R. S. Elliott, and G. J. Stern, "Optimising the synthesis of shaped beam antenna patterns," *IEE Proc. H,* Vol. 132, No. 1, 63–68, 1985.
5. Ares, F., R. S. Elliott, and E. Moreno, "Optimised synthesis

of shaped line-source antenna beams," *Electron. Lett.,* Vol. 29, 1136–1137, 1993.
6. Ares, F. and J. A. Rodriguez, "Asymmetric-shaped beam patterns from a continuous linear aperture distribution," *Microwave and Optical Technology Letters,* Vol. 15, 288–291, 1997.
7. Kirkpatrick, S., C. D. Gelatt, and M. P. Vecchi, "Optimization by simulated annealing," *Science,* Vol. 220, No. 4598, 671–679, 1983.
8. Richie, J. E. and H. N. Kritikos, "Linear program synthesis for direct broadcast satellite phased arrays," *IEEE Trans.,* Vol. AP-36, No. 3, 345–348, 1988.

Juan M. Cid-Alvarez was born in Torneiros (Allariz), Spain, in 1976. He received his B.S. degree in Physics from the University of Santiago de Compostela, Spain. At present, he is preparing his M.S. degree about antenna array pattern synthesis. His general research interests include numerical methods for solving electromagnetic problems and pattern synthesis.

Juan A. Rodriguez-Gonzalez was born in Orense, Spain, in 1972. He received his B.S. and M.S. degrees in Physics from the University of Santiago de Compostela, Spain and for two years taught subjects related to electromagnetics at the National Open University Centre in Pontevedra, Spain. At present, he is preparing his Ph.D. in Physics on antenna array pattern synthesis. His general research interests include numerical methods for solving electromagnetic problems and pattern synthesis. He is also interested in computer programming and software engineering in general.

Francisco J. Ares-Pena received B.S. and M.S. degrees in Physics from the University of Santiago de Compostela, Spain, in 1986 and 1987 respectively, and the Ph.D. from the same institution in 1993. He is currently an Associate Professor in the Department of Applied Physics at the University of Santiago de Compostela. He has published more than 80 journal and conference papers. Dr. Ares is a Senior Member of IEEE and a member of the New York Academy of Sciences. His main research interests are antenna array pattern synthesis and the design of slot arrays.

9-D-9? (ICEAA 94)

SHAPED POWER PATTERNS PRODUCED BY EQUIESPACED LINEAR ARRAYS: OPTIMIZED SYNTHESIS USING ORTHOGONAL sin(Nx)/sin(x) BEAMS.

J. M. Cid, J. A. Rodriguez, F. Ares, and E. Moreno.

Departamento de Física Aplicada
Facultad de Física, Universidad de Santiago de Compostela
15706 Santiago de Compostela
SPAIN

The problem and the solution:

Multi-beam antenna arrays have applications in the field of electronic countermeasures, in satellite communications, and in adaptive nulling [1]. For these systems, the most natural method for synthesizing multiple beams is the Woodward-Lawson method; which can be implemented using lossless orthogonal beam-forming networks such as the Butler matrix [2]. The major objections to the Woodward-Lawson method have been its inability to control either the amplitude of the ripple in the shaped region of the pattern, or the heights of side lobes in the unshaped region [2,3]. Another telling objections is that the excitations it prescribes often have very high dynamic range rations, and may not be physically realizable in the presence of mutual coupling [4,5]. These weaknesses are ultimately due partly to the fact that the Woodward-Lawson method constrains all the beams with which it synthesizes the desired pattern to have the same phase, so that the far field pattern is real, and partly to its zero tolerance of deviation from the desired field at the points at which it samples this field. These major defects of the Woodward-Lawson of shaped pattern synthesis (lack of control over side lobes and ripple, and high dynamic range ratios) can be overcome by perturbing the field samples weighting the component sin(Nx)/sin(x) beams. If a real field is not necessary, further improvement (especially as regards dynamic range ratio) can be achieved by optimizing the phases of the coefficients of the component beams.

Example:

Suppose that we require a 20-element ($\lambda/2$)-spaced linear array to produce a flat-topped power pattern with a -3 dB beamwidth of $\cos^{-1}(0.4)$ and side lobe levels of -40 dB for the two inner lobes and -20 dB for the others. Fig. 1 ("real field" pattern) shows that the specified side lobe levels and ripple levels of about ±0.01 dB can be achieved by optimizing just the amplitudes of the beam coefficients. If the amplitudes are now fixed at these values and the phases of the beam coefficients are optimized, there is virtually no change in the power pattern but the dynamic range ratio of the excitation distribution falls from 17.09 to 6.83, an improvement of 60%. Results for a cosecant-squared pattern wil be shown in the conference.

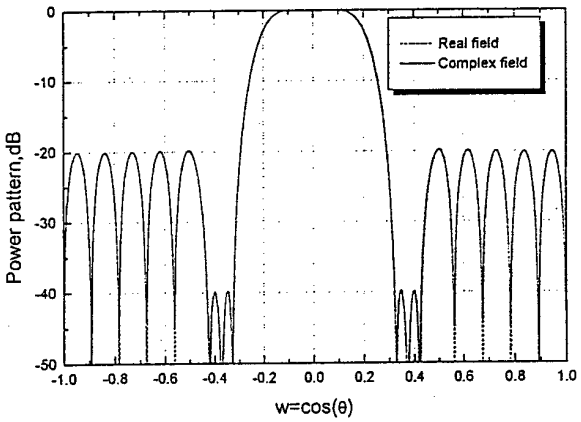

Figure 1. Flat-topped power patterns obtained by optimizing the amplitudes of a linear combination of sin(Nx)/sin(x) beams (real field) and then optimizing their phases (complex field).

References:

[1] Hansen, R. C., *Phased Array Antennas,* 330-335, John Wiley & Sons, Inc., New York, 1998.
[2] Mailloux, R. J., *Phased Array Antenna Handbook,* 116-119, Artech House Inc., Norwood, MA, 1994.
[3] Elliott, R. S. and G. J. Stern, "A new technique for shaped beam synthesis of equispaced arrays," *IEEE Trans.,* Vol. AP-32, No.10, 1129-1133. 1984.
[4] Orchard, H. J., R. S. Elliott, and G. J. Stern, "Optimising the synthesis of shaped beam antenna patterns," *IEE Proc. H,* Vol. 132, No. 1, 63-68, 1985.
[5] Ares, F., R. S. Elliott, and E. Moreno, "Optimised synthesis of shaped line-source antenna beams," *Electron. Lett.,* Vol. 29, 1136-1137, 1993.

MINIMISING THE VARIABILITY OF CHARACTERISTIC IMPEDANCES IN MULTISECTION QUARTER-WAVELENGTH TRANSFORMERS

M.Vicente-Lozano, F. Ares-Pena, and E. Moreno.

Departamento de Física Aplicada.

Facultad de Física, Universidad de Santiago de Compostela

15706. Santiago de Compostela

SPAIN

E-mail: faares@usc.es

Abstract

The widely used first-order polynomial representation of the voltage reflection coefficient in multisection quarterwavelength transformers is assumed. The roots of this polynomial are displaced iteratively to obtain, through the simulated annealing technique, low variability between the characteristic impedances of adjacent transformers. Besides, for each problem configuration, the bandwidth is maintained close to its maximum possible value. An example is presented obtaining an important decrease in the characteristic impedances variability of the transformers.

I. INTRODUCTION

Quarter-wavelength transformers are used as intermediate matching sections between a primarily resistive load R_L and a waveguide structure of characteristic impedance $Z_0 \neq R_L$. They are also used to connect two transmission lines with different characteristic impedances, caused by a change in dimensions or dielectric. When a match over a narrow frequency band is sufficient, a single-section quarter-wavelength transformer may be

adequate. However, for good performance over an extended band of frequencies it may be necessary to use two or more sections in tandem.

Elliott [l] obtained results for a tandem of quarterwavelength transformers with a ripple-like frequency response with a moderate loss in bandwidth. Orchard procedure [2] was used to calculate the roots of the polynomial associated to the reflection coefficient. Several solutions were possible and the one that implies less variability between the characteristic impedances of adjacent transformers was chosen. However, using this technique we have not the guarantee to obtain, for a desired frequency response, the solution with less variability and with low loss in bandwidth in an optimal sense.

In this letter we propose a new technique to obtain a desired frequency response with low variability in characteristic impedances of consecutive transformers. This implies that the dimensions (or the dielectric) of adjacent transformers are similar and the physical implementation is easier since discontinuity effects are minimised. Furthermore, the bandwidth is also taken into account optimising its value according to input parameters. This procedure consists in minimising a cost function through the simulated annealing technique [3].

II. THEORY

Given N sections of common length l and characteristic impedances Z_n, connecting a mismatched load R_L to a line of characteristic impedance Z_0, it is well known that, to first order, the voltage reflection coefficient seen at the end of the main line (i.e. at the input to the first transformer section) is given by [l]:

$$\Gamma = \sum_{n=0}^{N} \Gamma_n e^{j2n\beta l} \tag{1}$$

where

$$\Gamma_n = \frac{Z_{n+1} - Z_n}{Z_{n+1} + Z_n} \tag{2}$$

By means of the following change of variable:

$$\psi = -2\beta l \tag{3}$$

$$w = e^{j\psi} \tag{4}$$

Equation (1) can be transformed in:

$$\Gamma = \sum_{n=0}^{N} \Gamma_n w^n \tag{5}$$

which can be factorised to give:

$$\Gamma = \Gamma_N \prod_{n=1}^{N} (w - w_n) \tag{6}$$

The synthesis of a desirable set of section reflection coefficients Γ_n can be obtained by first determining a desirable set of roots w_n and the study of the frequency behaviour of the input reflection coefficient Γ can be performed by using (6). By means of (2) is possible to calculate the characteristic impedance of each quarter-wavelength transformer.

The synthesis procedure consists on calculate the appropriate reflection coefficients in order to obtain a desired frequency response and also to adjust the bandwidth to desired specifications. The searching of these coefficients will be accomplished through the roots w_n. In (4) was shown the expression of these roots, but in general, they adopt the following form:

$$w_n = e^{a_n + j\psi_n} \tag{7}$$

where the factor a_n indicates the radial displacement of the nth root in the unit circle representation of the roots.

With the assumption of negligible losses, all section characteristic impedances are pure real and also the reflection coefficients, therefore the roots w_n must occur in complex conjugate pairs or be in the real axis. In this case:

$$\left(\frac{\rho}{\rho_n}\right)^2 = \prod_{n=1}^{N}(w-w_n)(w-w_n)^* = \prod_{n=1}^{N}\left[1-2^{a_n}\cos(\psi-\psi_n)+e^{2a_n}\right] \tag{8}$$

where $\rho = |\Gamma|$ and $\rho_n = |\Gamma_n|$.

It can be seen from the above expression that, except for level, $\left(\rho/\rho_n\right)^2$ does not depend on the a_n sign, thus there are 2^N sets of roots w_n that will produce the same frequency response.

The simulated annealing technique [3] allows us to obtain desirable frequency response while maintaining low variability between the characteristic impedances of each transformer. In this technique there exist two key factors: the construction of a cost function that the algorithm minimises and the perturbations introduced to the variables in this cost function, which are the roots w_n. As starting solution a Chebyshev distribution of the section reflection coefficients was chosen, which has all the lobes at the same height and yields the maximum bandwidth in the frequency response for a given N. The cost function used was:

$$C = \left|M_{id} - M_{io}\right|^2 k_1 + \left|Z_{i+1} - Z_i\right|^2_{max} k_2 + \left|P_d - P_0\right|^2 k_3 \tag{9}$$

where M_{id} and M_{io}, are the desired and the obtained maxima in the frequency response of each transformer, the second term is the maximum difference between the characteristic

impedance of two consecutive transformers, which we define as variability. Finally P_o and P_d are the obtained and maximum desired percentage of loss in bandwidth respectively of the multisection transformer. These percentages are taken in relation to the bandwidth corresponding to the Chebyshev distribution. The factors k_i are weights used to give more importance to one factor than to another in order to search for the best solution. In the weights selection the greater factor is k_2 but a reasonable relation with the others factors (k_1 and k_3) is always maintained.

III. EXAMPLE

In this example a tandem of $N = 6$ transformers was chosen, the load at the end of the line was R_L = 140 ohms and the input impedance was Z_o= 60 ohms. With this load configuration the selected value of ρ_{max} was 0.1, so the maxima (M_{id}) were all set to 0.1. The bandwidth, defined as the frequency range over which the magnitude ρ of the reflection coefficient does not exceed the specified level ρ_{max}, was controlled by the percentage of deviation from the bandwidth of the Chebyshev pattern (P_d parameter in (9)). In Table I there are shown, for several values of P_d, the results about initial and final beamwidth (BW_i and BW_f respectively), initial and final variability (V_i and V_f respectively) and the relative percentage of gain or loss in each factor. In Fig. 1 it is shown the frequency response when P_d is chosen to 2%. It can be seen that as long as the desired percentage of loss increases, the variability decreases.

IV. CONCLUSIONS

The variability of the multisection quarter-wavelength transformers characteristic impedances was improved by using the simulated annealing technique. Furthermore the

bandwidth of the frequency response was taken into account to acquire more practical and realisable solutions for the construction of multisection quarter-wavelength transformers. Due two the multiplicity of solutions there are 2^N sets of roots w_n that will give the same optimal response function $\rho(\beta l)$. Each of these sets gives a different solution for the section reflection coefficients and characteristic impedances. In addition, the method is also applicable in cases where all the zones in the frequency range have not the same lobe level, i.e., different ρ_{max}'s in different zones in the passband.

At present the extension of this method to tapered transmission lines, described in [4], is under study. Finally this method is directly applicable to the problem analysed in [5] about multihole directional couplers.

V. ACKNOWLEDGEMENTS

This work was supported by the Xunta de Galicia under Project XUGA 20601B98, by the U.S. European Office of Aerospace Research and Development (EOARD) and by the U.S. AirForce Office of Scientific Research (AFOSR).

REFERENCES

[1] Elliott R. S., *An Introduction to Guided Waves and Microwave Circuits*, Englewood Cliffs, New Jersey: Prentice-Hall International Editions, 1993, pp. 208-231.

[2] Orchard R. S., Elliott R. S., and Stern G. J., "Optimizing the Synthesis of Shaped Beam Antenna Patterns", Proc. IEE, Part H, 1985, **132**, pp. 63-68.

[3] Press W.H., Vetterling W.T., Teukolsky S.A., and Flannery B.P., *Numerical Recipes in C*, Second Edition, Cambridge, 1992, pp. 444-445.

[4] Mahon, J. P. and Elliott R. S., "Tapered Transmission Lines with a Controlled Ripple Response", IEEE Trans. Microwave Theory Tech., 1990, **38**, pp. 1415-20.

[5] Elliott R. S. and Kim Y. U., "Improved Design of Multihole Directional Couplers Using an Iterative Technique", IEEE Trans Microwave Theory Tech., 1990, **38** ,pp 411-415.

Legends for Figure and Table.

Figure 1. Frequency response for a tandem of $N = 6$ quarter-wavelength transformers, $\rho_{max} = 0.1$. The maximum desired percentage of loss in bandwidth is $P_d = 2\%$. The load used was $R_L = 140$ and the input impedance $Z_o = 60$.

Table I. Results obtained in the example, $N = 6$.

Table I.

P_d	BW_i	BW_f	%	V_i	V_f	%
2.0	4.92	4.84	-1.62%	18.51	12.55	-32.18%
1.5	4.92	4.88	-0.81%	18.51	13.70	-26.01%
0.5	4.92	4.92	0.00%	18.51	15.46	-16.49%

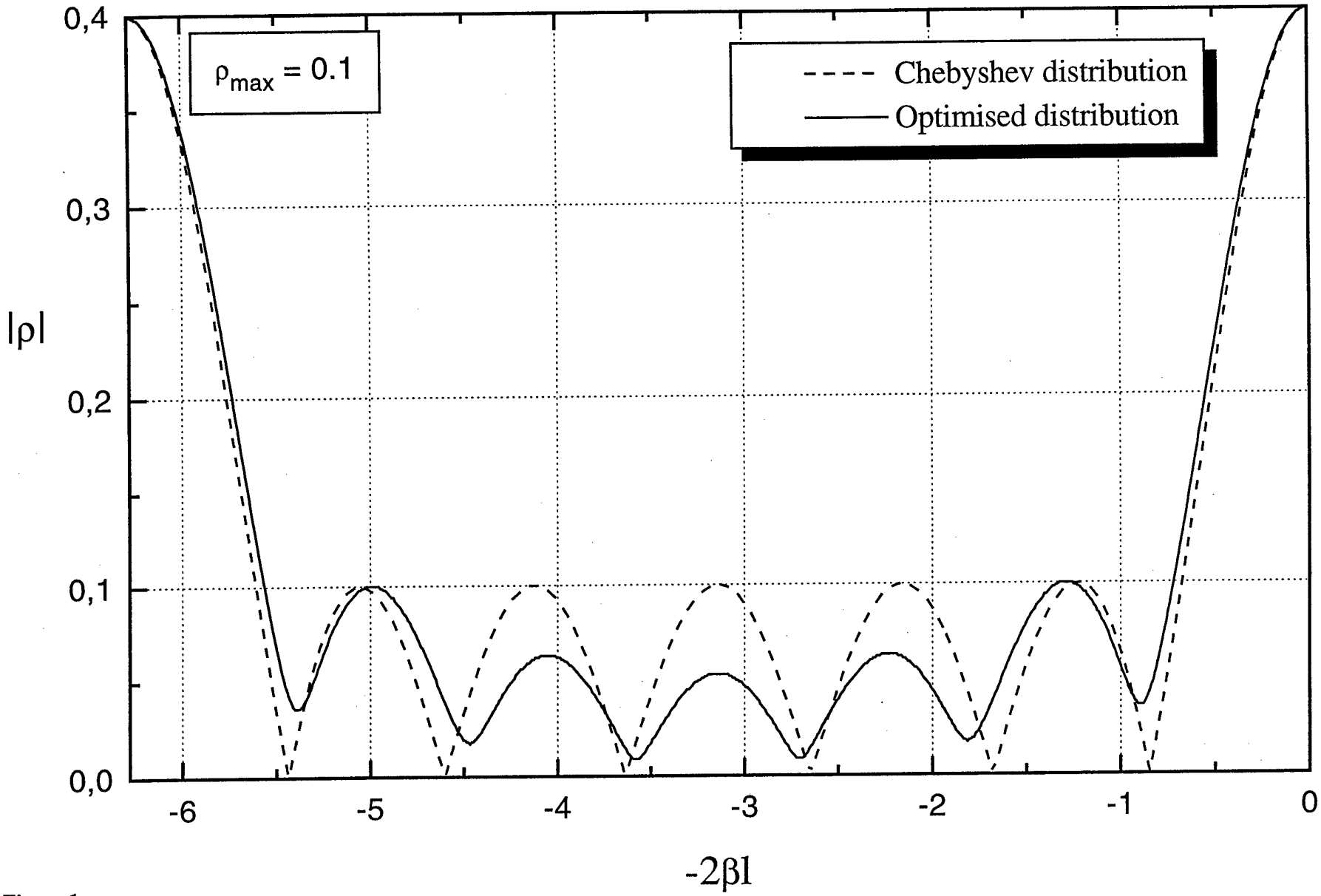
0,4
0,3
0,2
0,1
0,0
|ρ|
ρmax = 0.1
Chebyshev distribution
Optimised distribution
-6
-5
-4
-3
-2
-1
0
-2βl

Figure 1

ISRAMT'99 (17-II-99)

MINIMISING THE VARIABILITY OF CHARACTERISTIC IMPEDANCES IN MULTISECTION QUARTER-WAVELENGTH TRANSFORMERS

M.Vicente-Lozano, F. Ares-Pena, and E. Moreno.
Departamento de Física Aplicada.
Facultad de Física, Universidad de Santiago de Compostela
15706. Santiago de Compostela
SPAIN
E-mail: faares@usc.es

Abstract

The widely used first-order polynomial representation of the voltage reflection coefficient in multisection quarterwavelength transformers is assumed. The roots of this polynomial are displaced iteratively to obtain, through the simulated annealing technique, low variability between the characteristic impedances of adjacent transformers. Besides, for each problem configuration, the bandwidth is maintained close to its maximum possible value. Examples for several numbers of transformers and maximum reflection coefficients are presented obtaining an important decrease in the characteristic impedances variability of the transformers.

I. INTRODUCTION

Quarter-wavelength transformers are used as intermediate matching sections between a primarily resistive load R_L and a waveguide structure of characteristic impedance $Z_0 \neq R_L$. They are also used to connect two transmission lines with different characteristic impedances, caused by a change in dimensions or dielectric. When a match over a narrow frequency band is sufficient, a single-section quarter-wavelength transformer may be adequate. However, for good performance over an extended band of frequencies it may be necessary to use two or more sections in tandem.

Elliott [1] obtained results for a tandem of quarterwavelength transformers with a ripple-like frequency response with a moderate loss in bandwidth. Orchard procedure [2] was used to calculate the roots of the polynomial associated to the reflection coefficient. Several solutions were possible and the one that implies less variability between the characteristic impedances of adjacent transformers was chosen. However, using this technique we have not the guarantee to obtain, for a desired frequency response, the solution with less variability and with low loss in bandwidth in an optimal sense.

In this paper we propose a new technique to obtain a desired frequency response with low variability in characteristic impedances of consecutive transformers. This implies that the dimensions (or the dielectric) of adjacent transformers are similar and the physical implementation is easier since discontinuity effects are minimised. Furthermore, the bandwidth is also taken into account optimising its value according to input parameters. This procedure consists in minimising a cost function through the simulated annealing technique [3].

II. THEORY

Given N sections of common length l and characteristic impedances Z_n, connecting a mismatched load R_L to a line of characteristic impedance Z_0, it is well known that, to first order, the voltage reflection coefficient seen at the end of the main line (i.e. at the input to the first transformer section) is given by [1]:

$$\Gamma = \sum_{n=0}^{N} \Gamma_n e^{j2n\beta l} \tag{1}$$

where

$$\Gamma_n = \frac{Z_{n+1} - Z_n}{Z_{n+1} + Z_n} \tag{2}$$

By means of the following change of variable:

$$\psi = -2\beta l \tag{3}$$

$$w = e^{j\psi} \tag{4}$$

Equation (1) can be transformed in:

$$\Gamma = \sum_{n=0}^{N} \Gamma_n w^n \qquad (5)$$

which can be factorised to give:

$$\Gamma = \Gamma_N \prod_{n=1}^{N} (w - w_n) \qquad (6)$$

The synthesis of a desirable set of section reflection coefficients Γ_n can be obtained by first determining a desirable set of roots w_n and the study of the frequency behaviour of the input reflection coefficient Γ can be performed by using (6). By means of (2) is possible to calculate the characteristic impedance of each quarter-wavelength transformer.

The synthesis procedure consists on calculate the appropriate reflection coefficients in order to obtain a desired frequency response and also to adjust the bandwidth to desired specifications. The searching of these coefficients will be accomplished through the roots w_n. In (4) was shown the expression of these roots, but in general, they adopt the following form:

$$w_n = e^{a_n + j\psi_n} \qquad (7)$$

where the factor a_n indicates the radial displacement of the nth root in the unit circle representation of the roots.

With the assumption of negligible losses, all section characteristic impedances are pure real and also the reflection coefficients, therefore the roots w_n must occur in complex conjugate pairs or be in the real axis. In this case:

$$\left(\frac{\rho}{\rho_N}\right)^2 = \prod_{n=1}^{N} (w - w_n)(w - w_n)^* \qquad (8)$$
$$= \prod_{n=1}^{N} 1 - 2e^{a_n} \cos(\psi - \psi_n) + e^{2a_n}$$

where $\rho = |\Gamma|$ and $\rho_n = |\Gamma_n|$.

It can be seen from the above expression that, except for level, $\left(\rho/\rho_n\right)^2$ does not depend on the a_n sign, thus there are 2^N sets of roots w_n that will produce the same frequency response.

The simulated annealing technique [3] allows us to obtain desirable frequency response while maintaining low variability between the characteristic impedances of each transformer. In this technique there exist two key factors: the construction of a cost function that the algorithm minimises and the perturbations introduced to the variables in this cost function, which are the roots w_n. As starting solution a Chebyshev distribution of the section reflection coefficients was chosen, which has all the lobes at the same height and yields the maximum bandwidth in the frequency response for a given N. The cost function used was:

$$C = |M_{id} - M_{io}|^2 k_1 + |Z_{i+1} - Z_i|^2_{max} k_2 + |P_d - P_o|^2 k_3 \qquad (9)$$

where M_{id} and M_{io}, are the desired and the obtained maxima in the frequency response of each transformer, the second term is the maximum difference between the characteristic impedance of two consecutive transformers, which we define as variability. Finally P_o and P_d are the obtained and maximum desired percentage of loss in bandwidth respectively of the multisection transformer. These percentages are taken in relation to the bandwidth corresponding to the Chebyshev distribution. The factors k_i are weights used to give more importance to one factor than to another in order to search for the best solution. In the weights selection the greater factor is k_2 but a reasonable relation with the others factors (k_1 and k_3) is always maintained.

III. EXAMPLES

A. *Example 1*

In this example a tandem of $N = 6$ transformers was chosen, the load at the end of the line was $R_L = 140$ ohms and the input impedance was $Z_o = 60$ ohms. With this load configuration the selected value of ρ_{max} was 0.1, so the maxima (M_{id}) were all set to 0.1. The bandwidth, defined as the frequency range over which the magnitude ρ of the reflection coefficient does not exceed the specified level ρ_{max}, was controlled by the percentage of deviation from the bandwidth of the Chebyshev pattern (P_d parameter in (9)). In Table I there are shown, for several values of P_d, the results about initial and final beamwidth (BW_i and BW_f respectively), initial and final variability (V_i and V_f respectively) and the relative percentage of gain or loss in each factor.

P_d	BW_i	BW_f	%	V_i	V_f	%
2.0	4.92	4.84	-1.62	18.51	12.55	-32.18
1.5	4.92	4.88	-0.81	18.51	13.70	-26.01
0.5	4.92	4.92	0.00	18.51	15.46	-16.49

Table I. Results obtained in the example, $N = 6$.

In Fig. 1 it is shown the frequency response when P_d is chosen to 2%. It can be seen that as long as the

desired percentage of loss increases, the variability decreases.

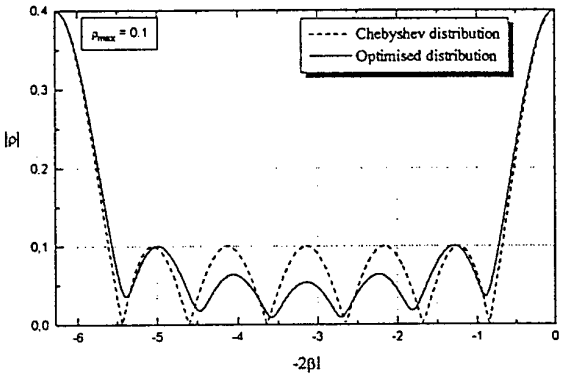

Figure 1. Frequency response for a tandem of $N = 6$ quarter-wavelength transformers, $\rho_{max} = 0.1$. The maximum desired percentage of loss in bandwidth is $P_d = 2\%$. The load used was $R_L = 140$ and the input impedance $Z_o = 60$.

B. Example 2.

In this case the parameters of the problem were: $N = 7$, $R_L = 100$ ohm, $Z_o = 60$ ohm and $\rho_{max} = 0.05$. The results for three values of P_d are shown in Table II. The initial and final frequency response are shown in Figure 2.

P_d	BW_i	BW_f	%	V_i	V_f	%
2.0	4.96	4.88	-1.62	6.98	5.34	-23.42
1.5	4.96	4.92	-0.81	6.98	5.33	-23.52
0.5	4.96	4.96	0.00	6.98	5.49	-21.38

Table II. Results obtained in the example, $N = 7$.

This example gives similar results for each P_d, all over the 20% of improvement in the variability. The most important factor in this case is the greater difference between $|R_L-Z_o|/|R_L+Z_o|$, which is the reflection coefficient at $\psi = 0$, and the desired ρ_{max}. Other examples performed showed the same behaviour, the smaller is this difference, the better is the improvement in the variability.

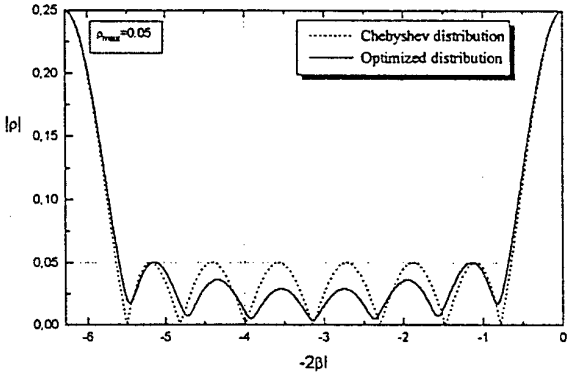

Figure 2. Frequency response for a tandem of $N = 7$ quarter-wavelength transformers, $\rho_{max} = 0.05$. The maximum desired percentage of loss in bandwidth is $P_d = 2\%$. The load used was $R_L = 100$ and the input impedance $Z_o = 60$.

IV. CONCLUSIONS

The variability of the multisection quarter-wavelength transformers characteristic impedances was improved by using the simulated annealing technique. Furthermore the bandwidth of the frequency response was taken into account to acquire more practical and realisable solutions for the construction of multisection quarter-wavelength transformers. Due two the multiplicity of solutions there are 2^N sets of roots w_n that will give the same optimal response function $\rho(\beta l)$. Each of these sets gives a different solution for the section reflection coefficients and characteristic impedances. In addition, the method is also applicable in cases where all the zones in the frequency range have not the same lobe level, i.e., different ρ_{max}'s in different zones in the passband.

At present the extension of this method to tapered transmission lines, described in [4], is under study. Finally this method is directly applicable to the problem analysed in [5] about multihole directional couplers.

V. ACKNOWLEDGEMENTS

This work was supported by the Xunta de Galicia under Project XUGA 20601B98, by the U.S. European Office of Aerospace Research and Development (EOARD) and by the U.S. AirForce Office of Scientific Research (AFOSR).

REFERENCES

[1] R. S. Elliott, *An Introduction to Guided Waves and Microwave Circuits*, Englewood Cliffs, New Jersey: Prentice-Hall International Editions, 208-231,1993.

[2] H. J. Orchard, R. S. Elliott, and G. J. Stern, "Optimizing the Synthesis of Shaped Beam Antenna Patterns", Proc. IEE, Part H, vol. 132, 63-68, February 1985.

[3] W.H. Press, W.T. Vetterling, S.A. Teukolsky, and B.P., Flannery, *Numerical Recipes in C*, Second Edition, Cambridge, 444-445, 1992.

[4] J. P., Mahon, and R. S. Elliott, "Tapered Transmission Lines with a Controlled Ripple Response", IEEE Trans. Microwave Theory Tech., vol. 38, 1415-20, October 1990.

[5] R. S. Elliott and Y. U. Kim, "Improved Design of Multihole Directional Couplers Using an Iterative Technique", IEEE Trans Microwave Theory Tech., vol. 38, 411-415, April 1990.